

Centre for Geo-Information

Thesis Report GRS-2007-17

---

**The influence of slope in the quantification of soil iron content with spectral reflectance based iron indices.**



V.L. Mulder

October 2007



WAGENINGEN UNIVERSITY

WAGENINGEN UR



# **The influence of slope in the quantification of soil iron content with spectral reflectance based iron indices.**

Vera Leatitia (Titia) Mulder  
Registration number 84-01-26-589-120

## Supervisor:

Harm Bartholomeus

A thesis submitted in partial fulfillment of the degree of Master of Science  
at Wageningen University and Research Centre,  
The Netherlands.

October, 2007  
Wageningen, The Netherlands

Thesis code number: GRS-80424  
Thesis Report: GRS-2007-17  
Wageningen University and Research Centre  
Laboratory of Geo-Information Science and Remote Sensing

## Foreword

This thesis gave me the perfect opportunity to combine both my specializations for graduation. My first masters degree is Soil Science and my second degree is Geo-Information Science and Remote Sensing. It was very interesting to combine both these specializations into one thesis subject. I started this thesis when I got back from my field practical for Soil Science which was located in Alora, Spain. The coincident was that the research area for this thesis was exactly the same area so it was easy for me to visualize the field conditions under which the soil samples were taken and to do another type of research in the same area.

The last four months, I have enjoyed working on this subject. It gave me a new view on Soils Science for I am trained as a field geologist and earth observation from remote distances is not familiar to me. Also, it deepened my knowledge in Remote Sensing for I have learned to work with new software packages and got acquainted with imaging spectroscopy.

I would not have come to these results if it was not for the help I received from several persons, who I would like to thank;

Firstly, I would like to deeply thank Harm Bartholomeus for his supervision. Thanks to Harm, I was able to combine my two specializations, Remote Sensing and Soil Science, together in one thesis. He has provided me with good comments, questions and suggestions to improve the results greatly. I truly appreciate that you have taken the time to answer all my questions.

Secondly, I would like to thank Aldo Bergsma for his help with the encountered difficulties while working with ArcMap. I learned now to work with ArcMap and to organize my data with a clear structure.

I would also want to thank Gerard Heuvelink for his advice on the statistical measures that I have used and Jetse Stoorvogel for his comments on the methods and the suitability for Soil Science.

I want to thank Jeroen van Bruggen for reviewing my report and patience that he has given me during the thesis work. Finally, I want to thank my family for their involvement and support.

Titia Mulder, Wageningen, 28-09-2007.

## Summary

Soil iron is an important indicator in the soil science; iron is an indicator for soil fertility, the usability of an area to cultivate specific crops and it can indicate the age of the deposits (Bartholomeus et al., 2007). Determining the spatial distribution of different types of iron with traditional fieldwork and laboratory analysis is time-consuming and expensive. Remote sensing has proven to be a useful tool to determine the presence of iron in extended areas and various research fields (Bartholomeus et al., 2007).

There are chemical and physical properties that influence the reflectance. They originate from the chemical and physical properties of the surface, the soil and from the set up of the spectrometer. These properties are so called spectral chromophores. For the soil reflectance the most important chemical chromophores are minerals, organic matter content and water. The most important physical chromophores are texture, surface roughness, viewing angle, radiation intensity, incident angle and azimuth angle of the source (Ben-Dor et al., 1999). With airborne imaging spectroscopy some characteristics of the terrain, like slope and aspect, do influence the reflectance. With PARGE/ATCOR the bias of these characteristics is corrected for though slope is not corrected over the whole reflectance spectrum. The effects of slope and aspect are still present because the PARGE/ATCOR model is not performing well for rugged terrain (Schläpfer and Richter, 2002).

The main objective of this research is to quantify the effect of slope on the prediction of soil iron content using spectral reflectance based iron indices.

The laboratory experiment will give the data to assess the influence of slope on the prediction of soil iron content. An experimental set up is designed where the slope of the sample can be varied, resulting in different illumination angles.

From these reflectance data the iron indices are calculated and a model is developed to predict the soil iron content. Three different indices are used in order to estimate the soil iron content; the ratio based Redness Index and the area and standard deviation after the continuum-removal. With multiple regression and general statistics the relation between slope and the prediction of soil iron content is quantified. From these relations a slope correction model is created with multiple linear regression to correct for the error caused by slope. In order to make the link with the "real world", the laboratory results are compared with airborne imaging spectroscopy data. Analyses are performed to assess the performance of a ROSIS- image, taken in the same area as the soil samples, in the prediction of soil iron content (Appendix A).

Paired-Samples T-tests are used to address the significant difference in the estimated soil iron content between measurements done under a certain slope and measurements from nadir. The ratio based Redness Index is not influenced by slope, the other indices are influenced by slope.

The slope has little influence on the  $D550_{\text{area\_lab}}$  and minimum and maximum errors are present up to 10% for slopes of  $10^0$  or smaller. With increasing slope, the influence of the slope increases as well but there is not a clear trend.

$D550_{\text{S.D.}_\text{lab}}$  is influenced by slope. On average, the index does significantly deviate from the nadir measurements up to an error of 2.5% and the minimum and maximum errors are up to 5%. The influence of slope is larger for steeper slopes and a so called "V-shape" is formed when results are plotted.

For both the area and the standard deviation of  $D880_{\text{lab}}$  the slope is clearly influencing the indices. The iron content is significantly deviating from the nadir measurements and the average deviates up to 5% with minimum and maximum errors deviating around this average of 5%. The effect is stronger for the negative facing slopes; this might be due to the retroreflectance properties of the material and the surface roughness.

In order to correct for the error caused by the slope, a slope correction model is developed with a linear regression for each slope and for each index.

The results for both the area and the standard deviation for  $D550$  and  $D880$  are improved and more accurate. Both the slope correction models for  $D550_{\text{area\_lab}}$  and  $D550_{\text{S.D.}_\text{lab}}$  can be classified as a class B model according to Chang et al. (2001). The developed slope correction models for  $D880_{\text{area\_lab}}$  and  $D880_{\text{S.D.}_\text{lab}}$  have a better performance and can be classified as a class A model according to Chang et al. (2001).

Finally, it is concluded that the ratio based Redness Index is not influenced by slope and the other indices are indeed influenced by slope. The slope correction model for the slope is performing well for D880<sub>\_area\_lab</sub> and D880<sub>\_S.D.\_lab</sub> and the performance of the slope correction model is less for D550<sub>\_area\_lab</sub> and D550<sub>\_S.D.\_lab</sub>.

The estimation of soil iron content with ROSIS data is not accurate. There are several reasons why the ROSIS image has a bad performance in the estimation of soil iron content:

- The ROSIS-image has a strong noise in the data and due to the applied MNF some signal is lost.
- Due to the rugged terrain the atmospheric and topographic corrections are not accurate and the reflectance is deviating strongly from the laboratory measurements.
- The result of the SMA is not optimal due to the coarse resolution of the image and the influence of mixed pixels is large. The mixed pixels consist of bare soil and olive trees.
- The interpolation of the masked pixels is not the most accurate method.
- The texture map is based on too few samples and therefore inaccurate.

Taken all these possible errors into account, the correlation (R) between soil iron calculated with RI<sub>\_rosis</sub> and the original iron content is 0.26. When the interpolated pixels and the correct texture is taken into account than the correlation increases up to 0.40, which is still very low.

If the expected error of the slope for D550<sub>\_S.D.\_rosis</sub> is compared with the overall error than it turns out that the error caused by the data quality and the field conditions is 8.96 times as big as the error caused by the slope.

The effect of slope is negligible when the ROSIS-image is being used for the quantification of soil iron content because the field conditions have more influence than slope and the indices require very accurate reflectance measurements.

For improvement of the slope correction model, it is most important that the standard deviation of the error caused by slope is minimized. For the spatial determination of soil iron content it would be recommended to use an orthorectified image with a finer resolution. With better data, the reflectance will probably better correspond to the reflectance measured under laboratory conditions and the amount of mixed pixels will be lower for the SMA.

The texture map must be of good quality, the best way to collect this data is to go into the field and take samples which are then analyzed in the laboratory.

More field samples of the iron content are needed in order to get insight into the spatial variability of the iron. All the calculated statistics are based on a relative small data set; the reliability of these statistics can be enhanced when more samples are taken into account (Isaaks and Srivastava, 1989).

# INDEX

<b>1. INTRODUCTION</b>	<b>1</b>
1.1 Background	1
1.2 Problem definition	1
1.2 Research objectives	2
1.3 Research questions	3
1.4 Outline of the report	3
<b>2. THEORETICAL BACKGROUND</b>	<b>4</b>
2.1 General information	4
2.1.1 Directional Reflectance Factors	4
2.1.2 Imaging spectroscopy	5
2.2 Microscopic interactions of soil particles	5
2.2.1 Vibrational transitions	6
2.2.2 Electronic transitions	6
2.3 Macroscopic interactions of soil particles	6
2.3.1 Directional distribution of soil bidirectional reflectance	7
2.3.2 Surface roughness and soil texture	7
2.3.3 Spectral chromophores	8
2.4 Landscape properties	10
2.4.1 Solar altitude and radiation intensity	10
2.4.2 Catena position	10
2.4.3 Spectral chromophore: Slope	10
2.4.4 Spectral chromophore: Aspect	11
2.5 Atmospheric and topographic correction for the ROSIS image	11
2.6 Viewing geometry	13
2.6.1 Calculation of the Ground projected Field of view	14

<b>3. METHODOLOGY</b>	<b>15</b>
<b>3.1 Soil samples</b>	<b>15</b>
<b>3.2 Soil reflectance measurements</b>	<b>16</b>
3.2.1 Imaging spectroscopy	16
3.2.2 Measuring device: ASD fieldspec Profr	16
3.2.3 Airborne measurements: ROSIS	16
<b>3.3 Methods for iron indices</b>	<b>17</b>
3.3.1 Ratio based Redness Index	17
3.3.2 Continuum-removal	18
3.3.3 Prediction of soil iron content.	18
3.3.4 Slope correction model	20
3.3.5 Performance of the slope correction model	21
<b>3.4 Soil iron content prediction with airborne imaging spectroscopy</b>	<b>23</b>
3.4.1 Data preprocessing	23
3.4.2 Prediction of soil iron content with ROSIS	24
<b>3.5 Practical set up</b>	<b>24</b>
<b>3.6 Software</b>	<b>26</b>
<b>4. RESULTS AND DISCUSSION</b>	<b>27</b>
<b>4.1 Reflectance under different slopes</b>	<b>27</b>
<b>4.2 Correlation of reflectance with soil iron</b>	<b>28</b>
<b>4.3 Correlation (R) of iron indices with soil iron</b>	<b>29</b>
<b>4.4 Regression functions for the estimation of soil iron content</b>	<b>30</b>
<b>4.5 Effect of slope on the soil iron prediction</b>	<b>32</b>
4.5.1 Paired-samples T-Test to test the significant difference	32
4.5.2 Visualization of the error	33
<b>4.6 Slope correction model</b>	<b>36</b>
4.6.1 Error correction for D550 <sub>area_lab</sub> and D550 <sub>S.D._lab</sub>	37
4.6.2 Error correction for D880 <sub>area_lab</sub> and D880 <sub>S.D._lab</sub>	40
4.6.3 Discussion	43

<b>4.7 Preprocessing of the ROSIS-image and spatial data</b>	<b>45</b>
4.7.1 Destriping and unmixing of the ROSIS image	45
4.7.2 Masking	46
4.7.3 Spatial data	46
<b>4.8 Spatial determination of the soil iron content</b>	<b>47</b>
4.8.1 Differences between the ROSIS data and the laboratory data	47
4.8.2 Correction of the indices calculated with the ROSIS data	50
4.8.3 Performance of the ROSIS data set	51
4.8.4 The effect of the slope correction model on the spatial determination of the soil iron content	55
4.8.5 Discussion	56
<b>5. CONCLUSIONS AND RECOMMENDATIONS</b>	<b>59</b>
<b>5.1 Conclusions</b>	<b>59</b>
<b>5.2 Recommendations</b>	<b>60</b>
5.2.1 Recommendations for the laboratory experiment	60
5.2.2 Recommendations for the ROSIS analyses	61
<b>REFERENCES</b>	<b>62</b>
<b>Literature references</b>	<b>62</b>
<b>URL's</b>	<b>65</b>
<b>APPENDICES</b>	<b>66</b>

## List of figures

Figure 2.1: Angles for the bidirectional Reflectance Factor.	4
Figure 2.2: Light reflection from a) smooth surface and b) rough surface, source: physics archives.	8
Figure 2.3: Spectral reflectance of bare soil over 350 nm to 2500 nm.	9
Figure 2.4: Viewing geometry for spectroscopy.	13
Figure 2.5: Ground projected Field of View.	14
Figure 3.1 a: Spectral signature of bare soil.	18
Figure 3.1 b: Continuum removed spectrum with the convex hull method.	18
Figure 3.2: Experimental set-up for laboratory reflectance measurements.	25
Figure 3.3: Ground projected Field of View.	25
Figure 4.1: Spectral signature of bare soil under different slopes.	27
Figure 4.2: The Pearson's correlation coefficient (R) of the soil iron content and reflectance.	28
Figure 4.3: Boxplot with the error calculated as the difference of the predicted (slope (x)) and estimated (slope 0) soil iron content, for the different slopes and calculated by means of the ratio based Redness Index.	33
Figure 4.4a: Boxplot with error (%) for D550 <sub>area_lab</sub> .	34
Figure 4.4b: Boxplot with error (%) for D550 <sub>S.D._lab</sub> .	34
Figure 4.5 a: Boxplot with error(%) for D880 <sub>area_lab</sub> .	35
Figure 4.5 b: Boxplot with error (%) for D880 <sub>S.D._lab</sub> .	35
Figure 4.6: Soil texture ( $\mu\text{m}$ ) plotted against the error of the iron prediction for D880 <sub>area_lab</sub> .	37
Figure 4.7a: Mean error (%) of the predicted iron content for corrected and uncorrected data of the calibration set for D550 <sub>area_lab</sub> .	39
Figure 4.7b: Mean error (%) of the predicted iron content for corrected and uncorrected data of the calibration set for D550 <sub>S.D._lab</sub> .	39
Figure 4.8a: Mean error (%) of the predicted iron content for corrected and uncorrected data of the validation set for D550 <sub>area_lab</sub> .	39
Figure 4.8b: Mean error (%) of the predicted iron content for corrected and uncorrected data of the validation set for D550 <sub>S.D._lab</sub> .	39
Figure 4.9a: Mean error (%) of the predicted iron content for corrected and uncorrected data of the calibration set for D880 <sub>area_lab</sub> .	42
Figure 4.9b: Mean error (%) of the predicted iron content for corrected and uncorrected data of the calibration set for D880 <sub>S.D._lab</sub> .	42
Figure 4.10a: Mean error (%) of the predicted iron content for corrected and uncorrected data of the validation set for D880 <sub>area_lab</sub> .	42
Figure 4.10b: Mean error (%) of the predicted iron content for corrected and uncorrected data of the validation set for D880 <sub>S.D._lab</sub> .	42
Figure 4.11a: Spectral signature of bare soil before MNF.	45
Figure 4.11b: Spectral signature of bare soil after MNF.	45
Figure 4.12: Zoomed map of the unmixed vegetation.	45

Figure 4.13a: Reflectance after MNF of soil sample A03 in the field, measured with airborne imaging spectroscopy.	47
Figure 4.13b: Reflectance of soil sample A01 measured under laboratory conditions.	47
Figure 4.14a,b,c: Scatterplots of the indices calculated with the laboratory data versus the indices calculated with the ROSIS data.	49
Figure 4.15: Scatter plot of the $RI_{\text{rosis}}$ and $RI_{\text{lab}}$ for uncorrected and corrected ROSIS data.	51
Figure 4.16: Scatter plot of Fe (mg/kg) calculated with ROSIS compared with the original Fe content.	54

## List of tables

Table 2.1: Relation of incoming and reflected radiance terminology used to describe reflectance quantities (Scaepman-Strub et al., 2006).	5
Table 2.2: Calculated diameter (cm) for the Ground projected Field of View for different slopes.	14
Table 3.1: Characteristics of the calibration set and validation set.	15
Table 3.2: The explanation for the abbreviations of the indices used in this research.	19
Table 4.1: Pearson correlations (R) of soil iron and spectral reflectance based iron indices under different slopes.	29
Table 4.2: Regression functions and $R^2$ for the estimation of soil iron content (mg/kg) with linear regression for the different indices and data sets.	30
Table 4.3: Regression functions and $R^2$ for the estimation of soil iron content with multiple linear regression for the different indices and data sets.	31
Table 4.4: 2-tailed significance of the compared pairs, the significant differences are given in red.	32
Table 4.5: 2-tailed significance of the compared pairs from the validation set for the different indices and slopes.	36
Table 4.6: The calibration and prediction results based on the error correction functions for D550 <sub>area_lab</sub> .	37
Table 4.7: The calibration and prediction results based on the error correction functions for D550 <sub>S.D._lab</sub> .	38
Table 4.8: The calibration and prediction results based on the error correction functions for D880 <sub>area_lab</sub> .	40
Table 4.9: The calibration and prediction results based on the error correction functions for the S.D. of D880	40
Table 4.10: Calibration and prediction results from Bartholomeus et al. (2007).	43
Table 4.11: Pearson's correlation (R) for the indices.	48
Table 4.12: Regression functions to correct the indices and correlation coefficients of the functions.	50
Table 4.13: Statistics for the comparison of the ROSIS image	51
Table 4.14: General statistics for the ROSIS image with and without masked pixels	52
Table 4.15: General statistics for the iron content calculated with variable texture.	53
Table 4.16: General statistics on iron content (mg/kg) for different data sets	54
Table 4.17: 2-tailed significance of the data sets compared with the soil iron content of the soil samples.	55
Table 4.18: General statistics for the expected error and the real error.	55

# 1. Introduction

## 1.1 Background

Iron is an important indicator in the soil science; iron is an indicator for the fertility of the soil, the usability of an area to cultivate specific crops and it can indicate the age of the deposits (Bartholomeus et al., 2007). Iron oxide content and iron species are also an indicator that soil is being formed. Iron oxide is strongly correlated with the soil weathering process on the short and long term (Ben-Dor et al., 1999). Determining the spatial distribution of different types of iron with traditional fieldwork and laboratory analysis is time-consuming and expensive. Remote sensing has proven to be a useful tool to determine the presence of iron in extended areas and various research fields (Bartholomeus et al., 2007).

Several techniques to deduce the amount of iron in the soil from the reflectance properties have been available. Chemical and physical properties of the surface do influence the reflectance (Ben-Dor et al., 1999 and Irons et al., 1989). A lot of research has been done on the chemical properties and less effort is put in the physical properties like the influence of the surface slope on the reflectance.

Investigation of the influence of slope on the quantification of soil iron content with spectral reflectance based iron indices will enhance the insight of the factors influencing soil reflectance.

This research has been carried out for the department of Geo-information Sciences and Remote Sensing from Wageningen University.

## 1.2 Problem definition

When airborne measurements are taken in sloping areas the measured reflectance is influenced by the slope. This effect is wavelength dependent, so slope may cause an under- or overestimation of the iron indices which can be calculated from these reflectances. In this research, an experimental setup is designed to investigate the effect of the slope on the quantification of soil iron with iron indices.

Found results from the experiment will be applied on airborne imaging spectroscopy data and analyzed on the performance of the estimation of soil iron content.

Peer-reviewed articles often focus on the chemical chromophores and the influences of multiple scattering and shadow-casting. The point of view of these researchers lies on the physical formulas but they do not examine the more practical factors, like variable slope, influencing the spectral reflectance. End-users are generally not interested in the physics behind data that they use. They want to know if the data is correct and reliable and if not which corrections they need.

There are some simplifications needed in this research in order to perform the analyses. In small scale areas (<1 ha) parent material, vegetation cover and water availability are most likely homogenous. In this research area the samples are all taken down slope in a transect with intervals of approximately

10 m (Bartholomeus et al., 2007). Therefore, it is assumed that some chromophores, like organic matter content and soil roughness will not really vary in the samples. Soil moisture is not influencing the laboratory spectra because the samples are air dried. The small differences that are present might not even influence the outcome of the iron indices. The iron content and the topography vary. For these small areas, it is far more interesting to look at these influences than those working on the microscopic scale. From this point of view, it is justified to not take into account the influence of the mentioned chemical chromophores on reflectance in the laboratory experiment. This is not justified for the analyses of the ROSIS image because of the extend of the research area (1 km x 2 km) and these differences must be taken into account when the two data sets are compared with each other. In the laboratory the radiation intensity is constant. The assumption is that the surface roughness is equal for the samples. Texture might be important but that will turn out during the analyses. In the experimental setup, the viewing angle, incident angle and azimuth angle are taken into account.

## 1.2 Research objectives

The main objective of this research is to quantify the influence of the slope on the prediction of soil iron, using spectral reflectance based iron indices.

To answer to this objective first the existing theories and performed research on this subject must be known. The first objective is to understand the existing literature which can contribute to the research. The second objective is to design an experimental set up where the slope of the sample can be varied, resulting in different illumination angles. The laboratory experiment will give the data to assess the influence of slope on the prediction of soil iron.

From these reflectance data the iron indices are calculated and a model is developed to predict the iron content. Three different indices are used in order to estimate the soil iron content; the ratio based Redness Index, the area of the iron specific absorption features and the standard deviation of the absorption features after the continuum-removal. With multiple regression and general statistics the relation between slope and the prediction of the iron content is quantified. The prediction of the iron content and the quantification of the influence of slope on the prediction of soil iron is the third objective. From these relations a slope correction model is created with multiple linear regression to correct for the error caused by slope, as a fourth objective. In order to make the link with the “real world”, the laboratory results are compared with airborne imaging spectroscopy data. Finally, an assessment is made on the performance of a ROSIS-image on the predictability of the iron content. In appendix A a flow chart can be found with the several steps that are taken in this research in order to reach the objectives.

### 1.3 Research questions

The research objectives lead to the following research questions.

The main research question is:

*“Is the influence of the slope significant on the quantification of soil iron content with spectral reflectance based iron indices?”*

Sub questions are:

- Which spectral chromophores do influence the spectral reflectance?
- What is the influence of slope on the quantification of soil iron content with spectral reflectance based iron indices?
- Can a correction model for the error caused by the influence of slope be developed?
- Is the influence of slope significant when reflectance data from airborne imaging spectroscopy are used?

### 1.4 Outline of the report

In the second chapter, a theoretical background is provided on imaging spectroscopy and the specific soil characteristics that influence the reflectance spectrum. The third chapter describes the methodology followed during the research. In the fourth chapter, the results of the experiment and the performed analyses are presented and discussed. In the fifth chapter the conclusions are drawn and recommendations are given for further research.

## 2. Theoretical background

Although the emphasis in this research is on the influence of the slope in the quantification of soil iron content, it is important to understand the theories behind imaging spectroscopy and to understand the reflectance spectrum. From earlier research it is known that differences in reflectance are caused by chemical and physical spectral chromophores, varying from microscopic to macroscopic scale. Corrections on some chromophores are known but the effect of a lot of chromophores is still under debate. In this chapter the different chromophores and processes influencing reflectance are discussed starting from the microscopic and macro scale up to the influence of land surface properties (Irons et al., 1989). The microscopic scale of the sand particles concern the processes within particles and the macroscopic scale is the scale where soil particles interact with each other. The land surface properties concern slope and aspect. Then, the atmospheric and topographic correction for the ROSIS image is clarified and finally the important aspects of the viewing geometry are described. First, some general information is given about imaging spectroscopy.

### 2.1 General information

#### 2.1.1 Directional Reflectance Factors

A definition of spectral reflectance and the reflectance factor is needed to understand the principle of reflectance. A definition of reflectance is given by Lillesand et al. (2004):

*Reflectance is quantified by taking the ratio of spectral radiant flux reflected from a soil surface to the spectral radiant flux reflected from a reference material illuminated and viewed in the same manner as the soil surface. If the reference material can be considered as a lossless perfectly diffuse surface, then the ratio is precisely defined as a Spectral Reflectance Factor, instead of spectral reflectance.*

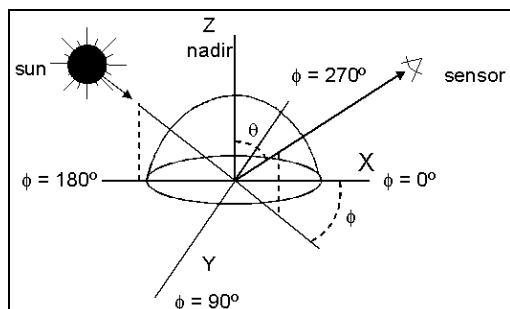


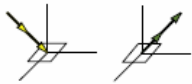
Figure 2.1: Angles for the bidirectional Reflectance Factor.

There are several reflectance factors, which are described by Schaepman-Strub et al. (2006). Two reflectance factors are relevant in this research namely, the Bidirectional Reflectance Factor (BRF) and the Hemispherical-Directional Reflectance Factor (HDRF) (table 2.1).

Under laboratory conditions the only irradiance is coming from one single direction of illumination (BRF), this means that all the incoming radiation is truly coming from the source (fig. 2.1).

Normally, measurements are done in the field or from the air. Under these conditions there is not one single direction of illumination but the irradiance comes from an entire hemisphere including the atmosphere and surrounding terrain, in that case the spectral reflectance factor is hemispherical (Schaepman-Strub et al., 2006). This means that under field conditions reflectance will deviate from the laboratory measured reflectance. This must be taken into account when field data and laboratory data are compared with each other.

Table 2.1: Relation of incoming and reflected radiance terminology used to describe reflectance quantities (Scaepman-Strub et al., 2006).

Incoming/Reflected	Directional
<i>Directional</i>	Bidirectional CASE 1
	
<i>Hemispherical</i>	Hemispherical-directional CASE 7
	

### 2.1.2 Imaging spectroscopy

The spectral reflectance of remote objects is measured with a spectrometer. Imaging spectroscopy is also referred to as hyperspectral sensing. With hyperspectral sensors images can be required in many, very narrow, contiguous spectral bands throughout the visible, near-IR, mid-IR and thermal IR portions of the spectrum, which enables the construction of an effectively continuous reflectance spectrum. The advantage of this system is that these systems can discriminate among earth surface features that have diagnostic absorption and reflection characteristics over narrow wavelength intervals that are lost within the relatively coarse bandwidths of the various bands of conventional multi spectral scanners. With imaging spectroscopy the absorption features of iron can be found (Lillesand et al., 2004).

## 2.2 Microscopic interactions of soil particles

At the microscopic scale there are radiation interactions with atoms and molecules. Vibrational, translational, rotational and electronic transitions take place due to the interaction of soil with solar radiation on the microscopic scale of soil particles. The translational and rotational transitions are restricted in most soil material and thus do not play a major role (Ben-Dor et al., 1999).

Electromagnetic radiation can only be emitted or absorbed when an atom or molecule makes a transition between energy states.

### **2.2.1 Vibrational transitions**

A molecule holds several modes of vibrations, depending on the number and arrangement of atoms in a molecule. Discrete energy levels may be associated with each vibrational mode of a molecule. The lowest allowable energy level for each mode is referred to as the ground level. Transitions between the energy level of each result in the emission or absorption of radiation at specific frequencies. The frequencies associated with transitions between a ground level and the next-highest energy level are called fundamental bands. The absorbed or emitted frequencies are so called overtone bands when a vibrational mode transits from one state to a state more than one energy level above or below the original state. Combination bands refer to frequencies associated with transitions of more than one vibrational mode. The vibrational transitions corresponding to the fundamental bands are generally more likely to occur than transitions corresponding to the combination and overtone bands. Absorption features in reflectance spectra are therefore usually strongest for the fundamental bands. The fundamental bands for most soil minerals occur in the infrared of wavelengths between 2500 and 50.000 nm. In this research this part of the spectrum will not be measured, only features can be observed between 300 nm and 2500 nm. The possible vibrational energy levels of the molecular soil components depend on the atomic composition and structure of the molecules (Ben-Dor et al., 1999 and Irons et al., 1989).

### **2.2.2 Electronic transitions**

Electronic transitions occur within the ultra violet and visible parts of the spectrum. Electronic transitions may be due to charge-transfer modes, crystal field transitions and transitions into the conduction band. For these transitions more energy is needed than for the vibrational transitions and so they will occur at the higher frequencies within the ultra violet and visible parts of the spectrum. The absorption bands are typically much broader than the bands corresponding to vibrational transitions (Irons et al., 1989), iron is a mineral that causes charge-transfers. Iron ions are soluble in certain conditions and are thus widely distributed by the soil solution. Further, iron ions can easily replace aluminium and magnesium ions in octahedral sites of soil mineral crystals and can even replace silica in some tetrahedral sites. This replacement of minerals by iron causes charge transfers and, besides the crystal field effects, cause the absorption features found in the visible part of the soil reflectance spectra (Ben-Dor et al., 1999).

## **2.3 Macroscopic interactions of soil particles**

Several interactions take place on the macroscopic scale of soil particles, which is the scale on which soil particles interact with each other. Parent material influences the direction and the amount of the reflectance. Texture and surface roughness determine the extend in which shadow-casting and multiple scattering occurs. Several chemical and physical chromophores cause specific absorption bands and influence the amount of reflectance. These parameters are discussed in this section.

### **2.3.1 Directional distribution of soil bidirectional reflectance**

In most studies of soil reflectance, soil surfaces were both illuminated from a single direction and viewed from a single direction. Soil surfaces, however, are not Lambertian surfaces. Soil reflectance is not only a function of wavelength, but also depends on the directions of illumination and viewing angle. Particulate materials having low absorption (e.g. desert sand), strongly scatter light in the forward direction, i.e., away from the direction of illumination, with a maximum reflectance at a view zenith angle greater than the zenith angle of specular reflectance. Retroreflectance was more pronounced by soils that highly absorb, such as clay and loamy soils. At a view zenith angle at nadir for all soils there is a reflectance minimum. The retroreflectance is attributed to the effects of mutual shadowing among particles. A sensor does not view shadows if the sensor views a particulate surface from the anti-illumination direction. The proportion of shadowed area in view increases as the sensor moves away from the anti-illumination direction. In materials having a low absorption, e.g. quartz, shadows are softened by light that is multiple scattered or transmitted through particles (Irons et al., 1989).

### **2.3.2 Surface roughness and soil texture**

A rough surface generally reflects less due to self shadowing effects and multiple scattering (Clevers et al., 2006). The texture of the soil influences the multiple scattering and the shadow-casting. Bidirectional reflectances of particulate soil minerals generally increase and the contrasts of absorption features decrease as particle size decreases for transparent materials. For opaque materials the bidirectional reflectances decrease as particle size decreases. Aggregation of clay particles and clods larger than sand grains can contribute to darker appearance of clayey soils (Irons et al., 1989).

#### *2.3.2.1 Multiple scattering*

Soil reflectance is based on the concept of multiple scattering by soil particles. The electric charges within any particle of matter are set into oscillatory motion by the electric field of an incident electromagnetic wave. The accelerated electric charges either transform the incident radiation into other forms of energy or reradiate the energy at the same frequency but in different directions. This secondary radiation from a particle is referred to as scattered radiation. Multiple scattering occurs when particles are in close proximity and are affected not only by the electromagnetic field from an external source, but also by the electromagnetic fields scattered from nearby particles. Given the close proximity of soil particles, reflection from soil surfaces is often modeled as a manifestation of multiple scattering by soil particles (Irons et al., 1989).

#### *2.3.2.2 Shadow-casting*

Particulate materials having low absorption (desert sand), strongly scatter light in the forward direction, i.e., away from the direction of illumination, with a maximum reflectance at a view zenith angle greater than the zenith angle of specular reflectance. Retroreflectance was more pronounced by soils that highly absorb, such as clay and loamy soils. At a view zenith angle at nadir for all soils there is a reflectance minimum. The retroreflectance is attributed to the effects of mutual shadowing among particles. A sensor does not view shadows if and only if the sensor views a particulate surface from the anti-illumination direction. The proportion of shadowed area in view increases as the sensor moves

away from the anti-illumination direction. In materials having a low absorption, quartz, shadows are softened by light that is multiple scattered or transmitted through particles. This softening of shadows reduces retroreflectance by low-absorption materials (Irons et al., 1989).

Corrections for the surface roughness and the shadow-casting are given by Hapke (1984) and (Hapke 1986). An arbitrary photometric function for the bidirectional reflectance of a smooth surface may be corrected to include effects of general macroscopic roughness. The correction involves only one arbitrary parameter, the mean slope angle  $\theta$ , and is applicable to surfaces of any albedo (Hapke 1984). A more practical solution for evaluating the effects of physical parameters is to evaluate the reflectance of a given target relative to a perfect reflector measured at the same geometry and viewing angle of the target in question. In reality such conditions are impossible to achieve in the field, and complex effects such as particle size effect cannot be removed absolutely (Ben-Dor et al., 1999).

Figure 2.2 gives a clear view on the problem of a rough surface and the spectral reflectance. On a smooth surface all reflected light obeys the relationship, called Snell's Law, that the angle of incidence equals the angle of reflection. When the surface is rough, the rays of light are reflected in many directions. The law of reflection is still obeyed, but the incident rays strike different regions which are inclined at different angles to each other. Consequently, the outgoing rays are reflected at many different angles and the spectral reflectance is disrupted (Ben-Dor et al., 1999).

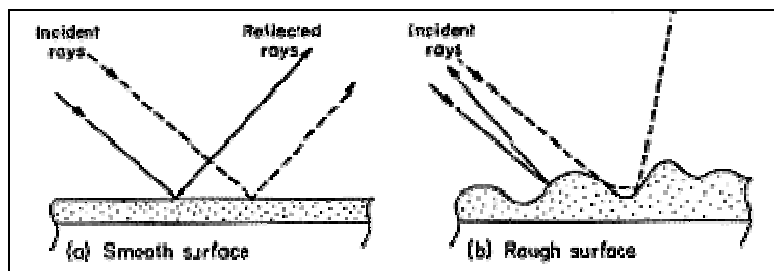


Figure 2.2: Light reflection from a) smooth surface and b) rough surface, source: physics archives.

### 2.3.3 Spectral chromophores

There are chemical and physical properties of objects influencing the reflectance, which originate from the chemical and physical properties of the surface, the soil and from the set up of the spectrometer. These properties are so called spectral chromophores. For the soil reflectance the most important chemical chromophores are minerals, organic matter content, water and iron content. The most important physical chromophores are texture, surface roughness, sample geometry, viewing angle, radiation intensity, incident angle and azimuth angle of the source (Ben-Dor et al., 1999). In this section the processes at macroscopic scale of soil particles is expound. The importance of texture and surface roughness has already been explained in section 2.3.2.

### 2.3.3.1 Mineralogical composition, Iron

Many of the absorption features in soil reflectance spectra are due to the presence of iron in some form (fig 2.3). The absorption features are caused by either crystal field effects or charge transfers involving iron ions. Steep decrease in reflectance toward the blue and ultraviolet wavelengths is a characteristic of almost all soil reflectance spectra. This decrease is due to a strong iron-oxygen charge transfer band that extends into the ultraviolet. Other absorption bands often occur near 700 nm and 880 nm due to electronic transition of ferric iron. Electronic transitions involving ferrous iron can cause strong absorption bands near 880 nm as well.

Several weaker absorption bands between 400nm and 550 nm are present due to one or the other iron ion. In iron rich soils the iron absorption in the middle infrared can be strong enough to obliterate the water-absorption band at 1400 nm and 1900nm (Irons et al., 1989).

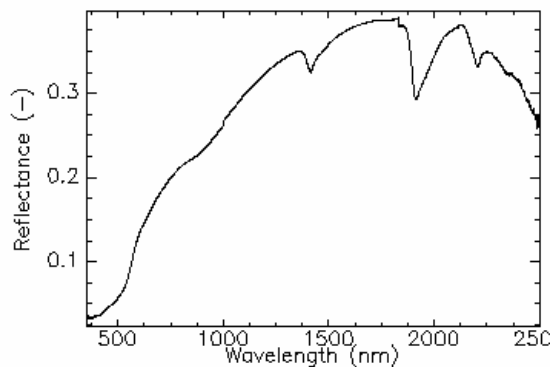


Figure 2.3: Spectral signature of bare soil over 350 nm to 2500 nm.

### 2.3.3.2 Viewing geometry

Escadafal and Heute (1991) did research on the viewing geometry on the spectral properties of soils. Bidirectional Reflectance Factors (BRF) in the 400 to 900 nm wavelength range and color coefficients were computed from measurements made along the principal plane of the sun with a portable spectroradiometer. A strong backscatter effect was observed in the antisolar direction. This nonlambertian behavior is related to the surface roughness and can be interpreted with existing models. Viewing geometry also influenced the shape of the soil spectral reflectance curves and resulted in an increase in color hue in the antisolar direction and maximum color saturation at nadir. This was attributed to multiple reflections of direct light and diffuse illumination of the shadowed parts of rough surfaces. These viewing effects on soil surface spectral signatures are relatively small when compared to spectral variances normally encountered among soils.

### 2.3.3.3 Organic matter content

Organic matter leads to a decrease in reflectance, soils with an organic matter content of 2% or more will mask absorption features. Organic matter itself has no distinct absorption features (Clevers et al., 2006). The influence of organic matter on the absorption features is dependent on the decomposition level, parent material and texture (Ben-Dor et al., 1999).

#### 2.3.3.4 Soil moisture

Water surrounds soil particles and fills the air spaces between them. This will reduce the amount of multiple scattered light. Moist soils will have lower absorption features in the SWIR region where water absorption increases significantly with increasing wavelength. The absorption bands for water can be found near 1.4  $\mu\text{m}$ , 1.9  $\mu\text{m}$  and 2.7 $\mu\text{m}$ . There is also a link between soil moisture and texture; clay can hold water more tightly, in this material the spectra will show more clearly the absorption bands than the spectra of sand (Clevers et al., 2006).

## 2.4 Landscape properties

Field conditions are not as stable as the laboratory conditions, there are several processes and terrain characteristics that will influence the reflectance. First of all, the solar altitude and the radiation intensity will vary every moment of the day and influence the reflectance during the data acquisition. The variability in altitude and sloping of the terrain will influence the reflectance as well, as will the aspect of the rugged terrain (Richter and Schläpfer, 2002). These properties are discussed in this paragraph.

### **2.4.1 Solar altitude and radiation intensity**

The solar altitude changes every second of the day. With that the angle of incoming radiation and irradiance angle also changes. This means that the viewing geometry and the incoming radiance is variable and influence the reflectance of the soil. When field measurements are taken during the day a correction should be made on the varying solar radiation and irradiance angle.

### **2.4.2 Catena position**

Different catena positions on a mountain are crest, up slope, down slope, valley. Due to the differences in soil redistribution and soil formation different iron contents can be expected. On top of a mountain, usually all soils are eroded and bare rock lies at the surface. Up slope, gradients are usually higher and soils erode which means that soil development is absent or marginal. Iron only occurs in developed soils, so expected is that the iron content on upslope positions will be lower. Down slope, gradients are less and sedimentation from upslope takes place in this area. The iron formed upslope is transported down slope, also the soil development contributes to iron in the soil, overall this will give a higher iron content in the soil. A valley can have a good soil development if soil is not eroded away by water transported from the mountain (Berg van Saparoea et al., 2007).

### **2.4.3 Spectral chromophore: Slope**

The main topographical property which influences the reflection parameters is slope in combination with aspect. Earlier research from Cierniewski (1987) shows that for soil on gradients of more than 20° the shadowing coefficient decreases when solar altitude increases from 0° to 90°. Cierniewski developed a model which indicates that the relationship for soils sloped with a surface roughness lower than 0.5 may be the opposite ( Ben-Dor et al., 1999).

Cierniewski has performed research on the same subject but the outcomes are too general. He only looked at the shadowing coefficient, and the range he defined for the slopes is too broad for topographical analysis. Usually soils occur at gradients ranging from  $0^{\circ}$  to maximal  $34^{\circ}$ , on larger slopes the soil suffers from erosion (Watson, 1987). It is more interesting to know what happens between the ranges that Cierniewski has defined, not only looking at the micro scale but also taken into account the macro scale properties like viewing geometry.

#### **2.4.4 Spectral chromophore: Aspect**

Depending on the aspect of the slope, the surface will receive more or less radiation. If reflectance is measured from an airplane the aspect might be important for the determination of the iron indices. On the sun side, more reflected radiation is received and on the shadow side the opposite takes place (Schläpfer and Richter, 2002). The aspect is present at the large scale; sun and shadow side of a mountain, but also at smaller scales caused by e.g. gullies or hilly, irregular surfaces.

Research has been carried out by (Schläpfer et al., 2004) for corrections on digital terrain models obtained from airborne measurements. They perform a radiometric nadir normalization of the HDRF surface, a so called parametric orthorectification. This normalization increases the validity of the DTM and decreases the shadowing effect but does not correct for a specific absorption feature under a specific aspect or slope (see section 2.5).

### **2.5 Atmospheric and topographic correction for the ROSIS image**

The ROSIS image is calibrated and converted to reflectance values by the operator (DLR), using the PARGE/ATCOR model. The described parametric geocoding procedure (PARGE) considers the aircraft and terrain geometry parameters and uses a forward transformation algorithm to create an orthorectified image. Correction is needed because airborne optical scanner images suffer from distortions due to the sensor movement during data acquisition. Even mechanically stabilizing platforms built into the carrier cannot remove these effects completely as residual movements of the stabilizing systems remain. Distortions become relevant if pixel or even sub-pixel accuracy is required. A higher accuracy can be obtained when working at a nominal spatial resolution of actual instruments between 4m and 20m, the generic accuracy requirement is in the range of 2–10 m (Schläpfer and Richter, 2002).

The influence of the atmosphere and topography is corrected for with ATCOR 4. A radiometric correction is performed on the geocoded orthorectified image obtained with the PARGE procedure. ATCOR4 takes into account the flight and solar geometry, the range of ground elevations, atmospheric parameters such as aerosol type and optical depth, water vapour and ozone contents, and the resampling with the spectral response function of the sensor channels (Richter and Schläpfer, 2002).

The created 'parametric geocoding' procedure (PARGE) reconstructs the scanning geometry for each image pixel using position, attitude and terrain elevation data. Slope is accounted for by means that the reflectance is been recalculated as if it would be at nadir. This means that when the slope is taken into account only a correction is made for the bias and that the influence of slope is assumed to be not wavelength dependent (Schläpfer and Richter, 2002).

In order to correct for the HRDF conditions accounted in the field ATCOR4 includes an interface to scene dependent bidirectional reflectance (BRDF) models. ATCOR4 first performs the atmospheric/topographic correction based on the assumption of Lambertian surface elements after that correction the BRDF can be taken into account.

The so called SPECL code performs a spectral pre-classification of the reflectance cube based upon template spectra at the Landsat Thematic Mapper (TM) reference wavelengths (i.e. 0.48, 0.56, 0.66, 0.83, 1.6, 2.2  $\mu\text{m}$ ) and returns a map of class indices for each pixel. The template spectra consist of typical vegetation covers, soil, sand, and water taken from literature (Vermote et al. 1997). If the spectral reflectance signature agrees within a 10% margin at the reference wavelengths with one of the class template spectra it is put into this class, otherwise it belongs to the class undefined (Richter 2000). For each pixel of a certain class the viewing and solar geometry is known. Depending on the available range of angles, a three- or four-parameter fit can be applied with a user-defined BRDF model. This correction is wavelength dependent (Richter and Schläpfer, 2001).

Richter and Schläpfer (2001) state that the following aspects are of critically importance for the accurateness of the correction model:

- An accurate absolute calibration (Green, 1998).
- The estimation of atmospheric parameters (Schläpfer et al., 1998).
- The geometric accuracy (Schläpfer and Richter, 2002).
- The bidirectional reflectance effects (Borel and Gerstl, 1994).

In many cases, the spatial resolution of the available DEM is not adequate to the sensor's pixel size. Therefore, regions of steep slopes and rapid slope or aspect changes are not adequately represented in the interpolated DEM. In this case errors in the matching of imagery and DEM can lead to large relative reflectance errors exceeding 100% for critical geometries (principal plane, e.g. a mountain ridge with half a pixel offset between imagery and DEM; Richter, 1998). Thus, the nonavailability of the required DEM resolutions of 1–10m for airborne imagery in rugged terrain will limit the final accuracy of the geo-atmospheric image product in many cases

Large radiometric errors (over- or under-correction) can, therefore, be expected in those regions (Richter, 1998).

All these aspects are hard to deal with in rugged terrain and therefore the radiometric correction of airborne imagery of optical sensors acquired in this type of terrain will remain a challenging risk (Richter and Schläpfer, 2002).

## 2.6 Viewing geometry

The viewing geometry can be explained by the following terms. There is an irradiance source which might be a lamp when working under laboratory conditions or the sun, when working under field conditions. The irradiance source emits radiance on the object to be measured under a certain angle; the incidence angle of the irradiance source. The spectrometer measures the radiance of the object under a certain angle, which is the viewing angle. Measurements are taken from nadir and in the solar principle plane, this means that the object and the spectrometer are in a perfect horizontal alignment with the irradiance source and the angle between the centre of the spectrometer and the object is  $0^{\circ}$  (fig 2.4).

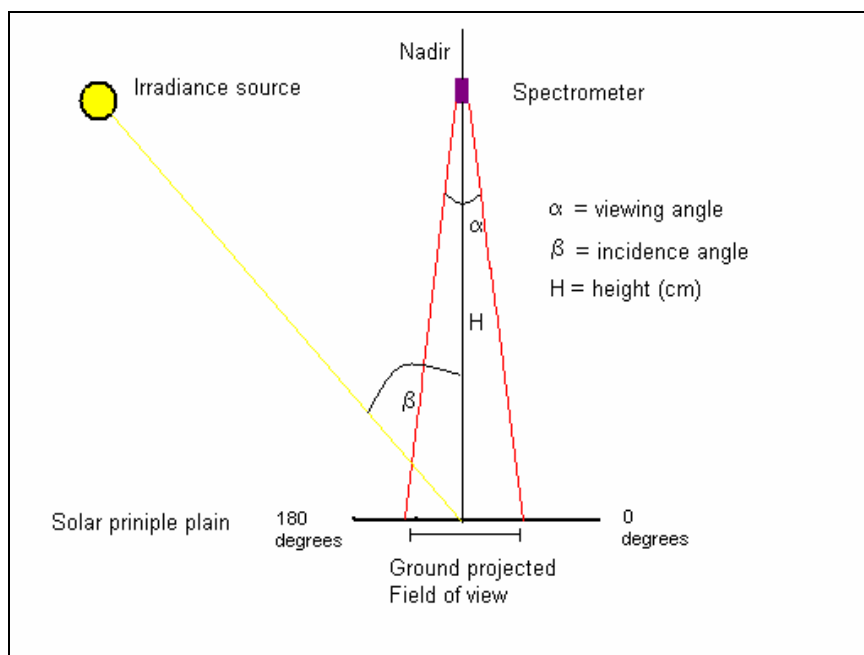


Figure 2.4: Viewing geometry for spectroscopy.

### 2.6.1 Calculation of the Ground projected Field of view

When the soil sample will be tilted under a certain angle, the ground projected field will change according to Pythagoras rules (fig. 2.5). This means that the amount of incoming and reflected radiation will deviate under different slopes. It might even influence the spectral reflectance based iron indices.

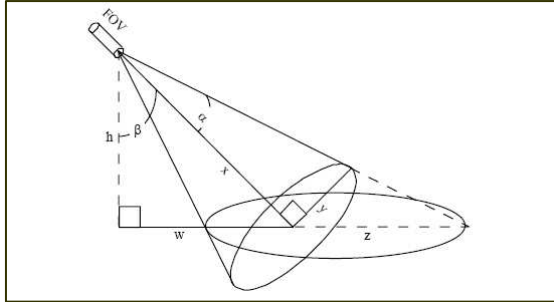


Figure 2.5: Ground projected Field of View (ENVI - The Remote Sensing Exploitation Platform).

The Ground projected Field of View from nadir can be calculated by:

$$x * \tan(\alpha) \tag{Equation 2.1}$$

Where  $\alpha$  is:

$$0.5 * (\text{for optic lens}) \tag{Equation 2.2}$$

For a changing viewing angle the Ground projected Field of View is variable. It is calculated with the law of sinus (TU Eindhoven, 2007).

$$a / \sin(\alpha) = c / \sin(\gamma) \tag{Equation 2.3}$$

Where  $a$  is the unknown variable, the Ground projected Field of View under a certain gradient and  $c$  is the Ground projected Field of View from nadir. Result for this experiment can be found in table 2.2.

Table 2.2: Calculated diameter (cm) for the Ground projected Field of View for different slopes.

Angle (°)	GFV (cm)
-25	4.79
-20	4.58
-15	4.43
-10	4.31
-5	4.24
0	4.2
5	4.19
10	4.21
15	4.26
20	4.35
25	4.48

### 3. Methodology

This chapter describes the methodology which is followed in this research. In appendix A the methodology is summarized by means of a flow chart.

#### 3.1 Soil samples

The soil samples to be measured are yet available, well selected and analysed for total iron content in the laboratory. They are taken from the slopes of El Hacho de Alora in Southern Spain and show a variety in iron content of 7 mg/kg up to 20 mg/kg. El Hacho is composed of material derived from tertiary marls and sands. Hematite is the major bearing iron mineral. Apart from the common iron absorption feature in the visible part of the spectrum, this will give an extra dip around 900 nm. For more information on the iron extraction method, the geological and topographical settings see Bartholomeus et al. (2007).

The texture of the soil samples can be of significant influence on the spectral reflectance of the soil samples as mentioned in the theoretical background. The marls have a very fine texture and the sands are coarse textured. The texture is determined manually by an expert according to the FAO classification system (FAO and ISRIC 1990).

The samples are taken in an area of about 300 m<sup>2</sup>. It is assumed that the variation in organic matter content is small due to the relative small size of the area. 48 Samples will be used which are air dried in the laboratory and sieved for the fraction < 2 mm. Due to the air drying, soil moisture is not influencing the spectral reflectance. For the experiment it is assumed that texture does not influence the iron indices. If prove is found that texture is really influencing the outcome of the indices it will be taken into account.

A calibration set and validation set is selected to calibrate and validate the models on. The sets are randomly selected with SPSS. The characteristics of both sets are given in table 3.1. For the calibration set the mean and standard deviation is higher and there are more samples with coarser texture included. The validation set consist of more fine textured samples. These differences can influence the results for the validation of the models.

Table 3.1: Characteristics of the calibration set and validation set.

	<b>Calibration set</b>	<b>Validation set</b>
N	24	24
Fe (mg/kg) Mean	14.41	11.41
Fe (mg/kg) S.D.	4.84	3.77
Texture >1000 µm	10	7
Texture <100 µm	3	6
Different parent material	3	3

## 3.2 Soil reflectance measurements

The ASD fieldspec ProFR spectrometer is used for data acquisition in the laboratory experiment in order to construct an effectively continuous reflectance spectrum. ROSIS is used for the airborne imaging spectrometer data, the data were collected in June 2001, during the DAISEX campaign (Berger et al., 2001).

### **3.2.1 Imaging spectroscopy**

The spectral reflectance is measured with a spectrometer. With hyper spectral sensors images can be acquired in many, very narrow, contiguous spectral bands throughout the visible, near-IR, mid-IR and thermal IR portions of the spectrum, which enables the construction of an effectively continuous reflectance spectrum. The advantage of this system is that these systems can discriminate among earth surface features that have diagnostic absorption and reflection characteristics over narrow wavelength intervals that are lost within the relatively coarse bandwidths of the various bands of conventional multispectral scanners. With imaging spectroscopy the absorption features of iron can be found (Lillesand et al., 2004).

### **3.2.2 Measuring device: ASD fieldspec ProFR**

The ASD Fieldspec Pro FR is used for the spectral reflectance measurements. This field spectrometer is an optical device that measures reflected light in the reflective part of the solar spectrum (350 nm - 2500 nm). The light enters the instrument through the fibre optic cable. Inside the instrument the light is divided over three sensors, which determine the intensity of the in coming light for each individual wavelength, for more technical detail see Barholomeus (2007a). The reference panel is made of spectralon and is assumed to be Lambertian per wavelength. The manual for the ASD Field-spec ProFR is used as described by Barholomeus (2007b).

### **3.2.3 Airborne measurements: ROSIS**

Airborne imaging spectrometer data were collected in June 2001, during the DAISEX campaign (Berger et al., 2001). ROSIS was built for the detection of absorption features especially in coastal and inland waters (Gege et al., 1998), but it is also used for land applications (Holzwarth et al., 2003). Airborne measurements are taken with a reflective optics system imaging spectrometer (RODIS) which covers the wavelength range from 416.9 up to 872.9 nm with a bandwidth of approximately 4 nm and a 4 nm sampling interval. The operating altitude of the aircraft was at flight level 120 resulting in a ground projected instantaneous field of view of 2m x 2m (Bartholomeus et al., 2007). ROSIS images were calibrated and converted to reflectance values by the operator (DLR), using the PARGE/ATCOR model (Schläpfer and Richter, 2002).

### 3.3 Methods for iron indices

There are several methods to determine the iron content of the soil samples; the ratio based Redness Index and the continuum-removal index by means of the convex hull normalization are the two most commonly used ((Hu et al., 2005);(Hu, 2007); and Bartholomeus et al., 2007).

The method used by researchers is depending on data and software availability. In this research both methods are used, and tested for robustness and performance. A random set of samples will be used for calibration and for the validation of the found relations.

#### **3.3.1 Ratio based Redness Index**

The ratio based Redness Index can be used as an indicator for soil iron because the redness of the soil is determined by iron oxides. Weathering products of iron bearing minerals contain iron oxides, when they become available to the soil, it will color the soil red (Irons et al., 1999). Soils with high amounts of iron oxide will appear redder and the ratio based Redness index will be higher for soil samples with higher iron content in the soil.

The spectral redness can be expressed as the reflectance in the visible red part of the spectrum divided by the sum of visible red, green and blue reflectances (Eq. 3.1):

$$r = \text{BRF}_r / (\text{BRF}_r + \text{BRF}_g + \text{BRF}_b), \quad \text{Equation 3.1}$$

Where  $\text{BRF}_r$  is the bidirectional reflectance in the visible red part of the spectrum (600-700 nm),  $\text{BRF}_g$  is the bidirectional reflectance in the visible green part of the spectrum (500–600 nm), and  $\text{BRF}_b$  is the bidirectional reflectance in the visible blue part of the spectrum (400–500 nm).

The  $\text{BRF}_n$  is then calculated by (Eq. 3.2):

$$\text{BRF}_n = R_t / R_c, \quad \text{Equation 3.2}$$

Where  $\text{BRF}_n$  is the bidirectional reflectance in wave band  $n$ ,  $R_t$  is radiance from the target surface, and  $R_c$  is the radiance from the reference panel (Bullard and White, 2002).

The Redness Index is calculated in IDL- ENVI 4.3 with the function “Band math”.

### 3.3.2 Continuum-removal

The normalization of the absorption features will be based on the convex hull method because this method is commonly used for normalization of soil reflectance spectra. E.g. Islam et al. (2005), evaluated the hypothesis that the convex hull biplot area of a geographical region is proportional to the soil variation found in that region. Withing et al. (2003) presents an approach to estimate soil moisture content through fitting an inverted Gaussian function to the continuum in soil spectra. Luo and Macleod (1992) presented the directed vein method and the convex hull method for automatic orientation analysis of soil microstructure. The mathematical theories behind the convex hull method are described by Hu et al. (2005) and Hu (2007). The normalization can also be done by using linear segments or with Gaussian band shapes (Kokaly, 2000). This method for continuum removal must be performed manually in Excel, although the Gaussian band shape is not an option because literature to perform the normalization is lacking. The normalization of the reflectance with convex hull can be performed with the software package IDL- ENVI 4.3. The characteristics of three absorption features for iron are taken into account; the dip between 390 to 600 nm, referred to as D550, the dip between 650nm to 750 nm, referred to as D700 and the dip between 800nm and 1000 nm, referred to as D880.

The convex hull method normalizes the absorption features to values up to 1, like a band is shaped around the curve and the band has a value of 1. Absorption features are falling under the band and do have a value smaller than one (fig. 3.1a & b).

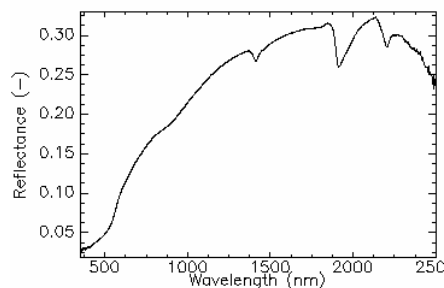


Figure 3.1a: Spectral signature of bare soil

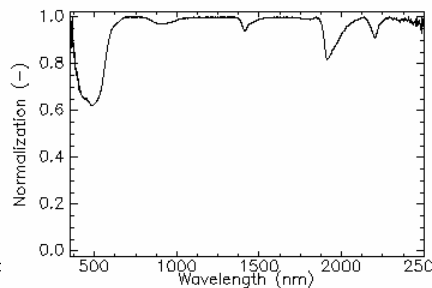


Figure 3.1b: Continuum removed spectrum with the convex hull method.

After the continuum removal, the area of the dip is calculated as indicator for iron. The depth and the width of the absorption dips are represented as well, in the standard deviation after continuum removal; the larger the width and depth of an absorption feature, the higher the standard deviation.

### 3.3.3 Prediction of soil iron content.

Once the indices are determined the effect of slope on the prediction of iron can be analyzed. Before the prediction function for iron can be derived for the different indexes, a check on the relation of iron with the indices must be determined. The Pearson correlation is calculated for the indices with iron for the ratio based Redness Index, D550, D700 and D880 (Putten, 2007). An R-value of at least 0.7 is good to proceed with the data analyses, if data series occur with R-value < 0.6 than it will not be used for further analyses. An R-value between 0.6 and 0.7 is mediocre but these results will be used for further

research, although it must be taken into account that the relation of the index with the iron content is mediocre. In this report the different indices are abbreviated as described in table 3.1.

Table 3.2: The explanation for the abbreviations of the indices used in this research.

<b><i>Abbreviation</i></b>	<b><i>Explanation</i></b>
RI <sub>lab</sub>	The ratio based Redness Index calculated with reflectance from the laboratory experiment.
D550 <sub>area_lab</sub>	The area of D550 calculated with reflectance from the laboratory experiment.
D550 <sub>S.D._lab</sub>	The standard deviation over the area of D550 calculated with reflectance from the laboratory experiment.
D700 <sub>area_lab</sub>	The area of D700 calculated with reflectance from the laboratory experiment.
D700 <sub>S.D._lab</sub>	The standard deviation over the area of D700 calculated with reflectance from the laboratory experiment.
D880 <sub>area_lab</sub>	The area of D880 calculated with reflectance from the laboratory experiment.
D880 <sub>S.D._lab</sub>	The standard deviation over the area of D880 calculated with reflectance from the laboratory experiment.
RI <sub>rosis</sub>	The ratio based redness index calculated with the reflectance from the ROSIS image.
D550 <sub>area_rosis</sub>	The area of D550 calculated with the reflectance from the ROSIS image.
D550 <sub>S.D._rosis</sub>	The standard deviation over the area of D550 calculated with the reflectance from the ROSIS image.
D700 <sub>area_rosis</sub>	The area of D700 calculated with the reflectance from the ROSIS image.
D700 <sub>S.D._rosis</sub>	The standard deviation over the area of D700 calculated with the reflectance from the ROSIS image.
D880 <sub>area_rosis</sub>	The area of D880 calculated with the reflectance from the ROSIS image.
D880 <sub>S.D._rosis</sub>	The standard deviation over the area of D880 calculated with the reflectance from the ROSIS image.

For the calculation of the estimated iron content for the samples measured from nadir ( $Fe_{est\_0}$ ), regression functions are derived with a linear regression for both the calibration and validation set for the indices with a R-value >0.6. The independent variable is the index and the dependent variable is the iron content measured in the laboratory (Bartholomeus et al., 2007). The formula will be in the form of equation 3.3.

$$Fe_{est\_0} = a + b * Index \quad \text{Equation 3.3}$$

A  $R^2$  of 0.7 will be good enough to proceed with the data analyses. If the  $R^2$  values are below 0.7 than a multiple regression might be needed to improve the regression results (Eq. 3.4). The independent variables are the index and the texture and the dependent variable is the iron content measured from nadir in the laboratory.

$$Fe_{est\_0} = a + b * Index + c * Texture \quad \text{Equation 3.4}$$

In order to find out what the influence of slope is on the determination of the iron content, the soil iron content for sloping samples is predicted with the functions derived for a nadir position ( $Fe_{pred\_slope(x)}$ ). The regression functions will be applied on the index values for different slopes on both the calibration and the validation set. Then, the difference between the predicted iron from nadir and the predicted iron with a slope is calculated by (Eq. 3.5).

$$((Fe_{est\_0} - Fe_{pred\_slope(x)}) / Fe_{est\_0}) * 100\% \quad \text{Equation 3.5}$$

The difference is calculated in percentages, in this way a comparison can be made between the different iron contents, otherwise the values are not normalized. This difference is the error caused by the effect of slope.

The significance of the error is determined by means of a Paired-Samples T-test because the difference between the mean estimated iron content from nadir measurements are compared with the mean predicted soil iron content under a certain slope. If the 2-tailed significance is smaller than 0.05 than the slope is significant on the determination of the iron content (Isaaks and Srivastava, 1989). A second method to present the differences is by means of box plots (Putten, 2007). The difference between slope measurements becomes visible and outliers can be labeled. By this method it becomes visible how the median and standard deviation deviate from the nadir measurement and which outliers frequently occur.

### 3.3.4 Slope correction model

Regression functions are calculated in order to correct for the error caused by the slope. The data from the calibration set is used to calculate these. The error is the difference between the estimation from nadir minus the iron content from the prediction under a certain slope. The data must be corrected in such a way that the mean error of the iron content under a certain slope will become the

same as the mean error obtained for nadir measurements (Eq. 3.6). The regression function must predict the correction needed per slope, per index (Eq. 3.7). Assumed is that the estimation functions for soil iron content for nadir is performing well, so it might be assumed as well that the corrected iron contents will be reliable. The units of the iron contents are mg/kg.

$$Fe_{\text{est}_0} - Fe_{\text{pred\_slope}} \approx 0 \quad \text{Equation 3.6}$$

$$Fe_{\text{corrected}} = a + b * Fe_{\text{uncorrected}} \quad \text{Equation 3.7}$$

The dependent variable is the error. The independent variable is the predicted iron content under a certain slope, as is described in section 3.3.3. There are 5 indices and 10 slopes, so finally there will be 50 regression functions to correct the iron content. The final function to calculate the correct iron content for each indices under different slopes can be described by equation 3.8 and the unit of  $Fe_{\text{corrected\_slope}(x)}$  is mg/kg .

$$Fe_{\text{corrected\_slope}(x)} = a + (1 + b) * (c + d*Index + e*Texture) \quad \text{Equation 3.8}$$

### 3.3.5 Performance of the slope correction model

In order to validate the correction functions, the functions are applied on the data from the validation set. A Paired-Samples T-test is performed to check whether the corrected iron content differ significantly from the iron content estimated from nadir. If the correction for slope is performing well the values should not significantly differ and the significance must be greater than 0.05.

A second method used to validate the results of the slope correction model is to calculate the standard error of calibration (SEC), standard error of prediction (SEP), bias and RPD values. The formulas are given by (Chang et al., 1998).

The SEC (Eq. 3.9) is the standard deviation of all the points from the reference values in the calibration set (Stevens et al., 2006).

SEP (Eq. 3.10) is an average prediction error estimate and can be used as an approximation of the standard deviation (S.D.) of the prediction error for all future prediction samples. The SEP overestimates the true prediction uncertainty since it includes measurement errors in the reference values (Stevens et al., 2006).

SEC and the SEP are related to the S.D. of the calibration and validation so; the lower the S.D., the lower the standard errors. Therefore, they have to be compared with their corresponding S.D.. The ratio of S.D. in the validation set to the SEP is referred to as the ratio of performance to deviation (RPD) and can be used as an index of model accuracy (Eq. 3.11) (Chang et al., 2001). Bias (Eq. 3.12) is also computed to assess the predictive ability of the model (Stevens et al., 2006).

There are two different ways for ranking the derived RPD values. According to Williams and Sobering (1993) the prediction of calibration equations is reasonable when the RPD value is  $\geq 3$ . The RPD rating was ranked as excellent ( $>10$ ), very good (7–10), good (5–7), fair (3–5), or unsatisfactory ( $<3$ ). The

higher the RPD value, the better the performance. According to Chang et al. (2001) the ability to predict values of soil properties can be grouped into three categories based on RPD values. Category A (RPD>2.0) includes properties with measured vs. predicted R<sup>2</sup> values between 0.8 and 1, the model prediction is good. Category B (1.4 < RPD > 2.0) includes soil properties with measured vs. predicted R<sup>2</sup> values between 0.5 and 0.8, the model prediction is moderate. Category C (RPD < 1.4) with measured vs. predicted R<sup>2</sup> values smaller than 1.4, the model prediction is insufficient. Chang et al. (2001) has adapted the ranking due to the high variation of different soil properties. To overcome the fact that all prediction were ranked as inaccurate according to Williams and Sobering (2003) he included the R<sup>2</sup> values in the classification because a high R<sup>2</sup> does mean that the prediction simulates reality fair enough concerning soil characteristics, by this the low RPD values can be defended. Chang et al. (2001) has classified the estimation of iron content with NIRS as a class B soil property which means that the prediction of iron content is less reliable. In accordance with these findings it is not expected in this research to find high RPD values, which means that the ranking of Chang et al. (2001) will be used.

The parameters in the formulas are described by; Y<sub>c</sub> and Y<sub>p</sub> are the values estimated from the model; Y<sub>r</sub> is the value from the laboratory; and n is the number of samples, and S.D. is the standard deviation of the data.

$$SEC = \sqrt{\frac{1}{n - m - 1} \sum_{i=1}^n (Y_r - Y_c)_i^2} \quad \text{Equation 3.9}$$

$$SEP = \sqrt{\frac{1}{n - 1} \sum_{i=1}^n \{(Y_r - Y_p) - \text{Bias}\}_i^2} \quad \text{Equation 3.10}$$

$$\text{Bias} = \frac{1}{n} \sum_{i=1}^n (Y_r - Y_p)_i \quad \text{Equation 3.11}$$

$$RPD = \frac{SD}{SEP} \quad \text{Equation 3.12}$$

To get insight in the change of the error, the results will be presented by means of a graph in which the uncorrected and corrected mean errors are plotted against slope. From this graph it can be seen where the slope correction model is performing well and where the slope correction model fails to correct properly for slope effects.

### 3.4 Soil iron content prediction with airborne imaging spectroscopy

To bring the found results into practice, the results from the laboratory experiment can be compared with airborne measurements. By this comparison it will become clear if the relations that exist in the laboratory do also hold in the field or that there are other factors more important and overshadowing the found relations for slope. In order to come to this comparison first some preprocessing of the ROSIS image and the available spatial data is needed. After this preprocessing the indices can be calculated and from those results the soil iron content can be estimated. With the iron content known it is analyzed what the differences are with the laboratory results and if the indices can be used for airborne imaging spectroscopy.

#### **3.4.1 Data preprocessing**

The spectra obtained from the ROSIS image have to be preprocessed before they can be used for the prediction of soil iron content. In order to improve the data quality, a forward and backward Minimum Noise Fraction rotation (MNF) is used to destripe the ROSIS data and smooth the spectral response. The soil reflectance is strongly influenced by vegetation cover and vegetation must be accounted for as stated by Bartholomeus et al. (2007). A spectral mixture analyses (SMA) is applied to determine the fractional vegetation cover for each pixel (Hurcom and Harrison, 1998). Pixels with vegetation covers of 25% or higher are masked out. The iron content of these pixels will be interpolated from the surrounding pixels with the nearest neighbor method because this is the only method possible in Arc Map for this type of image. The interpolation of the masked pixels is performed with the command Nibble, this is the only function that can cope with the amount of data. Ideally, the data is converted to a coverage or a feature file so better interpolation methods can be applied but the computation capacity is too low for this procedure.

There are several methods to determine the fractional vegetation cover as described by Xiao and Moody (2005). It is most important for the prediction of soil iron content that the bare soil is unmixed as good as possible and that the fraction of vegetation is determined. In this case the olive tree is the dominant vegetation present in the research area. This means that it is suited to use a two endmember SMA-model, the first endmember is the olive tree and the second endmember is bare soil. Two possible models exist for the SMA; the linear spectral unmixture model (Small, 2001) or the NDVI-regression method (Hurcom and Harrison, 1998). Hurcom and Harrison (1998) showed that NDVI provides a reliable and efficient measure of vegetation abundance. However, laboratory analyses have shown that vegetation fraction estimates based on spectral mixture modeling are less sensitive to background soil reflectance than those estimated using the NDVI-regression method (Elmore et al., 2000). From this it can be concluded that the linear spectral mixture model is the most suitable model for this research.

### 3.4.2 Prediction of soil iron content with ROSIS

The available bands from the ROSIS data are limited in comparison with the available bands used in the laboratory experiment for they only cover up to 872.9 nm, this means that the  $RI_{\text{roxis}}$ ,  $D550_{\text{area\_roxis}}$  and  $D550_{\text{S.D.}_\text{roxis}}$  can only be calculated and  $D880_{\text{area\_roxis}}$  and  $D880_{\text{S.D.}_\text{roxis}}$  are not available.

In order to calculate the iron content of the soil several maps are needed. First of all the slope and aspect must be derived from a digital elevation model and secondly a soil texture map. These maps must have the same extend, resolution and spatial reference.

The regression functions derived from the laboratory measurements can only be applied on the ROSIS image if there is no significant difference between the reflectance based indices of both the data sets. This can be tested with a paired-samples t-test. If there is no significant difference between the indices than the designed regression functions from the laboratory experiment can be applied on the ROSIS data. If there is a difference between the both data sets than new functions must be derived for the ROSIS data set to correct for this deviation.

Overall performance of the ROSIS data is analyzed in several steps because there are at least three parameters that can contribute to an error in the prediction of the soil iron content. The parameters are the ROSIS reflectance, the interpolated masked pixels and the texture. First the difference of the corrected and uncorrected ROSIS data with the laboratory data is being analyzed with the general statistics. Secondly, the influence of the masking is being tested and finally the contribution of texture is being analyzed.

As a last comparison the laboratory data, the ROSIS data with masked pixels and mismatched texture and the ROSIS data completely corrected are all being tested on the performance of the prediction of the soil iron content. The slope correction model developed from the laboratory experiment is applied on the ROSIS data and evaluated on its performance.

### 3.5 Practical set up

The experimental setup is presented in figure 3.2. Measurements are done in the solar principal plane. One tripod holds the irradiance source and is set to  $20^\circ$  off nadir at 30 cm from the surface. A second tripod will be used to hold the spectrometer. An  $8^\circ$  fore optic is used at approximately 20 cm distance from the soil sample. An uncalibrated white spectralon panel is used as reference radiance panel resulting in the relative reflectance values. The soil sample is placed on a plate that can tilt around its centre. By tilting the sample, the slope is changed.

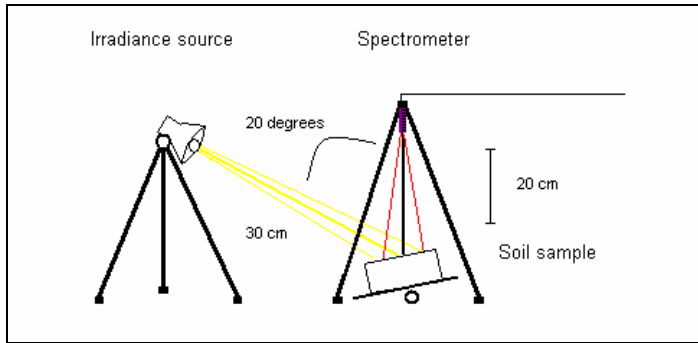


Figure 3.2: Experimental set-up for laboratory reflectance measurements.

In the experiment the sample will be rotated in steps of 5 degrees between  $+25^{\circ}$  and  $-25^{\circ}$ , which represents the slope of the surface. The positive angles are facing towards the irradiance source and the negative angles face off the irradiance source. The measured slopes of the soil samples were within this range in the field. When the slope is larger than  $25^{\circ}$  the soil will roll off the plateau, which is in contradiction with repose angles found for sand, the angle of repose for sand lies within  $31^{\circ}$  to  $34^{\circ}$  (Watson, 1987). This movement of the soil is caused by the smooth surface of the plateau. The sand particles can not grip and the resistance gets very low.

Measurements will be taken at a distance of approximately 20 cm from the surface and a fore optic of  $8^{\circ}$  is used. For measurements taken from nadir this results in a circular Ground projected Field of View of 4.2 cm diameter. Due to the change in slope the resulting circular Ground projected Field of View is variable. This means that the amount of incoming and reflected radiation will deviate under different slopes. It might even influence the spectral reflectance based iron indices. The circular Ground projected field of View (fig. 3.3) can be calculated with the law of sinus (Technische Universiteit Eindhoven, 2007).

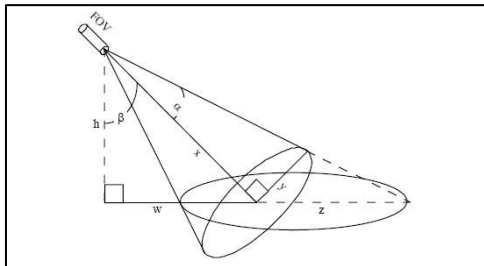


Figure 3.3: Ground projected Field of View (ENVI - The Remote Sensing Exploitation Platform).

### 3.6 Software

Microsoft Word will be used for reporting and Microsoft Excel and SPSS will be used for the analyses on the relation between slope and soil iron content. Endnote will be used to store the used references. After finishing the experiment and the report a presentation will be created in Microsoft Power Point for the colloquium to be held.

IDL-ENVI 4.3 and SAMS will be used for the spectral image analyses. IDL-ENVI 4.3 is a software package for the visualization, analysis, and presentation of all types of digital imagery (iitvs, 2007). The continuum-removal can be performed in IDL-ENVI 4.3. Spectral Analysis and Management System (SAMS) will be used to manage the spectral database from the laboratory experiment (Rueda and Wrona 2003). Arc Map will be used to model the soil iron content from the pre-processed ROSIS image, the Digital Elevation model and the texture map.

## 4. Results and discussion

### 4.1 Reflectance under different slopes

The reflectance of bare soil is different under different slopes (fig. 4.1). Up to 600 nm the differences are small. At higher wavelengths the deviation in reflectance from nadir increases. Around 1000 nm differences in reflectance for a negative slope deviates up to -6% and for positive slopes up to 2%. The maximum differences can be found around 1800 nm, with a difference up to -8% for the negative slopes and up to 3% for the positive slopes.

The absorption features from iron are clearly visible. The first absorption dip appears around 390 nm up to 600 nm and is caused by electronic transitions of both types of iron present in the soil (Ben-Dor et al., 1999). A second dip can be observed around 700 nm, but this is less strong attended than the dip around 550 nm. The third dip is found from 800 nm up to 1000 nm. The absorption that occurs near 700 nm and 880 nm is due to electronic transition of ferric iron (Irons et al., 1989). The absorption feature around 1400 nm is caused by oxygen-hydrogen stretching of OH-bearing minerals and is referred to as the first overtone band (Ben-Dor et al., 1999; Irons et al., 1989). Around 1900 nm and 2400 nm there is strong absorption by water molecules.

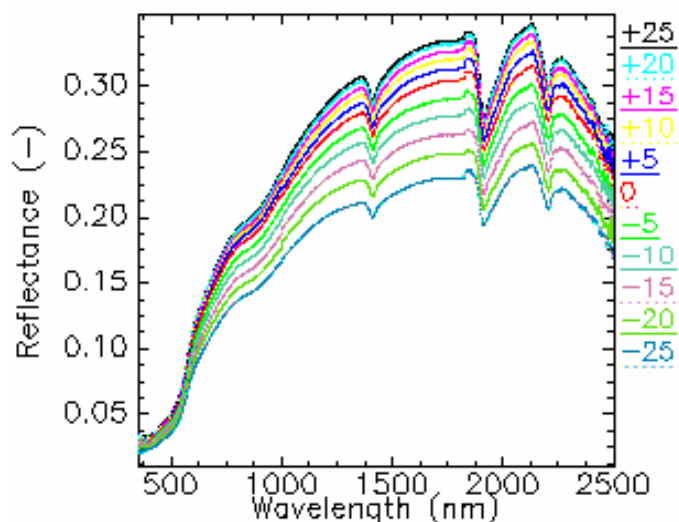


Figure 4.1: Spectral signature of bare soil under different slopes.

It can be concluded that the deviation from nadir is larger for the negative slopes than for the positive slopes. From these results nothing can be said yet about the influence of the slope on the estimation of soil iron content because; with the calculation of indices the reflectance is out weighted against each other. The ratio based Redness Index calculates the ratio of the reflectance in the red part with the whole visible part so the reflectance itself is not of importance. For the continuum removal the same holds, only the properties of the area of the absorption feature are taken into account regardless of the amount of reflectance. Though, figure 4.1 shows a nice trend for the reflectance.

## 4.2 Correlation of reflectance with soil iron

High negative correlations (R) are found in the spectrum from 400 nm up to 600 nm, with a maximum of 0.71 around 550 nm. Low correlations are found for the part of the spectrum ranging between 680 nm up to 790 nm, with the minimum of -0.53 around 750 nm. The correlation (R) is mediocre in the part of the spectrum ranging from 800nm up to 1000 nm, with a maximum of -0.63 around 900 nm (fig. 4.2).

When the correlation is lower than 0.5 then there is not a good relation, it is the same as a random fit of data. The highest negative correlations are found around 550 nm, for further analyses this absorption feature will perform best. The correlation for around 750 nm is too low to relate reflectance with soil properties because it approaches -0.5. This does not directly imply that the index will not work for this feature. Around 900 nm the correlation is mediocre, when working with results from this area this must be taken into account. The slope does not influence the correlation significantly between the reflectance and the iron content, as can be seen from figure 4.2. All the negative slopes have a lower correlation than the correlation for  $0^{\circ}$ . Slopes larger than  $15^{\circ}$  show the same trend. Slopes smaller than  $10^{\circ}$ , both positive and negative have similar correlation as  $0^{\circ}$ .

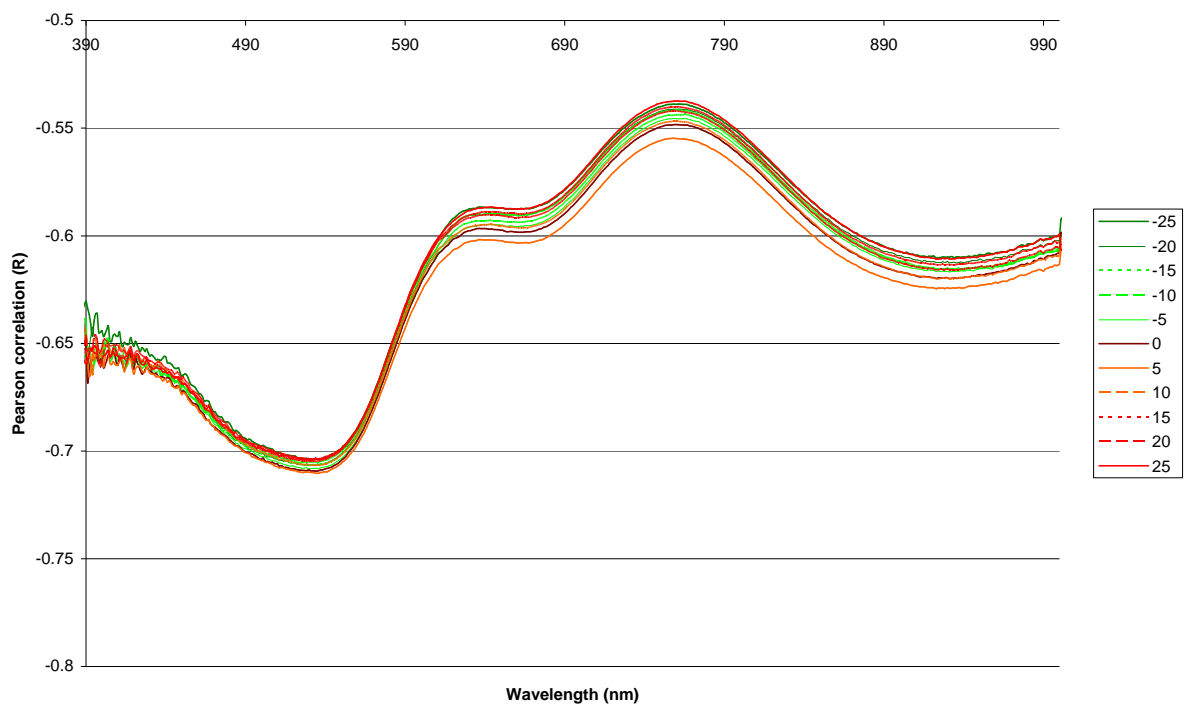


Figure 4.2: The Pearson's correlation coefficient (R) of the soil iron content and reflectance.

### 4.3 Correlation (R) of iron indices and soil iron

The correlation is calculated between the iron indices and the iron content of the soil samples measured in the laboratory. The properties of the absorption areas described in the previous paragraph are used for the calculation of the indices. The absorption feature ranging from 390 nm up to 600 nm is referred to as D550, the absorption feature ranging from 650 up to 750 nm is referred to as D700 and the absorption feature ranging from 800 nm up to 1000nm is referred to as D880.

The overall correlation (R) is given in table 4.1. For the ratio based Redness Index the correlation is on average 0.80. For D550<sub>area\_lab</sub> a negative correlation is found and a positive correlation is found for D550<sub>S.D.\_lab</sub>. The found correlation (R) for D550<sub>area\_lab</sub> is on average -0.82 for the area, this means with a decreasing area of the dip the iron content decreases as well. This is as expected, the higher the iron content, the larger the absorption feature. D550<sub>S.D.\_lab</sub> has a correlation of 0.82.

For D700<sub>lab</sub>, the correlations are much lower; the correlation between iron and D700<sub>area\_lab</sub> is on average 0.51 and for the standard deviation -0.53.

The correlation for D880<sub>area\_lab</sub> has an average of -0.84 and for D880<sub>S.D.\_lab</sub> an average correlation of 0.84. The correlation between iron content and the indices is not depending on slope because the standard deviation is very low.

RI<sub>lab</sub> has a good correlation which means that this index can be used for next research. For D550<sub>lab</sub> the correlation is high as well, so the data can be used for the next part of the research. D700<sub>lab</sub> has correlations almost as low as a random relation so this part of the spectrum will not be used for the next assessments. The correlation of D880<sub>lab</sub> with iron is high so the data can be used for the next part of the research.

From now on the D700 will be left out of all the coming analyses because they will not give reliable results.

Table 4.1: Pearson correlations (R) of soil iron and spectral reflectance based iron indices under different slopes.

<b>Slope ( ° )</b>	<b>RI<sub>lab</sub></b>	<b>D550<sub>lab</sub></b>		<b>D700<sub>lab</sub></b>		<b>D880<sub>lab</sub></b>	
	<b>400-700</b>	<b>Area</b>	<b>S.D.</b>	<b>Area</b>	<b>S.D.</b>	<b>Area</b>	<b>S.D.</b>
-25	0.796	-0.826	0.820	0.354	-0.408	-0.837	0.843
-20	0.801	-0.823	0.825	0.447	-0.48	-0.833	0.841
-15	0.796	-0.807	0.815	0.468	-0.509	-0.826	0.834
-10	0.796	-0.815	0.809	0.492	-0.524	-0.83	0.837
-5	0.795	-0.822	0.815	0.53	-0.527	-0.833	0.838
0	0.798	-0.816	0.816	0.536	-0.564	-0.832	0.838
5	0.797	-0.814	0.822	0.568	-0.531	-0.834	0.839
10	0.8	-0.818	0.816	0.572	-0.637	-0.837	0.839
15	0.8	-0.82	0.815	0.548	-0.572	-0.837	0.839
20	0.798	-0.819	0.818	0.555	-0.554	-0.842	0.842
25	0.798	-0.812	0.817	0.565	-0.568	-0.843	0.84
<b>Mean</b>	0.798	-0.817	0.817	0.512	-0.534	-0.835	0.839
<b>S.D.</b>	0.002	0.005	0.004	0.067	0.058	0.005	0.002

#### 4.4 Regression functions for the estimation of the soil iron content

Estimation of soil iron content can be done by use of regression functions. These regression functions are set with linear regression. As independent parameter the iron index is used and the dependent parameter is soil iron content. The regression functions to estimate the soil iron content are made for measurements from nadir. Table 4.2 shows the found regression functions and the corresponding  $R^2$  for the different indices.

Table 4.2: Regression functions and  $R^2$  for the estimation of soil iron content (mg/kg) with linear regression for the different indices and data sets.

<b>Data set</b>	<b>Index type</b>	<b>Regression function</b>	<b><math>R^2</math></b>
Calibration set	RI_lab	Fe =-55.218+129.771*RI	0.66
	D550_area_lab	Fe =66.965-0.314*D550_area_lab	0.68
	D880_area_lab	Fe =593.677-2.92 * 880_area_lab	0.62
	D550_S.D_lab	Fe =-1.095+159.94*D550_S.D_lab	0.69
	D880_S.D_lab	Fe =3.25+1156.112*D880_S.D_lab	0.62
Validation set	RI_lab	Fe =-60.194+134.637*RI_lab	0.68
	D550_area_lab	Fe =64.202-0.311*D550_area_lab	0.71
	D880_area_lab	Fe =567.519-2.802*D880_area_lab	0.76
	D550_S.D_lab	Fe =-2.953+155.507*D550_S.D_lab	0.70
	D880_S.D_lab	Fe =2.736+1111.865*D880_S.D_lab	0.77

Found correlation coefficients could be improved in order to make the prediction of soil iron content better. This can be obtained by adding texture as an extra variable and use a multiple linear regression. The Pearson correlation (R) of texture and iron content is -0.67 which means that there is a relation between texture and soil iron content. The independent parameters are the iron index and the texture, the dependent parameter is the soil iron content in the samples. The results are given in table 4.3.

The found correlation coefficients for the regression functions are higher when texture is added to the regression function (table 4.3). In order to improve these functions, more variables can be added to the multiple linear regression. It could be that organic matter is a suitable parameter and that the fit will increase significantly because organic matter content influences the spectral reflectance (Ben-Dor et al., 1999). When there are more variables included, a principle component analyses could be used instead of multiple linear regression for the principle component analyses is more sensitive for the variability of variables (Jolliffe, 2002).

The texture classification is performed by hand and the interpretation of a person is less reliable than a mechanical texture determination, the manual texture classification might reduce the  $R^2$  as well.

Overall, the multiple regression functions are good when texture is added as extra variable, and these functions (table 4.3) will be used for the next part of the research.

Table 4.3: Regression functions and  $R^2$  for the estimation of soil iron content with multiple linear regression for the different indices and data sets.

<b>Data set</b>	<b>Index type</b>	<b>Regression function</b>	<b><math>R^2</math></b>
Calibration set	RI_lab	$Fe = -39.086 + 104.313 \cdot RI_{lab} - 0.004 \cdot texture$	0.82
	D550_area_lab	$Fe = 59.050 - 0.253 \cdot D550_{area\_lab} - 0.004 \cdot texture$	0.82
	D880_area_lab	$Fe = 468.878 - 2.286 \cdot D880_{area\_lab} - 0.004 \cdot texture$	0.76
	D550_S.D._lab	$Fe = 4.247 + 128.688 \cdot D550_{S.D._lab} - 0.004 \cdot texture$	0.82
	D880_S.D._lab	$Fe = 8.123 + 907.207 \cdot D880_{S.D._lab} - 0.004 \cdot texture$	0.77
Validation set	RI_lab	$Fe = -52.684 + 122.373 \cdot RI_{lab} - 0.002 \cdot texture$	0.75
	D550_area_lab	$Fe = 60.44 - 0.284 \cdot D550_{area\_lab} - 0.002 \cdot texture$	0.77
	D880_area_lab	$Fe = 522.853 - 2.572 \cdot D880_{area\_lab} - 0.002 \cdot texture$	0.82
	D550_S.D._lab	$Fe = -0.774 + 141.564 \cdot D550_{S.D._lab} - 0.002 \cdot texture$	0.76
	D880_S.D._lab	$Fe = 4.336 + 1021.546 \cdot D880_{S.D._lab} - 0.002 \cdot texture$	0.82

## 4.5 Effect of slope on the iron prediction

The regression functions for measurements from nadir are used to predict the soil iron content under variable slope for the five different indices. By use of Paired-Samples T-Tests and Boxplots the error, induced by the effect of slope, in the estimation of soil iron content is examined and visualized.

### 4.5.1 Paired-samples T-Test to test the significant difference

The pairs that are compared are the prediction values of iron content under a certain slope with the estimation values of iron content measured at nadir. Values are tested on the 95% confidence interval for the error in iron content in mg/kg. If the 2-tailed significance is lower than 0.05 than the deviation of iron content is significant. The results are listed in table 4.4.

Table 4.4: 2-tailed significance of the compared pairs, the significant differences are given in red.

Slope ( ° )	RI <sub>_lab</sub>	D550 <sub>_lab</sub>		D880 <sub>_lab</sub>	
		Area	S.D.	Area	S.D.
-25	0.061	0.027	3.22E-11	1.81E-07	6.51E-19
-20	0.236	0.003	2.27E-08	4.74E-09	1.08E-21
-15	0.956	0.016	5.24E-09	2.56E-07	6.02E-21
-10	0.053	0.120	2.06E-07	7.40E-08	6.38E-21
-5	0.011	0.177	3.79E-07	1.07E-09	3.82E-24
5	0.467	0.022	0.139	0.433	1.26E-05
10	0.525	0.421	0	0.043	2.57E-10
15	0.644	0.030	2.22E-06	0.007	6.23E-11
20	0.872	0	2.84E-06	0	3.34E-14
25	0.791	0.001	5.72E-06	8.07E-05	1.25E-19

The differences between the estimated iron content at nadir and the predicted iron content under a certain slope do not significantly differ for RI<sub>\_lab</sub> except for a slope of -5°.

The differences for D550<sub>\_area\_lab</sub> are partly significant. For slopes larger than +15° and -15° the deviation is significant. For smaller slopes the model is robust, except for the slope of +5°. The significance for D550<sub>\_S.D.\_lab</sub> are all smaller than 0.05 except for +5°, which means that slope has significant influence on the iron prediction. For both the area and the S.D. of D880<sub>\_lab</sub> all values are smaller than 0.05 except for the D880<sub>\_area</sub> with +5°.

From this test it can be concluded that the RI<sub>\_lab</sub> is robust and performing well under varying slopes. The continuum-removed indices appear to be very sensitive to variations in slope, so research is needed to explain and to correct for the error induced by slope.

The differences are higher for the negative facing slopes; this might be due to the retroreflectance properties of the material (Ben-Dor et al., 1999) and the non-lambertian behavior of the surface. The retroreflectance is attributed to the effects of mutual shadowing among particles. A sensor does not view shadows if and only if the sensor views a particulate surface from the anti-illumination direction. The proportion of shadowed area in view increases as the sensor moves away from the anti-illumination direction (Irons et al., 1989). Surface roughness does influence the direction of reflection as well. The samples have a rough surface because they consist of loose sand particles. The rays of

light are reflected in many directions. This effect increases when the sample is tilted under a certain angle because the outgoing rays are reflected at many different angles and the spectral reflectance is disrupted (Ben-Dor et al., 1999).

The effect of surface roughness is stronger for the samples under a slope. There seems not to be a specific reason for the better performance of the indices at a slope of  $+5^{\circ}$  for it would be expected that the significance would be lower with increasing slope.

#### 4.5.2 Visualization of the error

The results are presented in boxplots in which the values are the error and described by: percentage of difference between the estimation at nadir ( $Fe_{est_0}$ ) minus the prediction under a certain slope ( $Fe_{pred\_slope(x)}$ ). The unit of the calculated error is in %, see equation 4.1.

$$\frac{(Fe_{est_0} - Fe_{pred\_slope})}{Fe_{est_0}} * 100\% \quad \text{Equation 4.1}$$

In figure 4.3 the errors (%) for the ratio based Redness Index are presented. The medians deviate with maximums of 1% from the nadir estimation. With increasing slope the variance increases and the minimum and maximum values deviate further from the median. There is a slight skewness towards the negative values. This means that the predicted iron content is overestimated. Even in the worse cases, slopes larger than  $+15^{\circ}$  and  $-15^{\circ}$ , the values are still within a deviation of 5%. This is in line with the Paired-Samples T-Test which also proved that the Redness Index is robust for varying slopes. There are outliers, but these are often the same samples for the different slopes, which means that other factors than the slope cause the outliers.

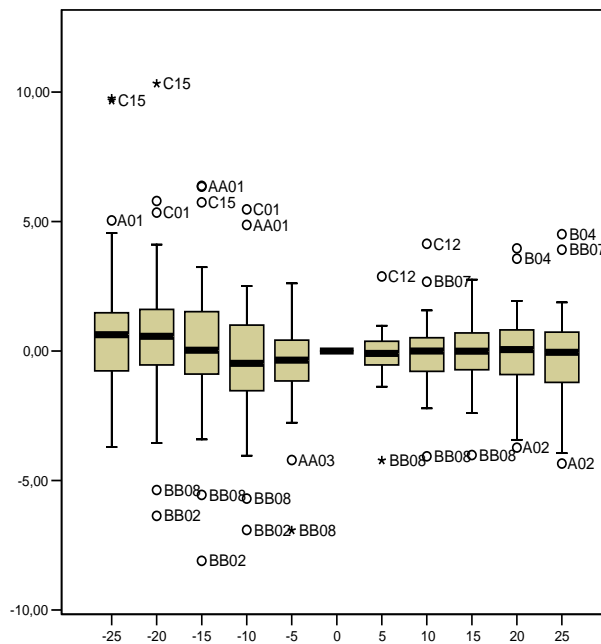


Figure: 4.3: Boxplot with the error calculated as the difference of the predicted (slope (x)) and estimated (slope 0) soil iron content, for the different slopes and calculated by means of the ratio based Redness Index.

For D550<sub>area\_lab</sub> the medians do not deviate much for the different slopes (fig 4.4a). Minimum and maximum values are higher with increasing slope. Differences are again higher for the negative slopes and increases with slope. The values for the slopes up to  $-10^0$  fall all within the limit of 5%. For the slopes of  $-15^0$  and higher, the predictions are underestimated up to a maximum of 7%, so for these slopes the prediction is not accurate, but the mean of the prediction of soil iron is quite robust. This is in accordance with the Paired-Samples T-Test.

Plotted results of D550<sub>S.D.\_lab</sub> show a so called “V-shape” (fig. 4.4b). The median increases with increasing slope and are within 2% deviation from the median from nadir estimations. Minimum and maximum errors are again increasing with increasing slope and the effect is stronger for the negative slopes. For the positive slopes the model predicts the iron content quite well, within 2.5 % error. The predictions for the negative slopes are not accurate, for slopes larger than  $-10^0$  the error in the prediction of soil iron is more than 5%. This is in accordance with the Paired-Samples T-Test.

There are more outliers for D550<sub>S.D.\_lab</sub> than for D550<sub>area\_lab</sub>, they are more present at the negative slopes and have a positive deviation which means that the iron content is underestimated.

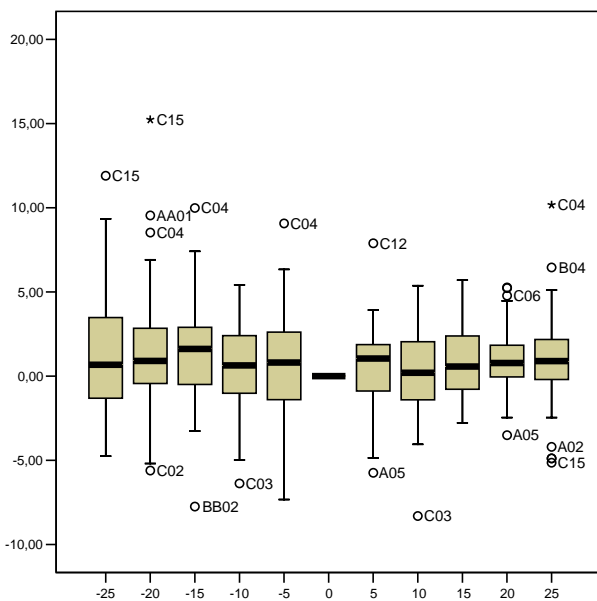


Figure 4.4a: Boxplot with error (%) for D550<sub>area\_lab</sub>.

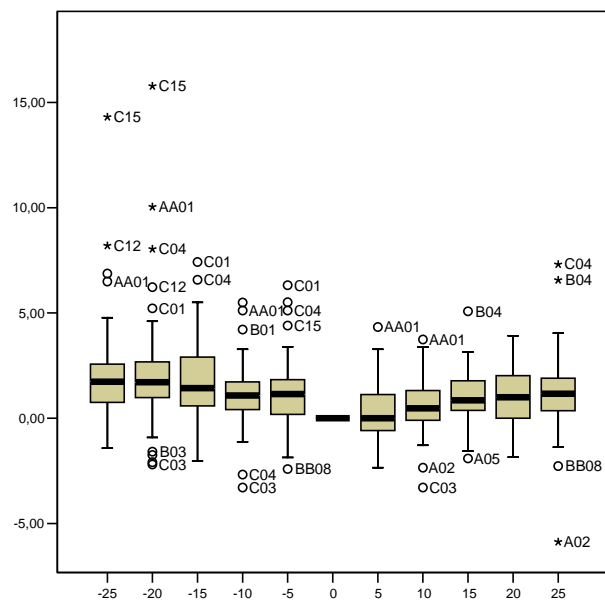


Figure 4.4b: Boxplot with error (%) for D550<sub>S.D.\_lab</sub>.

In figure 4.5a and b, which shows the boxplots of the error for the area and standard deviations of D880<sub>lab</sub>, there is a clear deviation of the medians and standard deviations with the estimation at  $0^0$ . A V-shape is present, with increasing slope, both the median and the deviations increases. The median, the minimum and maximum values deviate stronger for negative slopes than for the positive slopes. Errors fall outside the 5% limit. It can be concluded from these figures that the continuum-removal for D880<sub>lab</sub> does not predict the iron content well under a certain slope. This is in accordance with the performed Paired-Samples T-Test. The number of outliers is medium.

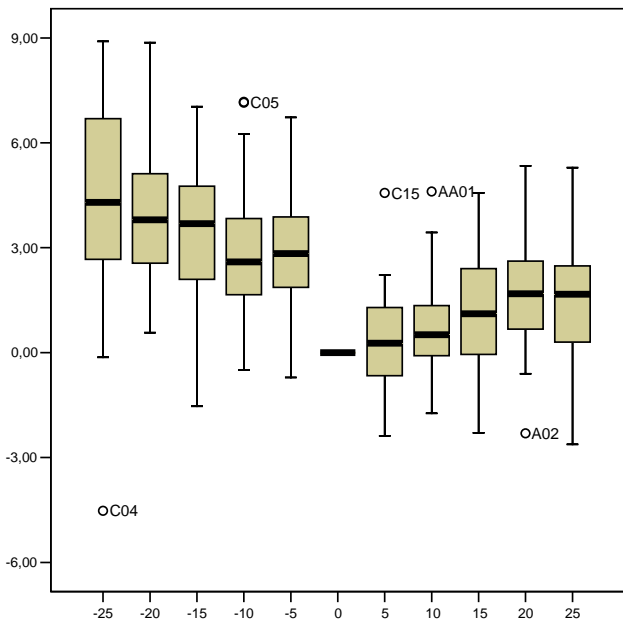


Figure 4.5 a: Boxplot with error(%) for D880\_area\_lab.

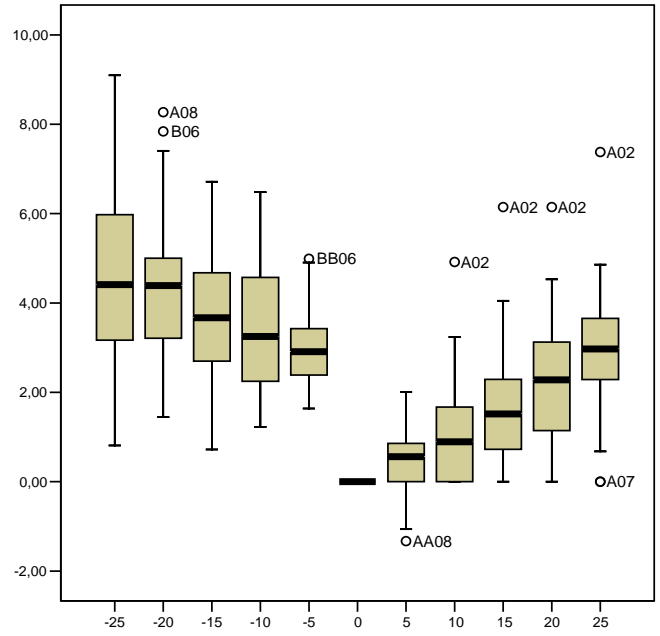


Figure 4.5 b: Boxplot with error (%) for D880\_s.D\_lab.

## 4.6 Slope correction model

The functions used for the correction of the iron content are given in appendix B. After the correction there is no longer a significant difference between the mean iron contents (table 4.5) except for D550<sub>S.D.\_lab</sub> under a slope of -20 and -10 degrees. From this it can be concluded that the slope correction model performs good enough. Both the area and the standard deviation of D550<sub>lab</sub> show the lowest significance values. This means that for these functions the performance is less on average.

Table 4.5: 2-tailed significance of the compared pairs from the validation set for the different indices and slopes.

<b>Slope (°)</b>	<b>RI<sub>lab</sub></b>	<b>D550<sub>lab</sub></b>		<b>D880<sub>lab</sub></b>	
		<i>area</i>	<i>S.D.</i>	<i>area</i>	<i>S.D.</i>
-25	0.056	0.19	0.392	0.93	0.983
-20	0.799	0.244	0.007	0.094	0.736
-15	0.658	0.075	0.646	0.959	0.665
-10	0.321	0.694	0.002	0.081	0.297
-5	0.585	0.756	0.923	0.752	0.526
5	0.946	0.468	0.631	0.758	0.917
10	0.106	0.262	0.776	0.133	0.657
15	0.334	0.162	0.626	0.432	0.083
20	0.853	0.706	0.951	0.688	0.378
25	0.859	0.641	0.902	0.583	0.216

The correction would be better if after the correction the standard deviation would become smaller because samples with higher deviations would be corrected for and the spread will become smaller. Unfortunately this is not the case (Appendix C) but this was expected because the regression functions only correct for the bias of the estimation.

Though, there are minor changes in the standard deviation after the application of the error correction slope model (Appendix C). The decrease in standard deviation is in most cases 0. The largest changes in standard deviations can be found for D880<sub>area\_lab</sub> with a maximum decrease of 0.07 for a slope of -25°. These minor changes are induced by the multiplication factors for the index and the texture in the regression function.

The standard deviation can only become smaller if the uncorrected data can be aggregated (Heuvelink 2007). Texture is the only parameter available to aggregate the samples, but this variable is already included in the regression function and is therefore not suited for the aggregation. Also, there is not a clear relation of the error of the iron content prediction with texture (fig. 4.6). It seems that for the corrected fine textured samples the iron content is overestimated and for the coarse textured samples there is an underestimation in iron content, although this relation cannot be found with statistical methods. The standard deviation decreased only with 0.0001 when regression functions for groups defined by texture were applied on the calibration set. A possible parameter to aggregate the samples with is the organic matter content. According to Ben-Dor et al. (1999), organic matter is

influencing reflectance. More research and data is needed to decrease the standard deviation and improve the slope model.

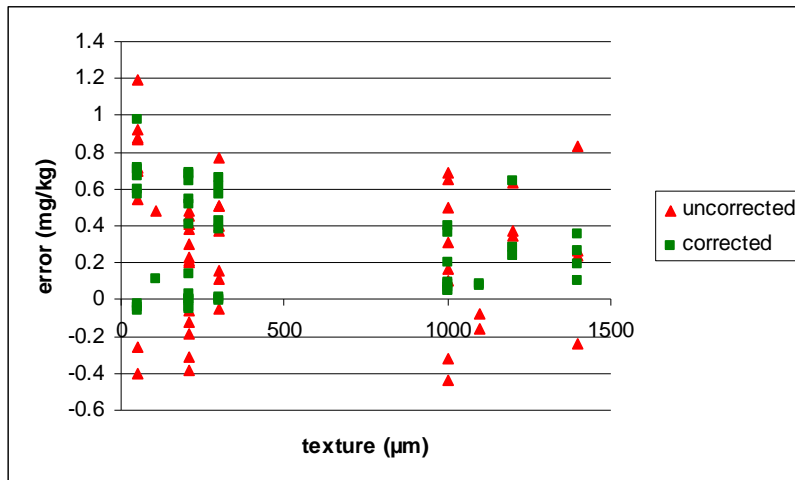


Figure 4.6: Soil texture (µm) plotted against the error of the iron prediction for D880<sub>area\_lab</sub>.

#### 4.6.1 Error correction for D550<sub>area\_lab</sub> and D550<sub>s.D.\_lab</sub>

Regression functions are derived which correct for the error caused by the influence of slope. Table 4.6 shows the result of the calibration of the slope model and the accurateness of the predicted soil iron content for D550<sub>area\_lab</sub>. For D550<sub>area\_lab</sub> the SEC values vary between 0.13 and 0.31 mg/kg, this means that the standard deviation of the iron content is at most 0.31 mg/kg. This standard deviation is acceptable because the samples have an iron content between 7 and 20 mg/kg, the standard deviation is at most 5% of the total amount of iron. The SEP values range between 1.95 and 2.12 mg/kg, this is higher than the SEC values which might be caused by the differences between the calibration and validation set (table 3.1). The bias values lie between -2.69 and -2.79 mg/kg, the values are negative so iron contents are being underestimated. There is a bias present at nadir measurements due to the error in the regression functions for the fit of these functions was not 1. The R<sup>2</sup> values varies between 0.70 and 0.75 and expect for the slope of -25 all RPD values are smaller than two. This means that the correction model for the estimation of the iron content with D550<sub>area\_lab</sub> can be classified as a class B model according to Chang et al. (2001).

Table 4.6: The calibration and prediction results based on the error correction functions for D550<sub>area\_lab</sub>.

<i>D550<sub>area_lab</sub></i>					
<b>Slope (°)</b>	<b>SEC (mg/kg)</b>	<b>Bias (mg/kg)</b>	<b>SEP (mg/kg)</b>	<b>RPD</b>	<b>R2</b>
-25	0.28	-2.69	1.95	2.03	0.75
-20	0.13	-2.69	2.02	1.98	0.73
-15	0.30	-2.68	2.10	1.90	0.71
-10	0.27	-2.75	2.06	1.91	0.72
-5	0.29	-2.75	2.08	1.92	0.72
0	0.29	-2.77	2.11	1.90	0.71
5	0.26	-2.80	2.02	1.95	0.73
10	0.27	-2.70	2.12	1.86	0.70
15	0.31	-2.69	2.01	1.96	0.73
20	0.26	-2.78	2.06	1.93	0.72
25	0.26	-2.79	2.07	1.91	0.72

Table 4.7 shows the result of the calibration of the slope model and the accurateness of the predicted soil iron content for D550\_<sub>S.D.\_lab</sub>. For D550\_<sub>S.D.\_lab</sub> the SEC values range between 0.13 and 0.44 mg/kg and the SEP values varies between 2.09 and 2.13 mg/kg. The bias values ranges between -2.69 and -2.80 mg/kg. Again the bias is negative so iron contents are being underestimated. The R<sup>2</sup> values are either 0.70 or 0.71 and the RPD values are all smaller than 2. This model can be classified as a class B model according to Chang et al. (2001).

Table 4.7: The calibration and prediction results based on the error correction functions for D550\_<sub>S.D.\_lab</sub>.

<b>Slope (°)</b>	<i>D550_<sub>S.D._lab</sub></i>				
	<b>SEC (mg/kg)</b>	<b>Bias (mg/kg)</b>	<b>SEP (mg/kg)</b>	<b>RPD</b>	<b>R<sup>2</sup></b>
-25	0.38	-2.81	2.09	1.92	0.71
-20	0.37	-2.68	2.10	1.91	0.71
-15	0.42	-2.80	2.12	1.89	0.71
-10	0.36	-2.89	2.13	1.88	0.70
-5	0.37	-2.78	2.10	1.92	0.71
0	0.40	-2.78	2.13	1.89	0.71
5	0.42	-2.76	2.13	1.87	0.70
10	0.38	-2.79	2.11	1.89	0.71
15	0.44	-2.80	2.13	1.88	0.70
20	0.40	-2.78	2.10	1.89	0.71
25	0.41	-2.77	2.10	1.90	0.71

The correction model for both the calibration and the validation set works quite well (fig. 4.7 and 4.8). Again for the calibration set the mean error lies around 0. The model for D550\_<sub>area\_lab</sub> deviates for the slope of -20 degrees, all other values are corrected well. The performance of the model is less for the validation set (fig. 4.8). The mean error for the validation set is not zero but is between 0% and 1% for all slopes. The correction of D550\_<sub>area\_lab</sub> works for all slopes except for +5 degrees, for this slope the corrected error is on average larger than the uncorrected error. The model for the standard deviation does not perform better for a slope of -10 degrees, the error is increased with -200% (fig. 4.7b). Although the models do not correct the errors well for all slopes, on average the error is significantly smaller and the data are more reliable when the correction models are applied on the data sets (table 4.5).

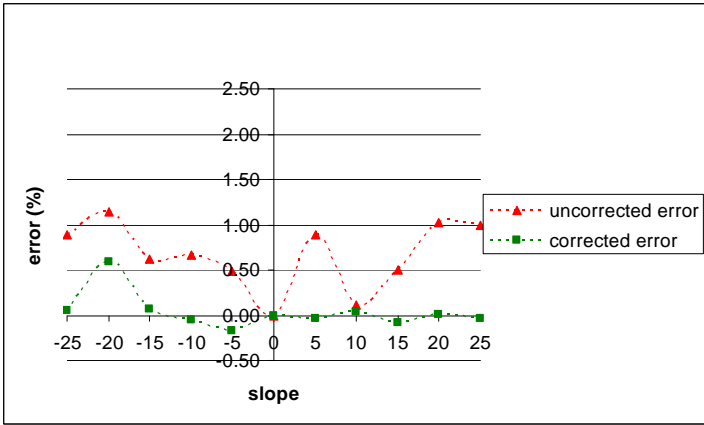


Figure 4.7a: Mean error (%) of the predicted iron content for corrected and uncorrected data of the calibration set for D550\_area\_lab.

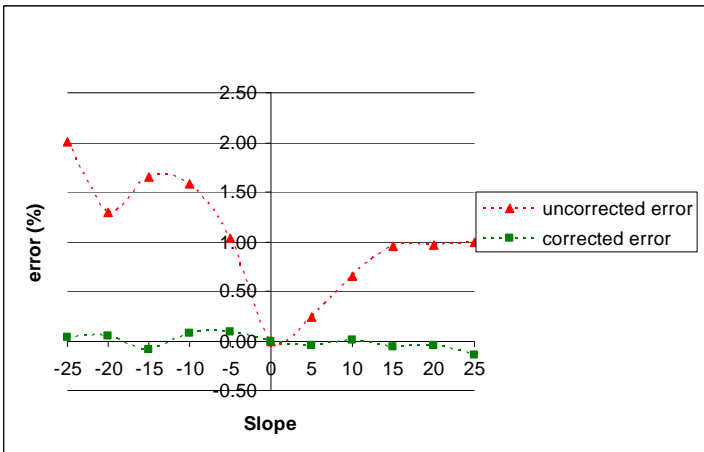


Figure 4.7b: Mean error (%) of the predicted iron content for corrected and uncorrected data of the calibration set for D550\_S.D.\_lab.

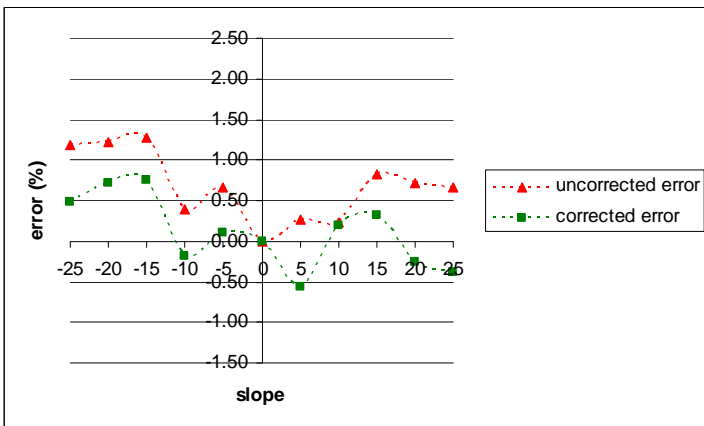


Figure 4.8a: Mean error (%) of the predicted iron content for corrected and uncorrected data of the validation set for D550\_area\_lab.

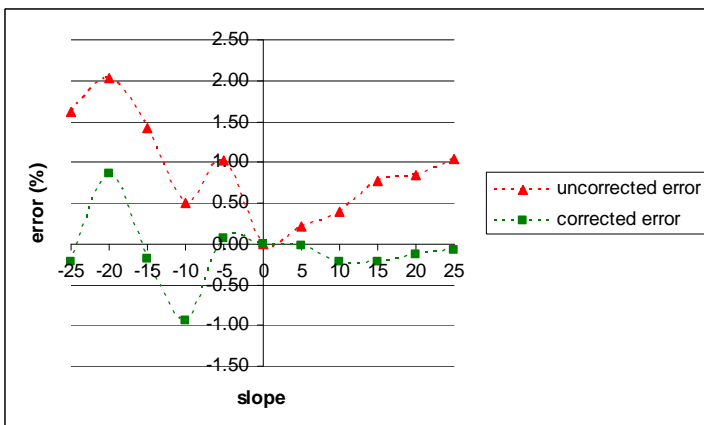


Figure 4.8b: Mean error (%) of the predicted iron content for corrected and uncorrected data of the validation set for D550\_S.D.\_lab.

#### 4.6.2 Error correction for D880<sub>area\_lab</sub> and D880<sub>S.D.\_lab</sub>

Table 4.8 shows the results of the calibration of the slope model and the accurateness of the predicted soil iron content for D880<sub>area\_lab</sub>. For D880<sub>area\_lab</sub> the SEC values vary between 0.45 and 0.50 mg/kg. The SEP values ranges between 1.27 and 1.89 mg/kg and are again much higher than the SEC values. The bias values lie between -1.81 and -1.94 mg/kg. The bias is negative so iron contents are being underestimated. The bias is relative small compared to the other indices. The R<sup>2</sup> values varies between 0.76 and 0.78 mg/kg and all RPD values are larger than 2. According to Chang et al. (2001) models with a RPD >2 can be classified as a class A model, this means that the model performance for D880<sub>area\_lab</sub> is good.

Table 4.8: The calibration and prediction results based on the error correction functions for D880<sub>area\_lab</sub>.

Slope (°)	D880 <sub>area_lab</sub>				
	SEC (mg/kg)	Bias (mg/kg)	SEP (mg/kg)	RPD	R <sup>2</sup>
-25	0.47	-1.87	1.89	2.08	0.76
-20	0.48	-1.93	1.35	2.92	0.76
-15	0.51	-1.87	1.35	2.92	0.76
-10	0.50	-1.94	1.33	2.96	0.76
-5	0.50	-1.88	1.31	2.99	0.77
0	0.49	-1.86	1.32	2.99	0.76
5	0.49	-1.86	1.30	3.04	0.77
10	0.47	-1.81	1.28	3.08	0.78
15	0.45	-1.84	1.31	3.01	0.77
20	0.49	-1.85	1.35	2.94	0.76
25	0.49	-1.88	1.27	3.09	0.78

For D880<sub>S.D.\_lab</sub> the SEC values range between 1.09 and 1.15 mg/kg and the SEP values varies between 1.87 and 1.94 mg/kg (table 4.9). The bias values ranges between -1.78 and -1.86 mg/kg. Again the bias is negative so iron contents are being underestimated. The bias is relative small compared to the area and S.D. of D550<sub>lab</sub>. The R<sup>2</sup> values are either 0.76 or 0.77 and the RPD values are all larger than 2. This model can be classified as a class A model according to Chang et al. (2001).

Table 4.9: The calibration and prediction results based on the error correction functions for the S.D. of D880

Slope (°)	D880 <sub>S.D._lab</sub>				
	SEC (mg/kg)	Bias (mg/kg)	SEP (mg/kg)	RPD	R <sup>2</sup>
-25	1.13	-1.83	1.89	2.10	0.77
-20	1.10	-1.85	1.94	2.05	0.76
-15	1.11	-1.82	1.92	2.07	0.76
-10	1.09	-1.86	1.90	2.08	0.76
-5	1.11	-1.81	1.90	2.08	0.76
0	1.12	-1.83	1.89	2.10	0.76
5	1.15	-1.83	1.87	2.12	0.77
10	1.15	-1.82	1.87	2.12	0.77
15	1.15	-1.78	1.91	2.09	0.76
20	1.11	-1.81	1.91	2.09	0.76
25	1.13	-1.87	1.87	2.12	0.77

The errors caused by slope are for both the standard deviation and the area of D880<sub>\_lab</sub> the largest in comparison to the other indices. It is only for these two methods that the average error is too large to produce reliable results for the estimation of soil iron content. Therefore, it is important that the model does correct the errors. For the calibration set both the mean error of D880<sub>\_area\_lab</sub> and D880<sub>\_S.D.\_lab</sub> are on average zero (fig. 4.9). The V-shape is no longer present and there is not a slope present that deviates from others slopes. The performance of the model when applied on the validation set is good (fig. 4.10). Again there are no slopes that deviate and the model has corrected for the so called “V-shape”.

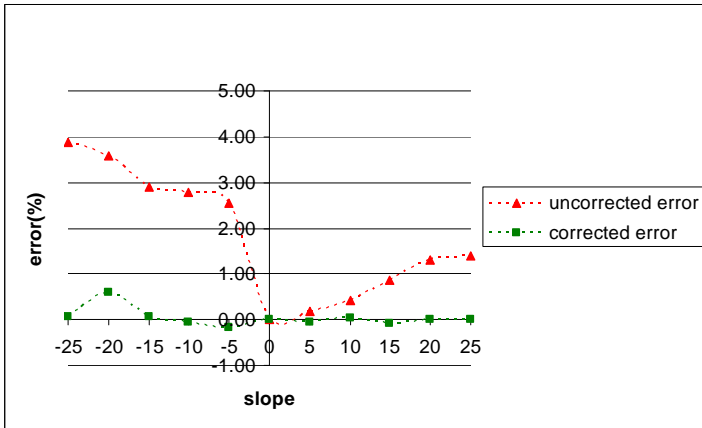


Figure 4.9a: Mean error (%) of the predicted iron content for corrected and uncorrected data of the calibration set for D880\_area\_lab.

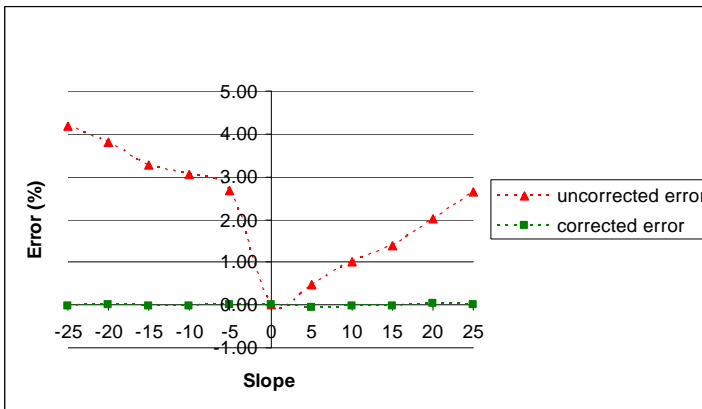


Figure 4.9b: Mean error (%) of the predicted iron content for corrected and uncorrected data of the calibration set for D880\_S.D.\_lab.

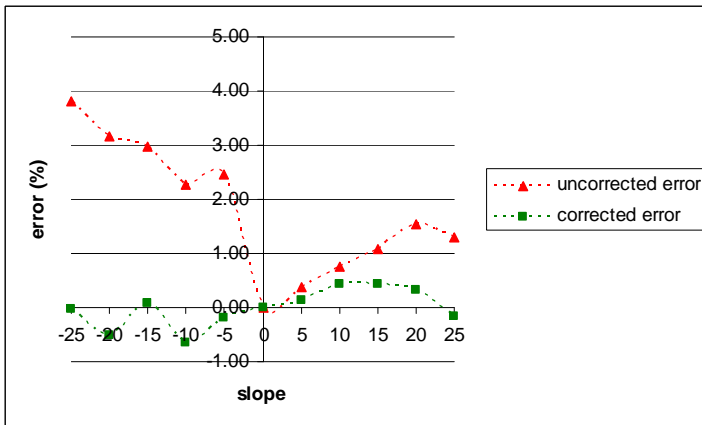


Figure 4.10a: Mean error (%) of the predicted iron content for corrected and uncorrected data of the validation set for D880\_area\_lab.

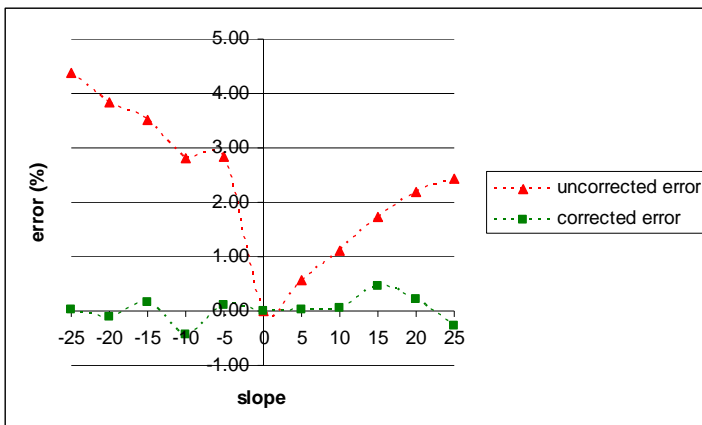


Figure 4.10b: Mean error (%) of the predicted iron content for corrected and uncorrected data of the validation set for D880\_S.D.\_lab.

### 4.6.3 Discussion

Overall, the slope correction model has proven to work well. The validation set has almost the same spread around the mean as the calibration set and the SEC values are low for all indices with a maximum of 1.3 mg/kg. SEP values of the area and S.D. of D550<sub>lab</sub> are on average 2.09 mg/kg and the SEP values are better for the area and S.D. of D880<sub>lab</sub> with an average of 1.63 mg/kg. The bias decreases for the different indices when  $R^2$  and the SEP values increase. Biases are smallest for both the area and S.D. of D880<sub>lab</sub> and the  $R^2$  are the largest for both the indices. The slope model has a lower performance when it is applied on the validation set, this might be caused by the fact that the mean iron content of the samples in the validation set is lower as well as the standard deviation. Bartholomeus et al. (2007) performed comparable analyses on the same data set in earlier research (table 4.10). All SEC and SEP values found in their research are larger than the values found in this research, from table 4.10 it can be concluded that there is a significant improvement made with the slope model and the addition of texture in the multiple linear regression.

Table 4.10: Calibration and prediction results from Bartholomeus et al. (2007).

	<b>Training set</b>		<b>Reference set</b>	
	<i>SEC</i>	<i>SEP</i>	<i>SEC</i>	<i>SEP</i>
Redness Index	3.29	5.01	4.2	3.19
Area of D550	4.18	3.92	2.78	3.21
S.D. of D550	3.81	3.98	2.66	2.59

From literature it is found that the prediction of iron as soil property is usually a class B model when working with imaging spectroscopy (Chang et al., 2001). The fact that for both the area and the S.D. of D880<sub>lab</sub> the correction model is of class A makes it a good result.

The two models for D880<sub>lab</sub> perform best in comparison with the area and standard deviation of D550<sub>lab</sub>. This is mainly caused by the higher  $R^2$  values of the regression functions. A second reason why D880<sub>lab</sub> performs better is that this absorption dip is caused by the mineralogical composition. The major bearing iron mineral is hematite which will give an absorption dip around 900 nm, soils that are rich in the secondary mineral hematite do often have a higher silt fraction coming from the secondary clay minerals, which might mean that the texture is finer for soils with high iron contents. Texture is used as a parameter for the regression, if it is true that only the mineralogical composition influences the dip at D880<sub>lab</sub> and texture is related to the mineral than this means that for the dip of D880<sub>lab</sub> the estimation is more accurate. The other absorption features can be influenced by other properties from which data is lacking. If there are more parameters available for the multiple regression than the other absorption features may perform better.

The correction model consists of two parts. The prediction of the iron content (B) and the correction for the slope (A), see equation 4.3. The prediction of the soil iron content performs well and the found  $R^2$  values are all above 0.75. The  $R^2$  values for part A are all below 0.5, this means that the correction is not robust. First of all, it only corrects for the bias and the standard deviations do not change significantly. The reason for working with the regression function of part A instead of only correcting

with the average is that with this formula outliers are more corrected for than values around the mean. This explains the small changes in the standard deviations. When this model would be applied on data from another region, it would probably not correct the values as good as in this research because the spread around the mean is different.

$$Fe_{\text{corrected\_slope}(x)} = \left| \frac{a + (1 + b)}{\mathbf{A}} \right| * \left| \frac{(c + d * \text{Index} + e * \text{Texture})}{\mathbf{B}} \right| \quad \text{Equation 4.3}$$

One aspect which is not taken into account in this research is the changing Ground Projected Field of view. This area is deviating per slope this means that the reflectance measured is not coming exactly from the same surface area. A correction for the surface area could be made in order to compare the reflectance per slope. The area and reflectance must be normalized to the Ground Projected Field of view that is used for the nadir measurements.

When the correction model is applied on airborne data the availability of data on texture might be a problem because detailed data is needed for the correction model. When this data is not available, the texture class must be divided in at least two groups. These texture classes can be obtained from a soil map, this leads to a decrease in the R<sup>2</sup> values of 0.1, but the model still corrects the errors well. The model is based on laboratory measurements in which the measured reflectance is the BRF, because the irradiance is coming from one single direction of illumination. Since, the airborne data is measured under different conditions, where there is not one single direction of illumination but from the entire hemisphere including the atmosphere and surrounding terrain, the HDRF holds (Schaepman-Strub et al., 2006). This means that under field conditions reflectance will deviate from the laboratory measured reflectance.

There are also other properties of the terrain influencing the reflectance which are not accounted for in the laboratory, e.g. aspect of the surface. These properties are taken into account in the next part of the research.

Finally, it can be concluded that the slope correction model is not as robust as desired but it is proven that the slope does influence the prediction of the iron content with reflectance based iron indices and that the prediction of iron contents can be improved if a slope correction model is used.

## 4.7 Preprocessing of the ROSIS-image and spatial data

In this section, the data needed for the estimation of soil iron content is adapted to the right format. First, the ROSIS image is corrected and the influence of vegetation is minimized. Secondly, the maps for slope, aspect and texture are developed.

### 4.7.1 Destriping and unmixing of the ROSIS image

The ROSIS image contains a strong noise. Therefore, the raw reflectance data cannot be used directly for the calculation of the indices (fig. 4.11a). A forward and backward minimum noise fraction (MNF) rotation (Green et al., 1988) was used to destripe the ROSIS image and smooth the spectral response (fig. 4.11b) (Bartholomeus et al., 2007). Band 1, 3 -5 and 7-10 from the MNF result are used for further research because these bands have the highest signal.

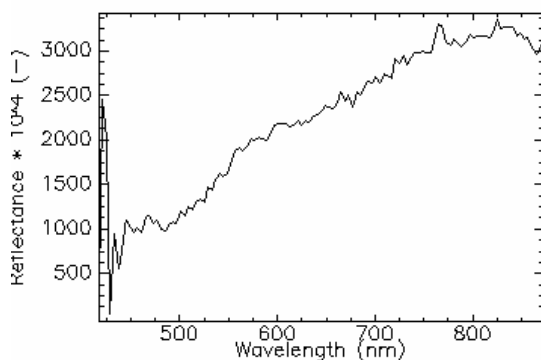


Figure 4.11a: Spectral signature of bare soil before MNF.

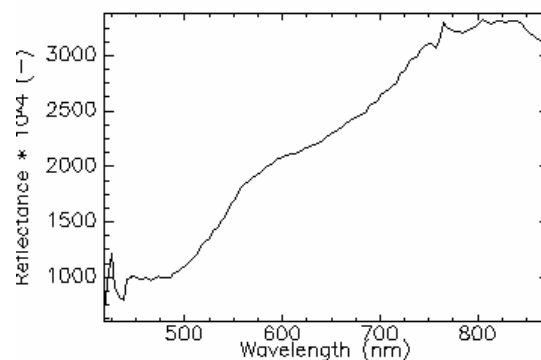
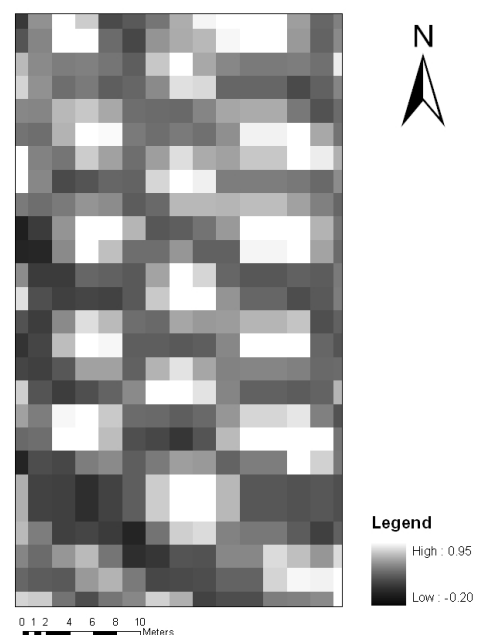


Figure 4.11b: Spectral signature of bare soil after MNF.

The spectral mixture analysis (SMA) with the endmembers bare soil and olive tree is performed on the forward MNF rotation image. The SMA is used to determine the fractional vegetation cover for each pixel (Appendix D). In this map the low values represent bare soil and the high values represent olive tree. Ideally, bare soil would have a value of 0 in this picture and vegetation a value of 1. If the vegetation cover does not lie within this range, it can be concluded that the SMA did not work well. The reason for this is probably the endmember selection for there was not an endmember of bare soil which was pure bare soil and the spectral signature for olive tree is influenced by the variable water content and chlorophyll content of olive trees (Clevers et al., 2006).

In figure 4.12 a map is presented which has



Titia Mulder, 14-09-2007, Wageningen University

Figure 4.12: Zoomed map of the unmixed vegetation.

zoomed in to a part of an olive tree orchard. The bright pixels have a high vegetation cover and represent olive trees. As can be seen from this map an olive tree does not cover 1 pixel but several. The pixel with the center of the olive tree has the highest value, the nearest neighbors are a bit lower and the grey pixels are low and represent bare soil. The nearest neighbors are mixed pixels of bare soil and vegetation because part of the olive tree crown fall into parts of these pixels, due to this mixing there are few perfect pixels present with only vegetation or bare soil. This has to be considered because in this vegetation research only bare soil is of interest.

#### **4.7.2 Masking**

From the unmixed image of the vegetation a mask can be created to exclude the pixels with a high vegetation cover. Several masks have been applied on the data set. A mask of 35% excludes all pixels with a vegetation cover of 35% which is 1.4 m<sup>2</sup> of one pixel with a resolution of 2m x 2m. This mask did not exclude enough pixels because some olive trees were still present in the masked picture. A mask of 20% did excluded 15 samples of the 36 which should be bare soil. Masking with a mask of 25% had the best performance; only 6 of the 36 field samples were masked (Appendix E).

In order to make a map with the reflectance of bare soil over the whole area the masked out pixels are interpolated with the nearest neighbor method, from these maps the indices are calculated.

Influence of vegetation is strong for there are no pure spectral signatures found for bare soil, all the samples show an increase near 700 nm due to the absorptance by chlorophyll (Clevers et al., 2006).

The lowest vegetation cover found for the locations of the pixels is 3% and 9 of the 36 samples have a vegetation cover in between 20% and 25%; this means that 25% of the samples are strongly influenced by vegetation for more than 1 m<sup>2</sup> is cover by vegetation within one pixel.

Vegetation does influence the estimation of soil iron content, as is discussed by Bartholomeus et al. (2007) and this effect should be taken into account in the next part of the research.

#### **4.7.3 Spatial data**

The slope derived from the Digital Elevation Model has an original pixel size of 25m x 25m, which has been resampled to 2m x 2m because the ROSIS data has this resolution. In order to compare the slopes of the research area with the slopes measured in the laboratory the slopes have been reclassified into 11 classes of 5 degrees ranging from -27.5<sup>0</sup> up to +27.5<sup>0</sup>.

The aspect derived from the Digital Elevation Model has 10 classes and a resolution of 25m x25m.

The resolution has been resampled to 2m x 2m. To compare the aspect with the aspect in the laboratory only 2 classes are needed; one class facing towards the sun and one class facing off the sun. The sun was standing in the South at the time of the flight campaign and the aircraft flew from South to North, this means that the aspect 90<sup>0</sup> up to 270<sup>0</sup> has a positive aspect and the aspect ranging from 270<sup>0</sup> up to 359<sup>0</sup> and 0<sup>0</sup> up to 90<sup>0</sup> have a negative aspect. In the laboratory the aspect and slope were combined and resulted in positive and negative slopes, so in order to compare the spatial data with the laboratory data the slope is multiplied with the aspect to obtain positive and negative slopes (Appendix F).

For the development of the texture map the 62 points of which the texture is known have been interpolated with the Nearest Neighbor method into a texture map (Appendix G).

## 4.8 Spatial determination of the soil iron content

In this section an analyses is performed on the quality of the ROSIS image and its performance in the quantification of soil iron content for there is a clear difference between the reflectance from the ROSIS image and the laboratory measured reflectance (fig. 4.13 a & b). The difference is large in the red part of the spectrum; the ROSIS image could be influenced by vegetation as is indicated by the sharp increase at 700 nm, while the determined vegetation cover is only 3%. This increase in reflectance is caused by the absorptance by the chlorophyll from plants (Clevers et al., 2006). Moreover, the spectral signature from ROSIS is not as smooth as the spectral signature from the laboratory, even after the MNF rotation.

First, the indices have been calculated from the ROSIS image and these indices are compared with the indices derived from the laboratory experiment. Secondly, the differences found between both data sets are minimized with a correction function. Than, the ROSIS image is analyzed on the performance in the estimation of soil iron content, by means of a comparison with the performance of laboratory spectroscopy. The performance is assessed with the Redness Index for this index is not influenced by slope. Finally, the influence of slope is compared with the other parameters that influence the estimation of soil iron content.

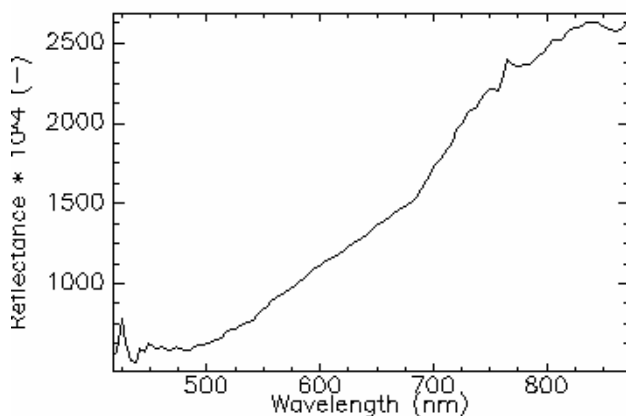


Figure 4.13a: Reflectance after MNF of soil sample A03 in the field, measured with airborne imaging spectroscopy.

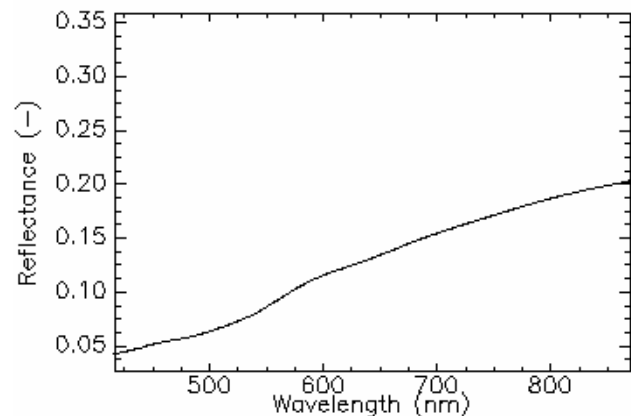


Figure 4.13b: Reflectance of soil sample A03 measured under laboratory conditions.

### 4.8.1 Differences between the ROSIS data and the laboratory data

From figure 4.14a it can be seen that the Redness Index calculated with the ROSIS ( $RI_{\text{rosis}}$ ) data is being overestimated. The samples A04, AA05, C13 and C14 are outliers. Figure 4.14b shows that  $D550_{\text{area\_rosis}}$  is being underestimated, and the samples AA05, C13 and C14 are outliers. The part of spectrum that is taken into account might contribute to this underestimation by ROSIS is smaller than the part of the spectrum taken into account in the laboratory. In the laboratory the area is calculated from 399 nm up to 600 nm and the ROSIS data starts at a wavelength of 416.9 nm and up to 600 nm. In figure 4.14c it can be seen that  $D550_{\text{s.D.}_\text{rosis}}$  is being overestimated and again the samples AA05, C13 and C14 are outliers.

The reason that these samples deviate strongly for all indices is not clear, they do not have a exceptional high vegetation cover or a specific texture so there must be other factors causing this deviation. The ROSIS data is deviating from the laboratory measurements which is caused by some characteristics of the data which complicate the estimation of the iron content. In the discussion an elaboration on these complications can be found.

From these graphs it can be concluded that there is a correlation for the different indices between both the data sets. This is supported by the Pearson correlation (table 4.11) for the indices of both datasets, after exclusion of the outliers. The correlation is highest for the Redness Index which might be caused by the robustness of the index. D550<sub>S.D.rosis</sub> has the lowest correlation which might be caused by the high sensitivity towards accurate spectral positioning.

Table 4.11: Pearson's correlation (R) for the indices.

	<b><i>Pearson's correlation</i></b>
RI	0.73
D550 <sub>area</sub>	0.63
D550 <sub>S.D.</sub>	0.60

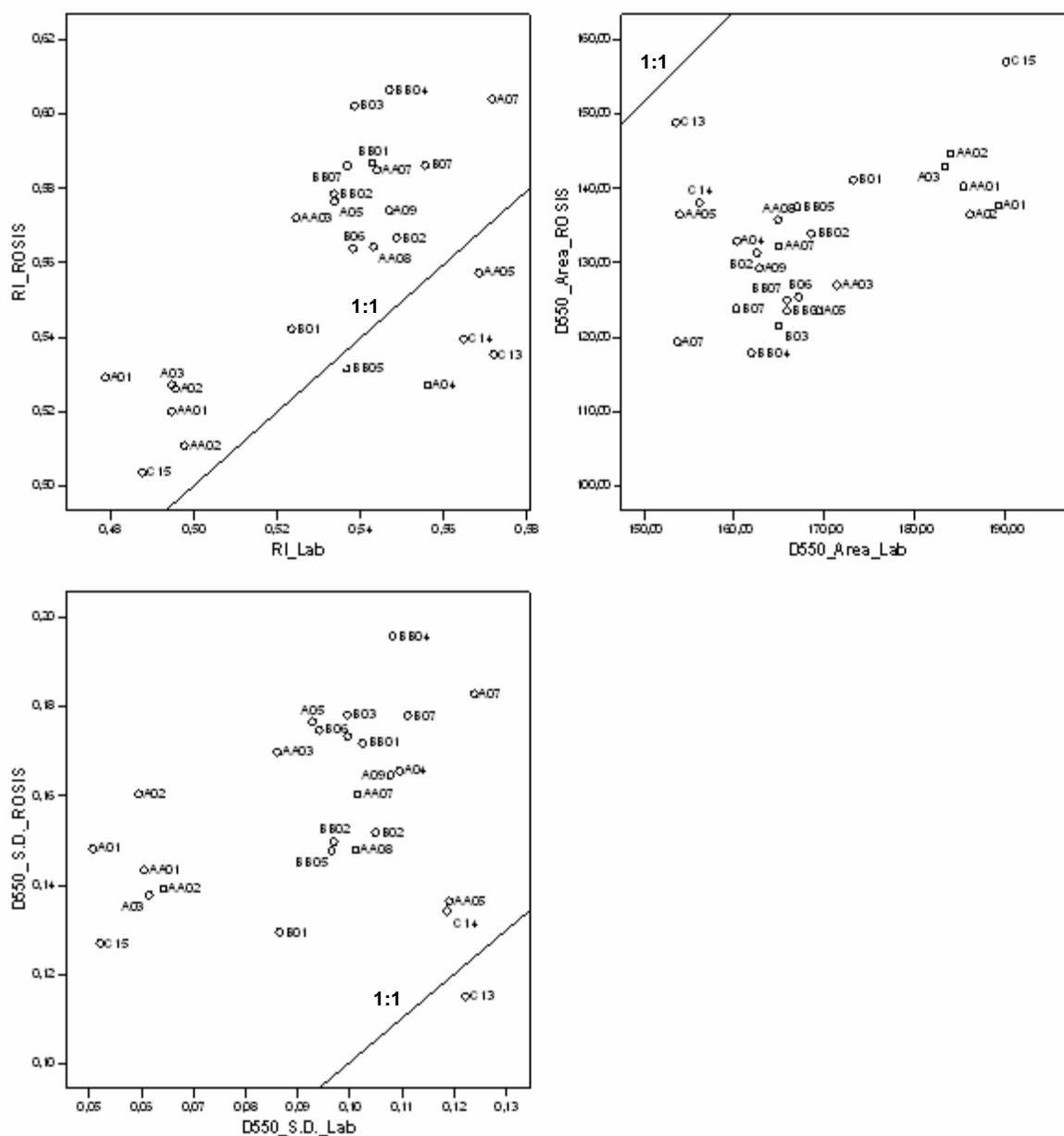


Figure 4.14a,b,c: Scatterplots of the indices calculated with the laboratory data versus the indices calculated with the ROSIS data.

#### 4.8.2 Correction of the indices calculated with the ROSIS data

In order to minimize the difference (fig. 4.13) between the ROSIS data and the laboratory data a regression function is calculated to correct for the deviation (table 4.12) of the different indices, the  $R^2$  is given as well to address the accurateness of the functions.

Differences in reflectance are caused by different parameters which will be corrected for with a formula. The disadvantage of this function is the fact that it will not give insight into the behavior of the parameters, it only corrects for it like a black box. In this research it is not possible to correct for all these parameters separately because the information and data is missing for this type of research. This formula is far from perfect but at least the data is corresponding better with the found indices in the laboratory.

The regression functions to correct the derived indices have a relative low  $R^2$ . The  $R^2$  of  $RI_{\text{rosis}}$  is high enough to proceed with analyses and the  $R^2$  for both the area and the S.D. of D550 is too low to proceed with. From this it should be concluded that only for  $RI_{\text{rosis}}$  the spatial variability can be mapped with reasonable accuracy. From the laboratory measurements it was concluded that the slope does not have a significant influence on the  $RI_{\text{lab}}$  and that the correction model was not needed for this indices. In order to work with the slope model, the iron content calculated with  $D550_{\text{S.D. rosis}}$  is mapped to show the spatial distribution of the iron content and the expected error caused by the slope because for this index the influence of the slope is most significant.

A paired-samples T-Test is applied on the uncorrected and corrected indices derived from ROSIS paired with the laboratory data for the different indices. The uncorrected samples all have a significance below 0.05 which means that the difference is too large between the two data sets to relate them. The corrected samples give a significance which are all small enough;  $RI_{\text{rosis}}$  : 0.861,  $D550_{\text{area rosis}}$  : 0.970 and  $D550_{\text{S.D. rosis}}$  : 0.965 this means that on average the regression functions corrects well. The function only corrects for the bias, this means that the standard deviation is unchanged.

Table 4.12: Regression functions to correct the indices and correlation coefficients of the functions.

	<b>Regression function</b>	<b><math>R^2</math></b>
$RI_{\text{rosis}}$	$RI_{\text{rosis}} = 0.211 + 0.557 * RI_{\text{ROSIS}}$	0.532
$D550_{\text{area rosis}}$	$D550_{\text{area rosis}} = 69.603 + 0.767 * D550_{\text{area ROSIS}}$	0.398
$D550_{\text{S.D. rosis}}$	$D550_{\text{S.D. rosis}} = -0.017 + 0.676 * D550_{\text{S.D. ROSIS}}$	0.358

### 4.8.3 Performance of the ROSIS data set

In order to analyze the overall performance of the ROSIS data, a comparison is made of  $RI_{lab}$  with  $RI_{rosis}$ . It was shown that the slope has no significant influence on the estimation of soil iron content so the data is compared in the settings from nadir. In appendix H a map can be found with the spatial distribution of the calculated iron content. For the calculation of the soil iron content different parameters have been used which can contribute to the error in the estimation. The following parameters will be analyzed in this paragraph; the index calculated with the reflectance from ROSIS, the vegetation influence, the interpolation of the masked out pixels and the spatial distribution of texture.

#### 4.8.3.1 Comparison of the $RI_{lab}$ with $RI_{rosis}$ .

In figure 4.15 a scatter plot is presented with the ROSIS data. If  $RI_{rosis}$  would be exact the same as  $RI_{lab}$  than the points would fall on the 1:1- line, which is not the case. The uncorrected  $RI_{rosis}$  are systematically underestimated because they lie under the 1:1 –line. This is caused by several parameters influencing the reflectance in the field, which will be discussed later. The  $RI_{rosis}$  lie around the 1:1 –line after the application of the correction function as given in paragraph 4.8.2 but the standard deviation does not decrease significantly (table 4.13), which is expected for the correction function only corrects for the bias. The minimum and maximum values are corrected for and the extremes are smoothed out (table 4.13). From these results it can be concluded that the correction is needed and that the reflectance data originating from ROSIS contribute strongly to errors in the estimation of the iron content. The possible causes for the strong deviation in reflectance are discussed in the following paragraphs.

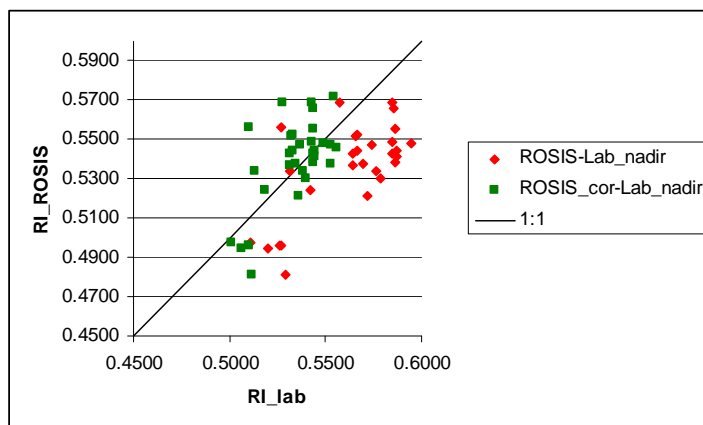


Figure 4.15: Scatter plot of the  $RI_{rosis}$  and  $RI_{lab}$  for uncorrected and corrected ROSIS data.

Table 4.13: Statistics for the comparison of the ROSIS image.

	<b>A*</b>	<b>B**</b>
Mean	0.03	0.004
S.D.	0.015	0.011
Minimum	0.003	0
Maximum	0.064	0.046
Median	0.031	0.011

\* (Fe (mg/kg)  $RI_{rosis\_uncorrected}$ ) – (Fe (mg/kg)  $RI_{lab\_nadir}$ )

\*\* (Fe (mg/kg)  $RI_{rosis\_corrected}$ ) – (Fe (mg/kg)  $RI_{lab\_nadir}$ )

#### 4.8.3.2 Interpolation of masked pixels

In paragraph 4.7.1 the results of the spectral unmixing of olive trees and bare soils is presented and in paragraph 4.7.2 the creation of the mask is explained, the results can be found in appendices D and E. The masked out areas have been interpolated in order to construct a map with solely bare soil.

The interpolation can cause an error in the determination of the soil iron content because the nearest neighbor method is used for interpolation and this method is discussed by Schläpfer and Richter (2002). For the imaging spectrometry data, nearest neighbor approaches are preferred in order to avoid spatial interpolation because this would lead to not-measured, 'unphysical' spectra but spectral integrity is thus preserved and is given higher priority than spatial quality and smoothness. However, new investigations by the authors have shown that spatial interpolation should be preferred for the resampling of direct neighbor pixels if more priority is put on geometric accuracy and not on spectral integrity. The nearest neighbors are derived by Delaunay triangulation (IDL 1999) or by optional fast buffering algorithms based on the output centre pixels (Schläpfer and Richter, 2002).

According to (Stoorvogel, 2007) is the nearest neighbor method not suitable for spatial interpolations in areas with high spatial variability. Some of the masked out areas are large ( $>20\text{m}^2$ ) and it might be that in the centre of the area the nearest neighbor will not give a correct value because there might be a different soil type or vegetation cover which will influence the iron content.

Though, in this research most of the areas to be interpolated are small (4 pixels) and the nearest neighbor is good enough. In order to test this hypothesis the general statistics are calculated for the data set with the calculated masked pixels included and compared with a data set in which the masked pixels are excluded (table 4.14). The masked cells have been interpolated and are all being more overestimated in comparison with the original values. The mean has decreased a bit because less samples are taken into account and the fact that the left out pixels were overestimated, the other statistics stay the same. The  $R^2$  is decreased from 0.72 to 0.68, which means that the interpolated pixels contribute to the error in the calculation of the iron content.

Table 4.14: General statistics for the ROSIS image with and without masked pixels.

	<b>A*</b>	<b>B**</b>
N	32	22
Mean	0.56	0.57
S.D.	0.03	0.03
Minimum	0.51	0.51
Maximum	0.61	0.61
Median	0.57	0.57
Correlation	0.72	0.68

\* Data set without masked pixel

\*\* Data set with the masked pixels included

#### 4.8.3.3 Influence of the spatial distribution of the texture

Some of the samples taken in the field are located on the borders of pixels. In case of the texture map, on borders of two pixels the points get the nearest neighbor as texture. This means that for some pixels the texture is deviating from the texture determined in the laboratory. This might influence the results as well. Only 16 of the 32 samples have been classified correctly. This might be due to the interpolation method that calculates the masked out pixels and the spatial distribution of the texture. In order to test this hypothesis the general statistics are calculated for the iron content calculated with the redness index from ROSIS data and the texture from the laboratory and compared with the iron calculated with both the Redness Index and the texture from the spatial data (Table 4.15). The differences between both data sets are not large, although half of the samples have been classified wrong for A. The correlation did not really decrease. From this it might be concluded that the misinterpretation of the texture does not contribute strongly to the error in the estimation of the iron content.

Table 4.15: General statistics for the iron content calculated with variable texture.

	<b>A*</b>	<b>B**</b>
N	32	22
Mean	15.11	14.95
S.D.	2.02	2.16
Minimum	11.34	11.34
Maximum	18.11	18.41
Median	15.28	14.67
Correlation	0.41	0.4

\* Texture from spatial data

\*\* Texture from laboratory data

#### 4.8.3.4 Prediction of soil iron content

In figure 4.16 a scatter plot is presented with the iron contents of three data sets against the original iron contents measured in the field samples. None of the data sets fall on the 1:1 line which means that none of the data sets corresponds with the original measured iron content. From this figure it seems that the iron content calculated under laboratory conditions does not perform better than the contents calculated based on the ROSIS data. All data sets have a large spread around the 1:1 –line. The general statistics provide better information (table 4.16).

The laboratory calculated iron contents have the highest correlation, this correlation is lower in this test than in the experiment because less samples have been taken into account. There are 32 samples instead of 48 samples because the other samples did not fall in the research area of the spatial data. It becomes clear from data set B that both the interpolated pixels and the texture do contribute to a significant error in the estimation of the iron content, the  $R^2$  is very low (0.25). The  $R^2$  does increase up to 0.4 if the interpolated pixels are excluded and the correct texture is taken into account but this is still significant lower than 0.62. This difference is caused by the quality of the ROSIS reflectance data or other factors that are not taken into account.

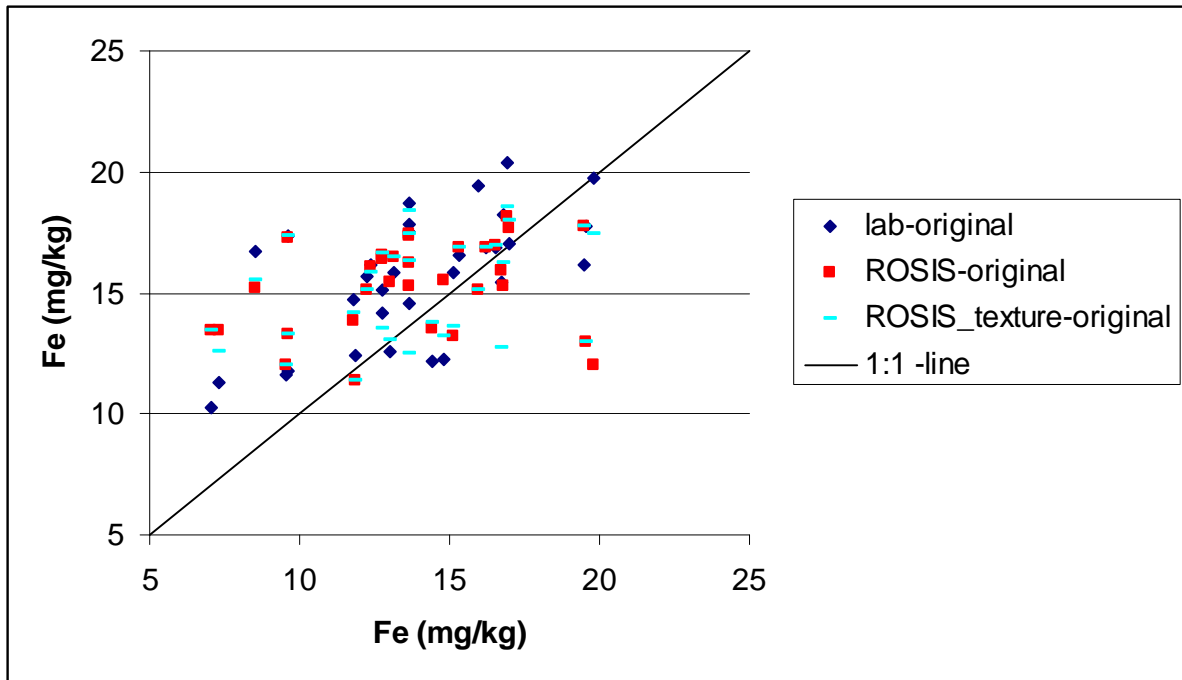


Figure 4.16: Scatter plot of Fe (mg/kg) calculated with ROSIS compared with the original Fe content.

Table 4.16: General statistics on iron content (mg/kg) for different data sets.

	<b>A*</b>	<b>B**</b>	<b>C***</b>	<b>D****</b>
Mean	13.78	15.59	15.3	14.95
S.D.	3.34	2.65	1.88	2.16
Minimum	7.08	10.26	11.34	11.34
Maximum	19.83	20.34	18.11	18.41
Median	13.66	16.01	15.46	14.67
Correlation (R)	-	0.62	0.26	0.4

\* Original iron content from the field samples

\*\* Iron content calculated in the laboratory with spectroscopy and texture included

\*\*\* Iron content calculated with the ROSIS data with the masked pixels and spatial determined texture

\*\*\*\* Iron content calculated with the ROSIS data without masked pixels and texture from the Laboratory

In order to determine the suitability of the ROSIS data to calculate the iron content with  $RI_{\text{rosis}}$  a paired samples T-Test is applied on the data set. The estimated iron content on the locations of the soil samples are compared with the iron content of the soil samples at a confidence level of 95%. The iron contents calculated with  $RI_{\text{lab}}$  do not significantly differ from the iron determined with the extraction method described by Bartholomeus et al. (2007) as described in section 4.5.1 and table 4.17. Both the ROSIS data sets do significantly deviate from the “true” iron content which would mean that ROSIS cannot be used if the data must comply with the 95% confidence level. The significance does increase if the correction is made for the texture. If users would agree on a confidence level of 97.5% than the ROSIS data can be used for the determination for the iron content after correction for the reflectance and a high quality texture map. It should be noted though that the data after the correction only just meet the significance criteria and that the prediction of iron content will still be a rough estimation. In section 4.8.5 the reasons for this low performance will be discussed.

A decrease in the significance is observed when the masked pixels are left out. Both the ROSIS data sets would not be suitable to determine the iron content, even at a confidence level of 97.5%. This result is not expected or supported with earlier found results. The reason for this result could be that the amount of samples is too low to get reliable results from this test.

Table 4.17: 2-tailed significance of the data sets compared with the soil iron content of the soil samples.

<b>Data set</b>	<b>Significance</b>
Laboratory	0.462
ROSI	0.016
ROSI_texture	0.026
Laboratory_masked	0.293
ROSI_masked	0.008
ROSI_texture_masked	0.015

#### **4.8.4 The effect of the slope correction model on the spatial determination of the soil iron content**

In ArcMap the spatial distribution has been modeled for the D550<sub>S.D.rosis</sub> because the influence of slope is the strongest for this index. The maps for the iron content and the expected error caused by slope can be found in appendix Ia and Ib. In this part of the research it is tested if the slope model has influence on the estimation of soil iron which has already an error caused by the quality of the used data, as described in the previous paragraph. To check if the correction model does improve the data a comparison is made between the iron content calculated with D550<sub>S.D.rosis</sub> and the iron content calculated with D550<sub>S.D.lab</sub> for the locations of the sample data.

The expected error and the real error calculated do not correspond, from the general statistics (table 4.18) it can be concluded that the real error is on average 8.96 times as big as the expected error. The expected error is modeled in Arcmap, the percentage of the expected error for each slope is multiplied with the estimated iron content from nadir. Only the error caused by the influence of slope is taken into account for this research is interested in the error caused by slope. The standard deviation, the minimum and maximum values all deviate significantly from the expected value. In appendix J the general statistics are presented for each slope. From these results still no resemblance can be found for the two error types.

From these results it can be concluded that the error caused by the quality and the characteristics of the ROSIS image, the texture map as well as the interpolation of masked pixels, is far more influencing the determination of the soil iron content than slope itself.

Table 4.18: General statistics for the expected error and the real error.

	<b>Error_exp (mg/kg)</b>	<b>Error (mg/kg)</b>
Mean	0.143	1.282
S.D.	0.066	3.59
Minimum	0.033	-7.51
Maximum	0.248	7.82
Median	0.118	1.02

## 4.8.5 Discussion

### 4.8.5.1 Field conditions

The reflectance measured in the field is deviating from the reflectance in the laboratory because the soil surface has other conditions. This give rise to the following discussion points;

1. The soil samples used for the laboratory spectral analysis were air-dried and sieved (<2 mm) while in the field the soil can form aggregates due to the ploughing, weeding and the clay content.
2. Aggregation of soil particles will be stronger when the soil has a higher clay content. In the laboratory the surface of the soil samples is flattened before measuring while in the field micro relief might be present again due to the aggregates and the ploughing. This influences the reflectance because the surface is rougher which enhances multiple scattering (Irons et al., 1989).
3. In the area several soils can be found that have properties that influence reflectance in a different way. These spatial variation of soils can be a reason of the spatial variability found in the deviation of the expected iron content in the area.
4. The research area suffers on erosion and there is poor soil development under the semi-arid conditions. On the steep slopes most of the soil has eroded away and shallow rocky soils (Leptosols) are found (Berg van Saparoea et al., 2007). These soils contain more stones and gravel than loose soil. These stony soils reflect the radiance strongly.
5. Organic matter content is not taken into account for both the laboratory experiment and the spatial analysis. In the spatial analysis though this might be important because organic matter influences the reflectance. In the research area there are some soils that contain a high amount of organic matter (Phaozems), they occur in accumulation areas like the valleys and flat areas and there are very poor and shallow soils that contain hardly any organic matter (Berg van Saparoea et al., 2007).
6. In the field the soil can be moist after rain events; this influences the reflectance ass well, especially for soils with high clay content because they can hold water more tightly (Clevers et al., 2006). Soil moisture should be estimated during field campaigns.
7. The incidence angle in the field is deviating from the angle used in the laboratory. On 28 June 2001 around 13.30 hours at a flight height of 3510 m the incidence angle of the sun is 21.22 degrees (Zimmerman, 2003). In the laboratory experiment the incidence angle is set on 20 degrees, this means that the incoming radiance is slightly different in the field compared to the laboratory radiance and will give a difference in the reflectance. The fly direction of the aircraft is from South to North, assumed is that all the slopes facing  $270^{\circ}$  up to  $90^{\circ}$  have a negative aspect but this is not true when the sun is not standing precisely in the South at the moment of measuring. At the moment of the flight campaign the sun was standing at  $165.75^{\circ}$  instead of  $180^{\circ}$ .

#### *4.8.5.2 Atmospheric and topographic correction*

The ROSIS image has been corrected for atmospheric and topographic effects in order to improve the data quality. This correction is of low accuracy due to the rugged terrain and the coarse resolution of the DEM. (Richter, 1998) state that with a coarse resolution (>10m) of the DEM the matching of the image and DEM can lead to large relative reflectance errors exceeding 100%. The calibration, the estimation of atmospheric parameters, the geometric accuracy and the correction for BRDF is not optimal for rugged terrain (Richter and Schläpfer, 2001). Apart from these corrections the image contains much noise and the bandwidth of 4nm is quite broad when working with continuum-removal. From these findings it can be concluded that the image is of poor quality and it may not be suited for the type of analyses performed in this research.

#### *4.8.5.3 Vegetation influence*

In the laboratory experiment the iron content is calculated for bare soil. In the field there are barely any spots that have only pure bare soil. The resolution of ROSIS is 2m x 2m and these pixels are a mixture of some landscape elements like bare soil, vegetation, water, houses etc. In order to calculate the iron content for bare soil SMA has been applied on the ROSIS data with a mask of 25% and the two endmembers soil and olive tree. This means that if a pixel has a olive cover of 1 m<sup>2</sup> than the pixel is masked out and that pixels with a vegetation cover of less than 1 m<sup>2</sup> are classified as bare soil. There are a lot of pixels with this vegetation cover because weeds and parts of olive tree crowns are very likely to fall in this class. The map with these unmixed values show that pixels surrounding the olive tree do indeed have a higher value than true bare soil pixels. These mixed pixels are treated as bare soil but the calculated iron content of these pixels will not be correct. In order to reduce this effect of vegetation, images should be acquired with a finer resolution so vegetation can be better masked out. It is very important to assess the vegetation cover properly because Bartholomeus et al. (2007) found that a fractional vegetation cover of 20% already give a difference in iron content of more than 6% when the ratio based Redness Index is being used to determine the iron content. They also state that when using the Redness Index at higher vegetation cover, the iron prediction shows a structural underestimation. Vegetation effects lead to a lower reflectance in the red part of the spectrum, while the reflectance in the green wavelengths shows a relative increase. Therefore, the Redness Index will always underestimate the iron content when the regression is established on bare soil under laboratory conditions and applied to partially vegetated spectra (Bartholomeus et al., 2007).

#### *4.8.5.4 Redness Index and the continuum removal*

In order to estimate the iron content with ROSIS only the ratio based Redness Index can be used to produce a reliable result after some corrections. The continuum removal has proven to be unsuitable for the ROSIS data. It might be that this method requires very accurate reflectance measurements. There are several reasons that can explain this. First of all, ROSIS has measured with a bandwidth of 4 nm instead of 1 nm so the absorption features are measured less accurately. The indices calculated are the area and the standard deviation over the area. In order to calculate the whole area the values measured in the band is multiplied by four, the changes per nanometer are smoothed by this multiplication in comparison with the laboratory measurements, e.g. the area calculated for the

continuum removed spectra is overestimated with 2%. Secondly, the ROSIS data has a low signal-to-noise ratio, to reduce this noise a forward minimum noise fraction (MNF) rotation has been applied to the image. When this rotation is applied too strict some signal can get lost and this would cause a lower performance of the continuum-removal. Finally, there is a mixed pixel bias for the available pixels are mosaics of different land cover types, the convex-hull derived endmember spectra are biased towards the centroid of the true endmember spectra (Stoner, 2003).

According to the laboratory experiment the indices calculated for D880<sub>lab</sub> have the highest correlation with the iron content and the slope model can correct the data best for sloping areas. It would be desirable to measure this indices in the field but this is not possible with ROSIS and probably D880<sub>lab</sub> would be too sensitive, as is D550<sub>lab</sub>. The second best indices are the area and the S.D. of D550<sub>lab</sub> for they need very accurate reflectance measurements. Only the ratio based Redness Index can be used to determine the soil iron content but from the laboratory it has proven to be a less accurate indices with the lowest correlation with the iron content. The ratio based Redness Index is more robust because the reflectance is taken over a large range and small differences are smoothed due to the ratio that is taken from the range.

#### *4.8.5.5 Other discussion points*

The texture map that has been used for the calculation of the iron content has a poor quality. There are only 62 points used for the interpolation of the whole area. Of these 62 points 48 were concentrated in the research area of Bartholomeus et al. (2007) where the sample location were positioned in two down slope transects and the others where located on 4 areas in a transect of crest, upslope, down slope and when present, a valley. The interpolation for the whole area is based on too few samples which are not representative for the whole area and therefore not accurate.

The indices calculated from ROSIS have been corrected with a regression function. This regression function is derived from a data set with only 23 samples. This is too little to make a good regression function (Isaaks and Srivastava, 1989) and can explain why the correction function for the area and standard deviation of D550 has a low  $R^2$ .

All the other statistics are calculated with this data set as well. More samples are needed in order to improve the reliability of the results.

The aspect is simplified into slopes facing towards the sun and off the sun. This means that a slope facing North-East of North-West is reclassified into North. A better reclassification would be the effective slope towards the North because a North facing slope receives less radiation than a slope facing North-East or North-West. In this research the slopes facing not completely North have an underestimated radiation and the inverse holds for slopes not facing exactly South. This simplification was needed in this research in order to compare the ROSIS data with the laboratory data because only two types of slope were taken into account in the laboratory measurements namely; facing towards the sun and facing off the sun. PARGE/ATCOR has corrected for the aspect effect but this correction is of a low quality for it only corrects the reflectance bias and not per wavelength and due to the terrain properties. The influence is still visible in the image, for this reason the aspect is taken into account for this research but the effect is smaller due to the correction.

## 5. Conclusions and recommendations

In this chapter, first the conclusions are drawn and the answers to the research questions are given. After the conclusions, the recommendations are given for further research.

### 5.1 Conclusions

At the start of this research, the main objective was to find out if the slope has a significant influence in quantification of soil iron content with iron indices. The main research question is:

*“Is the influence of the slope significant on the quantification of soil iron content with spectral reflectance based iron indices?”*

In order to understand the spectrum measured with imaging spectroscopy it is important to understand which spectral chromophores do influence the shape and reflectance of the spectrum. The most important spectral chromophores are:

- A. Mineralogical composition of the soil will give certain absorption features. Iron will give absorption bands near 400nm -600 nm, 700 nm and near 800 nm 1000 nm (Irons et al., 1989).
- B. Surface roughness, texture and parent material contribute to the self shadowing effects and multiple scattering (Clevers et al, 2006).
- C. Variations in slope and aspect will influence the incoming and reflected radiation (Schlöpfer and Richter, 2002).
- D. Organic matter leads to a decrease in reflectance but has no distinct absorption features (Clevers et al., 2006).
- E. Soil moisture will reduce the amount of multiple scattered light and there is a relation between soil moisture and texture (Clevers et al., 2006).

It is found that slope does significantly influence the quantification of soil iron content when the indices after continuum removal are being used:

The slope does not significantly influence  $RI_{lab}$ . The minimum and maximum found errors in the estimation of the iron content are within a deviation of 5% from the average. Although this indices has the lowest correlation with iron content, the ratio based Redness Index is a robust index and can be used for the determination of the soil iron content.

The slope has little influence on the  $D550_{area_{lab}}$  and minimum and maximum errors are present up to 10% for slopes of  $10^0$  or smaller. With increasing slope, the influence of the slope increases as well but there is not a clear trend visible. This index could be used for the prediction of iron content without a correction for slope if the slopes are smaller than  $10^0$ , otherwise a correction for slope is recommended.

D550<sub>\_S.D.\_lab</sub> is influenced by slope. On average, the index does significantly deviate from the nadir measurements up to an error of 2.5% and the minimum and maximum errors are up to 5%. The influence of slope is larger for steeper slopes and a so called “V-shape” is formed. In order to predict the soil iron content accurate, a correction for slope is needed.

For both the area and the standard deviation of D880<sub>\_lab</sub> the slope is clearly influencing the indices. The iron content is significantly deviating from the nadir measurements and the average deviates up to 5% with minimum and maximum error deviating around this average of 5%. Without a correction for slope, these two indices are not suitable for the determination of soil iron content.

In order to correct for the error caused by the slope a slope correction model is developed with a linear regression for each slope and for each index.

The results for both the area and the standard deviation for D550 and D880 are improved and more accurate. Both the slope correction models for D550<sub>\_area\_lab</sub> and D550<sub>\_S.D.\_lab</sub> can be classified as a class B model according to Chang et al. (2001). The developed slope correction models for D880<sub>\_area\_lab</sub> and D880<sub>\_S.D.\_lab</sub> have a better performance and can be classified as a class A model according to Chang et al. (2001).

For all the indices, the validation set has a lower performance but the results are still an improvement on the uncorrected data.

The influence of slope is negligible when airborne imaging spectroscopy data is being used.

Taken all the possible errors into account, the correlation of iron calculated with RI<sub>\_rosis</sub> with the original iron content is 0.26. When the interpolated pixels and correct texture is taken into account than the correlation increases up to 0.40, which is still very low.

When the expected error of the slope for D550<sub>\_S.D.\_rosis</sub> is compared with the overall error than it turns out that the error caused by the data quality and the field conditions is 8.96 times as big as the error caused by the slope under laboratory conditions. It can be concluded from these results that the influence of slope on the error in the estimation of the iron content is not of significant influence when the ROSIS image is used.

## 5.2 Recommendations

### **5.2.1 Recommendations for the laboratory experiment**

For further research it is most important that the standard deviation of the error caused by slope is minimized. This can be obtained by aggregating data and make several correction functions depending on a third property. A good aggregation parameter could be organic matter because from earlier research it is proven that organic matter does significantly influence reflectance properties (Ben-Dor et al., 1999). When there are more soil properties available than a principle components regression analyses would be the appropriate method to predict the iron content (Chang et al., 2001).

The slope model can be used to correct data from field spectroscopy measurements. The slope model is calibrated for the specific research area used in this research and should first be calibrated for other areas before it is applied.

### **5.2.2 Recommendations for the ROSIS analyses**

ROSI is not the most suitable spectrometer for this type of analyses in this specific research area because the band width is too wide and the resolution too coarse. With better data, the reflectance will probably better correspond to the reflectance measured under laboratory conditions and the amount of mixed pixels will be lower for the SMA. If the ROSIS image is being used for the estimation of soil iron content than a correction model must be developed to correct for the deviation of the reflectance. ROSIS can be used for a coarse classification of soil iron content, for areas with high soil iron content can be discriminated from areas with low soil iron content. This might be enough in extended areas when there is only need for an indication of soil iron. It is also recommended to use a spectrometer with only three bands, one in the blue, one in the green and one in the red, in combination with a lower fly height in order to get a finer resolution. This type of spectrometer will probably have less noise and the ratio based Redness Index can then be used to quantify the soil iron content.

The masked out pixels can be interpolated with ordinary kriging because this method will give more accurate results (Isaaks and Srivastava, 1989).

As discussed before, the aspect which is taken into account is too simplified. In order to make a better comparison with laboratory data measurements must be taken under the 9 different aspects.

The texture map must be of good quality, the best way to collect this data is to go into the field and take samples which are then analyzed in the laboratory. These laboratory analyses are expensive, so the texture can be determined manually but this is less accurate. If it is not possible to do field work than the texture can be derived from a soil map.

More field samples of the iron content are needed in order to get insight into the spatial variability of the iron. When this data is present relations can be found with e.g. different soil types, parent material, organic matter, texture and soil moisture. This information can improve the developed correction model. All the calculated statistics are based on a relative small data set; the reliability of these statistics can be enhanced when more samples are taken into account.

## References

### Literature references

- BARHOLOMEUS, H., 2007a, ASD Fieldspec Pro FR.
- BARHOLOMEUS, H., 2007b, Short manual Fieldspec Pro: Wageningen University.
- BARHOLOMEUS, H., EPEMA, G., and SCHAEPMAN, M., 2007, Determining iron content in Mediterranean soils in partly vegetated areas, using spectral reflectance and imaging spectroscopy. *International Journal of Applied Earth Observation and Geoinformation*, 9 194-203.
- BEN-DOR, E., IRONS, J., EPEMA, G., 1999, Soil reflectance, 3 edn: John Wiley & Sons, Inc.
- BERG VAN SAPAROE, V. D. R., 2007, Introduction to the field training project Alora.
- BERGER, M., RAST, M., WURSTEISEN, P., ATTEMA, E., MORENO, J., MUELLER, A., BEISL, U., RICHTER, R., SCHAEPMAN, M., STRUB, G., STOLL, M. P., NERRY, F., and LEROY, M. E., 2001, The DAISEX campaigns in support of a future land-surface-processes mission. *ESA Bulletin*, 105, 101-111.
- BOREL, C. C., and GERSTL, S. A., 1994, Nonlinear spectral mixing models for vegetation and soil surfaces. *Remote Sensing of Environment*, 47, 403-416.
- BULLARD, J. E., and WHITE, K., 2002, Quantifying iron oxide coatings on dune sands using spectrometric measurements: an example from the Simpson-Strzelecki Desert. *Journal of Geophysical Research*, 107.
- CHANG, C. W., LAIRD, D. A., MAUSBACH, M. J., and HURBURGH, C. R., 2001, Near-Infrared Reflectance Spectroscopy-Principal Components Regression Analyses of Soil Properties. *Soil Science Society of America Journal*, 65, 480-490.
- CHANG, W. H., CHEN, S., and TSAI, C. C., 1998, Development of a Universal Algorithm for use of NIR in Estimation of Soluble Solids in Fruit Juices. *American Society of Agricultural Engineers*, 41, 1739-1745.
- CIERNIEWSKI, J., 1987, A model for soil surface roughness influence on the spectral response of bare soils in the visible and near infrared range. *Remote Sensing of Environment*, 23, 98-115.
- CLEVERS, J. G. P. W., KOOISTRA, L., SCHAEPMAN, M. E., DE WIT, A. J. W., ROERINK, G. J., and BARTHOLOMEUS, H. M., 2006, Remote Sensing Lecture Sheets.
- ELMORE, A. J., MUSTARD, J. F., MANNING, S. J., and LOBELL, D. B., 2000, Quantifying Vegetation Change In Semiarid Environments: Precision and Accuracy of Spectral Mixture Analysis and the Normalized Difference Vegetation Index. *Remote Sensing of Environment*, 73, 87-102.
- ESCADAFAL, R., and HEUTE, A. R., 1991, Influence of the viewing geometry on the spectral properties (high resolution visible and NIR) of selected soil from Arizona. *Proceedings of the 5th International Colloquium on Physical measurements and Signatures in Remote Sensing*, 1, 401-404.
- FAO, and ISRIC, 1990, Guidelines for soil description (Rome).

- GEGE, P., BERAN, D., MOOSHUBER, W., SCHULZ, J., and PIEPEN, H. V. D., 1998, System analysis and performance of the new version of the imaging spectrometer ROSIS. , Remote Sensing Laboratories, University of Zurich.
- GREEN, A. A., BERMAN, M., SWITZER, P., and CRAIG, M. D., 1988, A transformation of ordering multispectral data in terms of image quality with implications for noise removal. *IEEE Trans. Geoscience for Remote Sensing*, 26, 65-74.
- HAPKE, B. W., 1984, Bidirectional reflectance spectroscopy: correction for macroscopic roughens. *Icarus*, 59, 41-59.
- HAPKE, B. W., 1986, Bidirectional reflectance spectroscopy: 4. The extinction coefficient and the opposition effect. *Icarus*, 49, 264-280.
- HEUVELINK, G., 2007, personal communication.
- HOLZWARTH, S., MULLER, A., HABERMEYER, M., RICHTER, R., HAUSOLD, A., THIESMANN, S., and STROBL, P., 2003, HySens-DAIS 7915/ROSIS Imaging Spectrometers at DLR. In: *Proceedings of the 3rd Earsel Workshop on Imaging Spectroscopy*.
- HU, T., 2007, Non-linear control design for linear differential inclusions via convex hull of quadratics. *Automatica*, 43, 685-692.
- HU, T., GOEBEL, R., TEEL, A. R., and LIN, Z., 2005, Conjugate Lyapunov functions for saturated linear systems. *Automatica*, 41, 1949-1956.
- HURCUM, S.J., HARRISON, A.R., 1998, The NDVI and spectral decomposition of semi-arid vegetation abundance estimation. *International Journal of Remote Sensing*, 19, 16,3109-3125.
- IRONS, J. R., WEISMILLER, R. A., and PETERSEN, G. W., 1999, *Soil reflectance: John Wiley & Sons, Inc.*
- ISAAKS, E. H., and SRIVASTAVA, R. M., 1989, *An introduction to applied geostatistics (Oxford: Oxford University Press, Inc)*.
- ISLAM, K., MCBRATNEY, A., and SINGH, B., 2005, Rapid estimation of soil variability from the convex hull biplot area of topsoil ultra-violet, visible and near-infrared diffuse reflectance spectra. *Geoderma*, 128, 249-257.
- JOLLIFFE, I. T., 2002, *Principal Components Analysis, 2 edn (-: Springer)*.
- KOKALY, R. F., 2000, Investigating a physical basis for spectroscopic estimates of leaf nitrogen concentration, . *Remote Sensing of Environment*.
- LILLESAND, T. M., KIEFER, R. W., and CHIPMAN, J. W., 2004, *Remote sensing and image interpretation, 5 edn*.
- LUO, D., and MACLEOD, J., 1992, Automatic Orientation analysis of particles of soil microstructures. *Geotechnique*, 42, 97-107.
- PUTTEN, V. B., 2007, *Lecture notes for spatial modeling and statistics*.
- RICHTER, R., 1998, Correction of satellite imagery over mountainous terrain. *Applied Optics*, 37, 4004-4015.
- RICHTER, R., 2000, *Model ATCOR4: Atmospheric/topographic correction for wide FOV airborne imagery*.

- RICHTER, R., and SCHLÄPFER, D., 2002, Geo-atmospheric processing of airborne imaging spectrometry data. Part 2: atmospheric/topographic correction. *International Journal of Remote Sensing*, 23, 2631-2649.
- RUEDA, C. A., and WRONA, A. F., 2003, SAMS user manual, University of California.
- SCHAEPMAN-STRUB, G., SCHAEPMAN, M., PAINTER, T., DANGEL, S., MARTONCHIK, J. , 2006, Reflectance quantities in optical remote sensing - definitions and case studies,. *Remote Sensing of Environment*, 103, 27-42.
- SCHLÄPFER, D., BOREL, C. C., KELLER, J., and ITTEN, K. I., 1998, Atmospheric precorrected differential absorption technique to retrieve columnar water vapor. *Remote Sensing of Environment*, 65, 353-366.
- SCHLÄPFER, D., KOETZ, B., GRUBER, S., and MORSDORF, F., 2004, The influence of DEM characteristics on preprocessing of DAIS/ROSIS data in high altitude alpine terrain: University of Zurich).
- SCHLÄPFER, D., and RICHTER, R., 2002, Geo-atmospheric processing of airborne imaging spectrometry data. Part 1: parametric orthorectification *International Journal of Remote Sensing*, 23, 2609-2630.
- SMALL, C., 2001, Estimation of urban vegetation abundance by spectral mixture analysis. *International Journal of Remote Sensing*, 22, 1305-1334.
- STEVENS, A., WESEMAEL, V. B., VANDENSCHRICK, G., TOURE, S., and TYCHON, B., 2006, Detection of Carbon Stock Change in Agricultural Soils Using Spectroscopic Techniques. *Soil Science Society of America Journal*, 70, 844-850.
- STONER, W. W., 2003, Towards a statistical error estimate for convex-hull derived endmembers. *Advances in Techniques for Analysis of Remotely Sensed Data*, IEEE, 129-142.
- STOORVOGEL, J. J., 2007, Inventory of natural resources: Wageningen University).
- VERMOTE, E. F., TANRE, D., DEUZE, J. L., HERMAN, M., and MORCRETTE, J. J., 1997, Second simulation of the satellite signal in the solar spectrum (6S). In *User Guide Version 2* (NASA Goddard Space Flight Center).
- WATSON, A., 1987, Variations in wind velocity and sand transport on the windward flanks of desert sand dunes. *Sedimentology*, 34, 511-520.
- WILLIAMS, P. C., and SOBERING, D. C., 1993, Comparison of commercial near infrared transmittance and reflectance instruments for analyses of whole grains and seeds. *Journal for Near Infrared Spectroscopy*, 1, 25-32.
- WITHING, M. L., LI, L., and USTIN, S. L., 2003, Predicting water content using Gaussian model on soil spectra. *Remote Sensing of Environment*, 89, 535-552.
- XIAO, J., and MOODY, A., 2005, A comparison of methods for estimating fractional green vegetation cover within a desert-to-upland transition zone in central New Mexico, USA. *Remote Sensing of Environment*, 98, 237-250.
- ZIMMERMAN, N. E., 2003, 7.3 supos.for.

## URL's

<http://www.itvis.com/envi/>

<http://www.phys.tue.nl/TULO/guldensnede/sinusregel.html>

<http://www.physicsarchives.com>

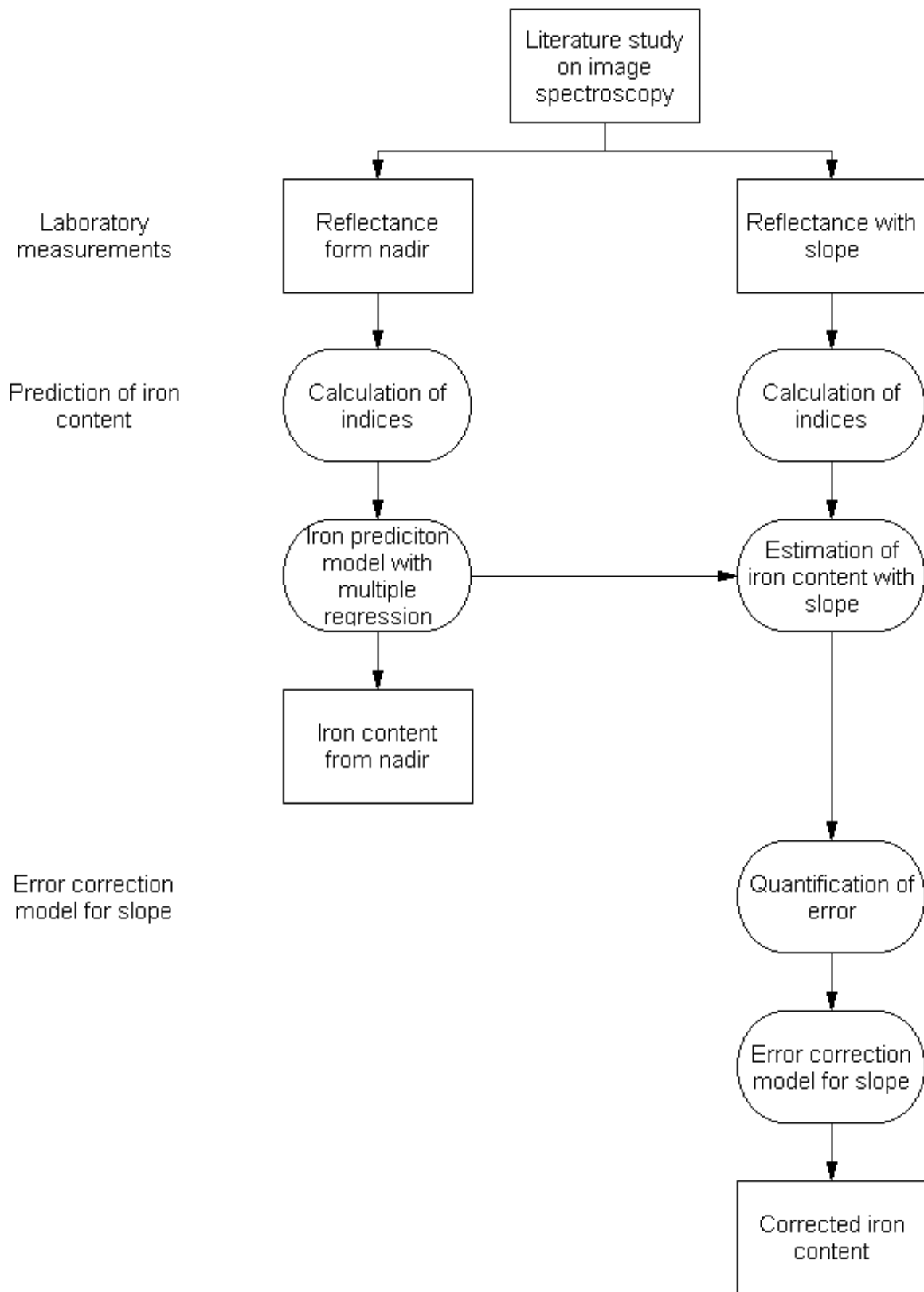
# Appendices

## Index:

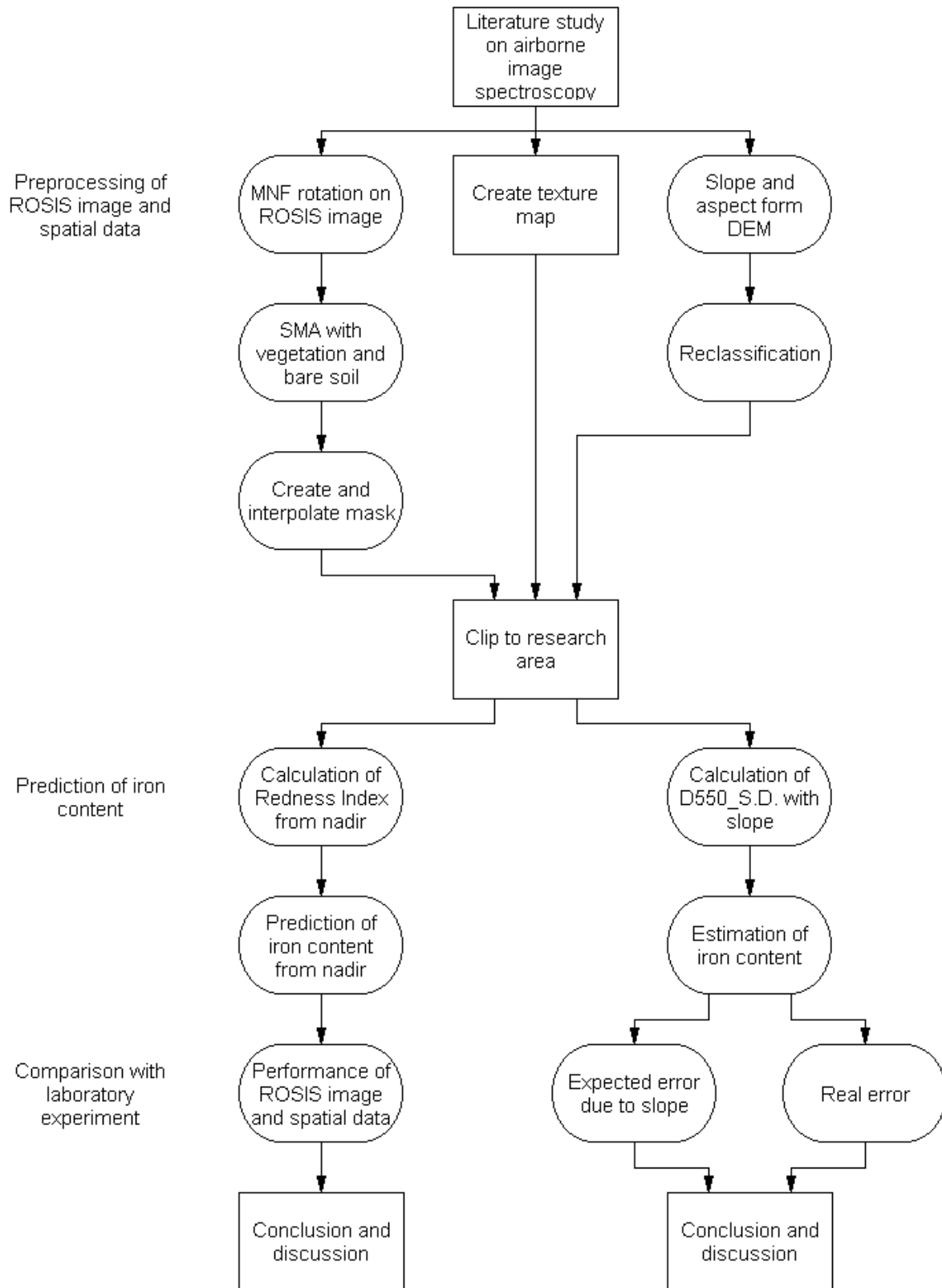
<b>Appendix A: flowchart of the methodology</b>	<b>I</b>
<b>Appendix B: Correction functions for iron contents per slope per index.</b>	<b>III</b>
<b>Appendix C: Standard deviations</b>	<b>V</b>
<b>Appendix D: Spectral unmixing for olive tree and bare soil</b>	<b>VI</b>
<b>Appendix E: Mask for vegetation</b>	<b>VII</b>
<b>Appendix F: Slope and aspect derived from DEM</b>	<b>VIII</b>
<b>Appendix G: Texture map</b>	<b>IX</b>
<b>Appendix H: Estimated soil iron content with RI_rosis</b>	<b>X</b>
<b>Appendix Ia: Estimated soil iron for D550_S.D._rosis</b>	<b>XI</b>
<b>Appendix Ib: Expected error for D550_S.D._rosis</b>	<b>XII</b>
<b>Appendix J: General statistics per slope</b>	<b>XIII</b>

# Appendix A: flowchart of the methodology

## PART 1: LABORATORY EXPERIMENT



PART 2: ESTIMATION OF IRON CONTENT WITH ROSIS



## Appendix B: Correction functions for iron contents per slope per index.

<i>Index</i>	<i>Slope</i>	<i>Function</i>
RI_lab	-25	$Y=0.23+0.991*(-39.086 + 104.313*RI_{lab} - 0.004*texture)$
	-20	$Y=0.192+0.99*(-39.086 + 104.313* RI_{lab} - 0.004*texture)$
	-15	$Y=0.098+0.994*(-39.086 + 104.313* RI_{lab} - 0.004*texture)$
	-10	$Y=0.008+0.997*(-39.086 + 104.313* RI_{lab} - 0.004*texture)$
	-5	$Y=-0.061+1.001*(-39.086 + 104.313* RI_{lab} - 0.004*texture)$
	5	$Y=0.009+0.999*(-39.086 + 104.313* RI_{lab} - 0.004*texture)$
	10	$Y=-0.008+0.998*(-39.086 + 104.313* RI_{lab} - 0.004*texture)$
	15	$Y=-0.079+1.004*(-39.086 + 104.313* RI_{lab} - 0.004*texture)$
	20	$Y=-0.094+1.006*(-39.086 + 104.313* RI_{lab} - 0.004*texture)$
	25	$Y=-0.131+1.008*(-39.086 + 104.313* RI_{lab} - 0.004*texture)$
	D550_area_lab	-25
-20		$Y=0.102+0.997*( 59.050 - 0.253* D550_{area\_lab} - 0.004*texture)$
-15		$Y=0.08+0.99*( 59.050 - 0.253* D550_{area\_lab} - 0.004*texture)$
-10		$Y=0.33+0.98*( 59.050 - 0.253* D550_{area\_lab} - 0.004*texture )$
-5		$Y=0.262+0.985*( 59.050 - 0.253* D550_{area\_lab} - 0.004*texture)$
5		$Y=0.223+0.991*( 59.050 - 0.253* D550_{area\_lab} - 0.004*texture)$
10		$Y=0.094+0.993*( 59.050 - 0.253* D550_{area\_lab} - 0.004*texture)$
15		$Y=0.217+0.988*( 59.050 - 0.253* D550_{area\_lab} - 0.004*texture)$
20		$Y=0.124+ 59.050 - 0.253* D550_{area\_lab} - 0.004*texture$
25		$Y=0.018+1.009*(59.050 - 0.253* D550_{area\_lab} - 0.004*texture)$
D550_S.D._lab		-25
	-20	$Y=0.201+0.996*(4.247 + 128.688* D550_{S.D. \_lab} - 0.004*texture)$
	-15	$Y=0.32+0.991*(4.247 + 128.688* D550_{S.D. \_lab} - 0.004*texture)$
	-10	$Y=0.16+1.002*(4.247 + 128.688* D550_{S.D. \_lab} - 0.004*texture)$
	-5	$Y=-0.005+1.01*(4.247 + 128.688* D550_{S.D. \_lab} - 0.004*texture)$
	5	$Y=0.096 +(4.247 + 128.688* D550_{S.D. \_lab} - 0.004*texture)$

---

	10	$Y=0.066+1.001*(4.247 + 128.688* D550_{S.D.}_{lab} - 0.004*texture)$
	15	$Y=0.051+1.006*(4.247 + 128.688* D550_{S.D.}_{lab} - 0.004*texture)$
	20	$Y=0.124+4.247 + 128.688* D550_{S.D.}_{lab} - 0.004*texture$
	25	$Y=0.078+1.005*(4.247 + 128.688* D550_{S.D.}_{lab} - 0.004*texture)$
D880_area_lab	-25	$Y=-0.174+1.055*(468.878 - 2.286* D880_{area\_lab} - 0.004*texture)$
	-20	$Y=-0.01+1.039*(468.878 - 2.286* D880_{area\_lab} - 0.004*texture)$
	-15	$Y=-0.188+1.046*(468.878 - 2.286* D880_{area\_lab} - 0.004*texture)$
	-10	$Y=0.011+1.029*(468.878 - 2.286* D880_{area\_lab} - 0.004*texture)$
	-5	$Y=0.048+1.023*(468.878 - 2.286* D880_{area\_lab} - 0.004*texture)$
	5	$Y=0.04+0.999*(468.878 - 2.286* D880_{area\_lab} - 0.004*texture)$
	10	$Y=-0.044+1.007*(468.878 - 2.286* D880_{area\_lab} - 0.004*texture)$
	15	$Y=-0.231+1.026*(468.878 - 2.286* D880_{area\_lab} - 0.004*texture)$
	20	$Y=-0.115+1.022*(468.878 - 2.286* D880_{area\_lab} - 0.004*texture)$
	25	$Y=0.092+1.007*(468.878 - 2.286* D880_{area\_lab} - 0.004*texture)$
D880_S.D_lab	-25	$Y=0.128+1.034*(8.123 + 907.207* D880_{S.D.}_{lab} - 0.004*texture)$
	-20	$Y=0.148+1.028*(8.123 + 907.207* D880_{S.D.}_{lab} - 0.004*texture)$
	-15	$Y=0.09+1.027*(8.123 + 907.207* D880_{S.D.}_{lab} - 0.004*texture)$
	-10	$Y=0.176+1.018*(8.123 + 907.207* D880_{S.D.}_{lab} - 0.004*texture)$
	-5	$Y=0.072+1.022*(8.123 + 907.207* D880_{S.D.}_{lab} - 0.004*texture)$
	5	$Y=0.03+1.003*(8.123 + 907.207* D880_{S.D.}_{lab} - 0.004*texture)$
	10	$Y=0.032+1.008*(8.123 + 907.207* D880_{S.D.}_{lab} - 0.004*texture)$
	15	$Y=-0.091+1.021*(8.123 + 907.207* D880_{S.D.}_{lab} - 0.004*texture)$
	20	$Y=0.001+1.02*(8.123 + 907.207* D880_{S.D.}_{lab} - 0.004*texture)$
	25	$Y=0.103+1.019*(8.123 + 907.207* D880_{S.D.}_{lab} - 0.004*texture)$

---

## Appendix C: Standard deviations

Standard deviation of the error for the uncorrected (A) differences and the corrected (B) differences.

<i>Slope</i>	<i>RI_lab</i>		<i>D550_area_lab</i>		<i>D550_S.D_lab</i>		<i>D880_area_lab</i>		<i>D880_S.D_lab</i>	
	<i>A</i>	<i>B</i>	<i>A</i>	<i>B</i>	<i>A</i>	<i>B</i>	<i>A</i>	<i>B</i>	<i>A</i>	<i>B</i>
-25	0.23	0.22	0.33	0.32	0.15	0.14	0.40	0.33	0.29	0.26
-20	0.29	0.29	0.29	0.29	0.23	0.23	0.29	0.25	0.22	0.19
-15	0.28	0.28	0.38	0.38	0.19	0.18	0.31	0.25	0.20	0.17
-10	0.23	0.23	0.28	0.27	0.13	0.13	0.26	0.24	0.19	0.17
-5	0.12	0.12	0.30	0.30	0.17	0.16	0.19	0.16	0.14	0.10
0	0.00	0.00	0.00	0.00	0.00	0.00	0.00	0.00	0.00	0.00
5	0.08	0.08	0.25	0.25	0.12	0.12	0.16	0.16	0.10	0.10
10	0.13	0.13	0.25	0.24	0.10	0.10	0.14	0.14	0.12	0.12
15	0.13	0.12	0.27	0.27	0.12	0.12	0.25	0.22	0.17	0.15
20	0.13	0.13	0.21	0.21	0.15	0.15	0.22	0.20	0.19	0.17
25	0.15	0.15	0.25	0.25	0.13	0.13	0.20	0.19	0.17	0.15

## Appendix D: Spectral unmixing for olive tree and bare soil

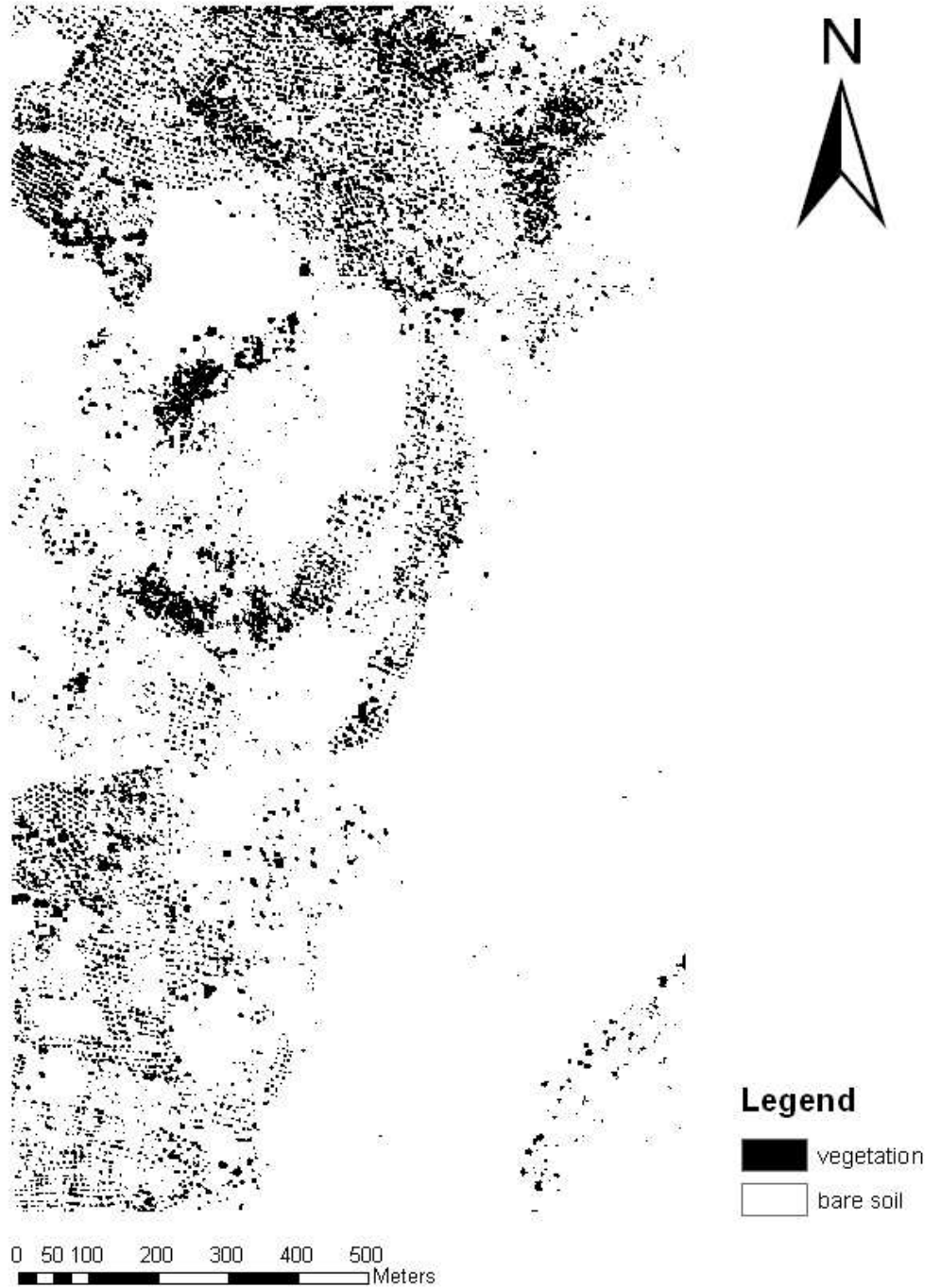
# Vegetation cover



Titia Mulder, 14-09-2007, Wageningen University

## Appendix E: Mask for vegetation

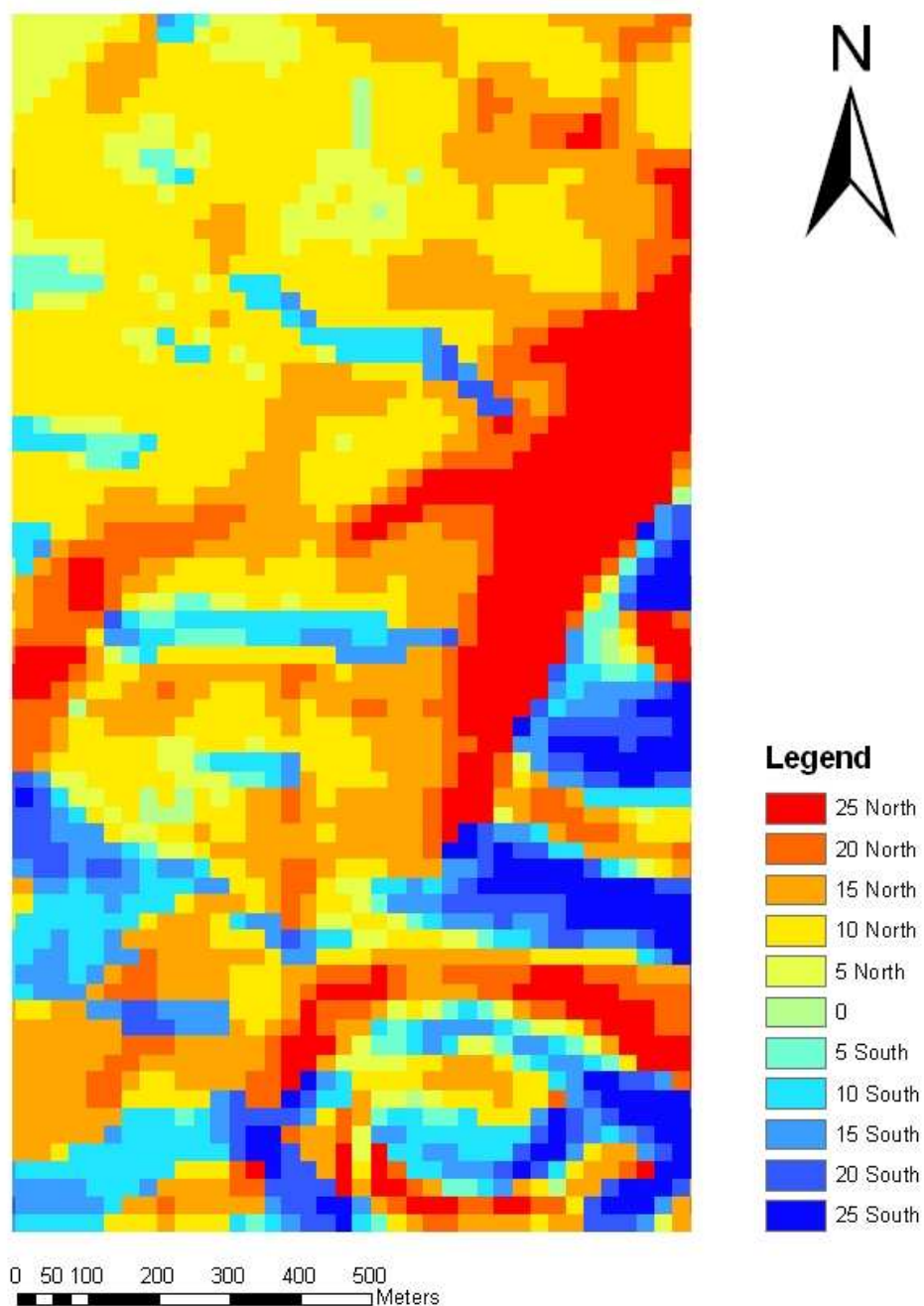
# Mask 25%



Titia Mulder, 14-09-2007, Wageningen University

## Appendix F: Slope and aspect derived from DEM

# Slope and aspect (degrees)



Titia Mulder, 14-09-2007, Wageningen University

## Appendix G: Texture map

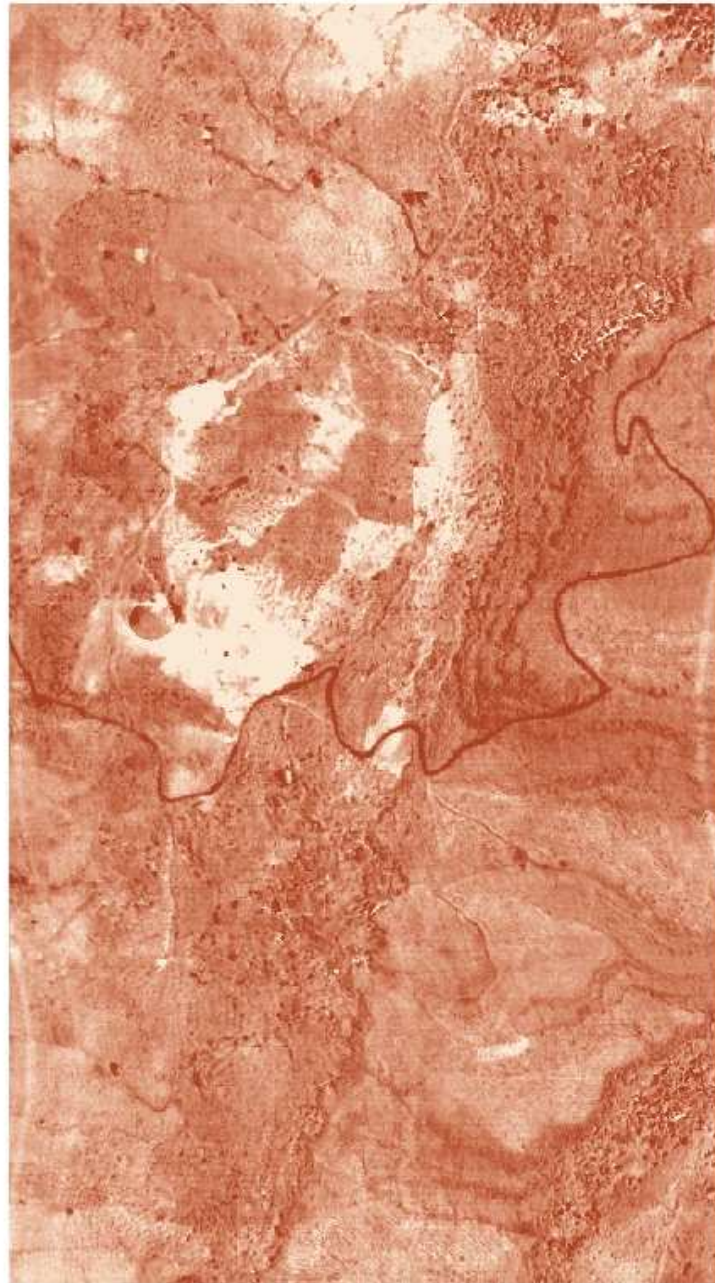
# Texture (qm)



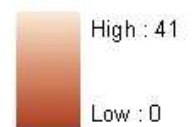
Titia Mulder, 14-09-2007, Wageningen University

Appendix H: Estimated soil iron content with RI<sub>rosis</sub>

# Fe (mg/kg) from nadir



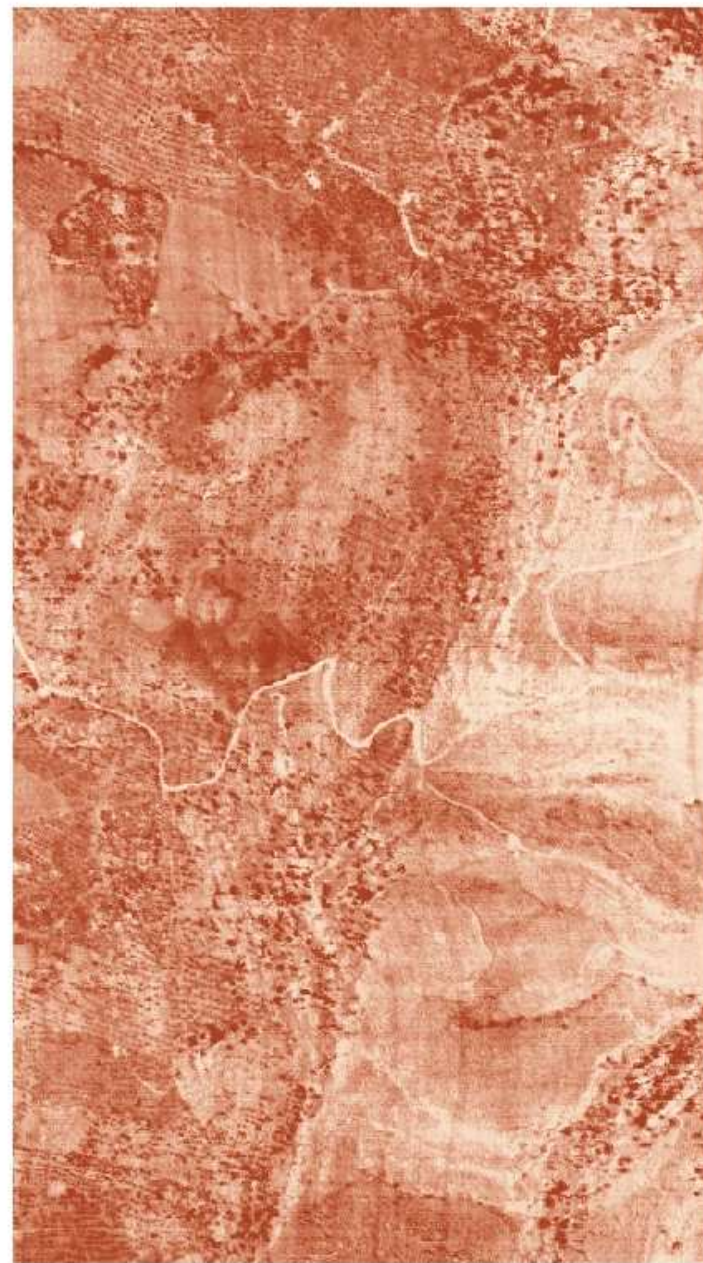
**Legend**



Titia Mulder, 14-09-2007, Wageningen University

Appendix Ia: Estimated soil iron for D550\_S.D.\_rosis

# Fe (mg/kg) from nadir



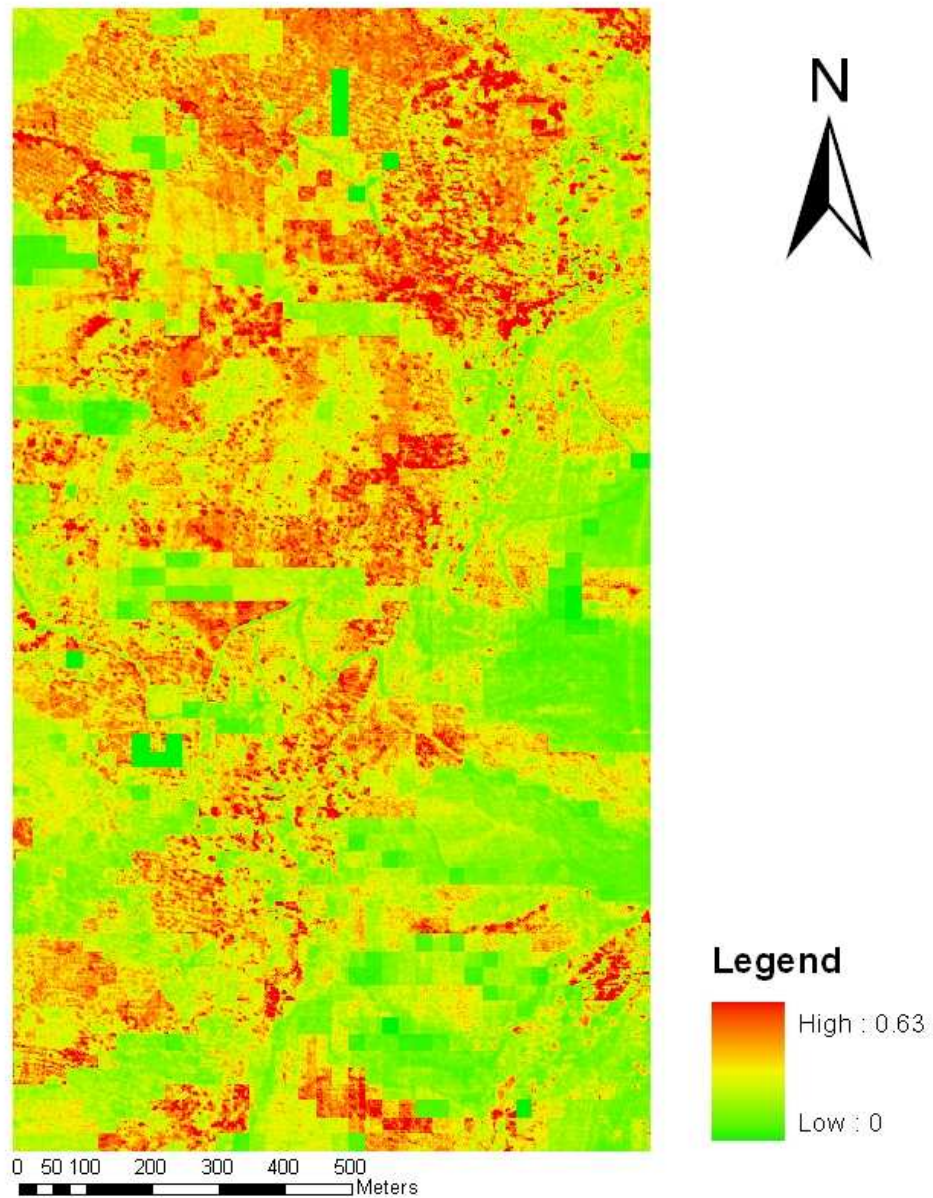
**Legend**



Titia Mulder, 14-09-2007, Wageningen University

## Appendix Ib: Expected error for D550\_s.D.\_rosis

### Expected error (mg/kg)



Titia Mulder, 14-09-2007, Wageningen University

## Appendix J: General statistics per slope

<i>Slope</i>	<b>-15</b>	<b>-10</b>	<b>-5</b>
	<i>error_exp</i>	<i>error</i>	<i>error_exp</i>
	<i>(mg/kg)</i>	<i>(mg/kg)</i>	<i>(mg/kg)</i>
Mean	0.23	2.74	0.15
S.D.	0.01	5.03	0.02
Minimum	0.22	-4.47	0.12
Maximum	0.25	7.82	0.17
Median	0.23	3.58	0.15

<i>Slope</i>	<b>5</b>	<b>10</b>
	<i>error_exp</i>	<i>error</i>
	<i>(mg/kg)</i>	<i>(mg/kg)</i>
Mean	0.04	2.08
S.D.	0.00	3.77
Minimum	0.03	-1.93
Maximum	0.04	5.45
Median	0.04	2.40

